Characterization of the excitation-contraction coupling in extraocular muscles

Inauguraldissertation

zur
Erlangung der Würde eines Doktors der Philosophie
vorgelegt der
Philosophisch-Naturwissenschaftlichen Fakultät
der Universität Basel

von

Marijana Sekulic

aus Serbien

Basel, 2016

Genehmigt von der Philosophisch-Naturwissenschaftlichen
Fakultät auf Antrag von:

Prof. Dr. Jean Pieters
Prof. Dr. Susan Treves
Prof. Dr. Christoph Handschin

Basel, den 08. Dezember 2015

Prof. Dr. Jörg Schibler

Dekan

ACKNOWLEDGMENTS

CONTENTS

ABSTRACT

Excitation-contraction coupling (ECC) is the physiological mechanism whereby an electrical signal detected by the dihydropyridine receptor, is translated into an increase in [Ca^{2+}], by activating ryanodine receptors. Mutations in *RYR1*, the gene encoding the ryanodine receptor 1, are the underlying cause of several congenital myopathies including Central core disease, Multiminicore disease, some forms of Centronuclear myopathy and Congenital fiber type disproportion. Patients with recessive but not dominant *RYR1* mutations show a significant reduction of ryanodine receptor protein in muscle biopsies as well as ophthalmoplegia or involvement of the extraocular muscles (EOM). This specific involvement indicates that this group of muscles may express different proteins involved in excitation-contraction coupling compared to limb muscles. The focus of this thesis is the characterization of the excitation-contraction coupling toolkit of human EOM. The main goal was to identify differences or similarities with other skeletal muscles in the context of the previously mentioned diseases which affect skeletal muscles. My results indicate that the transcripts of the main genes involved in skeletal excitation-contraction coupling are downregulated, while at the same time, we report increased expression of the ryanodine receptor 3, cardiac calsequestrin and alfa 1 subunit of the cardiac dihydropiridine receptor. In addition, the finding of increase in excitation-coupled calcium entry in the EOM compared to leg muscles (LM) completes the picture of the EOM muscles as a specific muscle group with a unique mode of calcium handling and their selective involvement in neuromuscular disorders.

Facial weakness and ptosis have also been described in patients with mutations in *RYR1*. Having this in mind, we were interested in investigating the relation between the facial muscle orbicularis oculi (OO), EOM and LM and the excitation-contraction coupling toolkit in human biopsies and myotubes derived from individuals which do not have any known neuromuscular disorder. According to our results, OO show more similarities to leg muscles than to EOM. In addition, we found high expression levels of dystrophin and utrophin and this is significant from the perspective of Duchenne muscular dystrophy (DMD). In fact in this condition EOM are spared from pathology and the same is true in mdx (dystrophin deficient) mouse models. In mdx

mice it is believed that utrophin compensates for the lack of dystrophin. Our findings that *UTRN* is expressed at higher level in OO compared to LM in normal conditions strongly support this theory of a compensatory effect by utrophin when dystrophin is missing.

Further investigations in my thesis focus on two isoforms of the ryanodine receptor, namely RyR1 and RyR3. Ryanodine receptor 1 plays a crucial role in the process of excitation-contraction coupling in skeletal muscle. According to our study on normal human EOM, the expression of this receptor is decreased compared to its expression levels in human leg muscles, however the expression level of RyR3 is significantly increased. Because of these latter results, we reasoned that the reported behavioral impairment reported in *RYR3* KO mice, may actually be due to alterations of EOM function. Our preliminary data show that in fact *RYR3* KO mice exhibit visual impairment as measured using their optokinetic reflex. We are currently investigating the role of RyR3 in EOM calcium homeostasis.

Taken all together, this thesis shows that different involvement of EOM and OO in neuromuscular disorders is due to their different excitation contraction coupling toolkit component. Furthermore, EOMs exhibit characteristics that deserve further attention as further investigations may lead to the discovery of protective mechanisms in neuromuscular disorders with potential therapeutic benefit.

LIST OF ABBREVIATIONS

2-APB	2-aminoethyl diphenylborate
4-CmC	4-chloro-m-cresol
ACTA1	α-skeletal actin 1
AP	Action potential
ARVD2	Arrhythmogenic right ventricular dysplasia type 2
BIN1	Bridging Integrator 1
CaM	Calmodulin
CaMKII	Ca^{2+}/calmodulin dependent protein kinase II
Ca_v	Voltage-gated calcium channel
CCD	Central core disease
CFTD	Congenital fiber type disproportion
CICR	Ca^{2+} induced Ca^{2+} release
CNM	Centronuclear myopathy
CNS	Central nervous system
COX	Cytochrome oxidase
CPVT	Catecholaminergic polymorphic ventricular tachycardia
CSQ	Calsequestrin
DHPR	Dihydropyridine receptor
DNM2	Dynamin 2
ECC	Excitation-contraction coupling
EOM	Extraocular muscles
FDHM	Full duration at half maximum
FKBP12	FK506-binding protein
FWHM	Full width at half maximum
H&E	Haematoxylin and eosin
IVCT	In vitro contracture test
JP45	Junctional SR protein 45
Mg29	Mitsugumin 29
MH	Malignant hyperthermia

MHS	Malignant hyperthermia susceptibility
MIFs	Multiply innervated fibers
MmD	Multi-minicore disease
MTM1	Myotubularin1
MyHC	Myosin heavy chain
NADH-TR	Nicotinamide adenine dinucleotide tetrazolium reductase
NCX	Na^+/Ca^{2+} exchanger
OO	Orbicularis oculi
PDE4D3	cAMP-specific phosphodiesterase type 4
PI3P	Phosphatidylinositol 3-phosphate
Pitx2	Paired-like homeodomain transcription factor 2
PKA	Protein kinase A
PMCA	Plasma membrane Ca^{2+}ATPase
PP1	Protein phosphatase 1
PP2A	Protein phosphatase 2
RyR	Ryanodine receptor
SAM	Sterile-α-motif
SARKO	Sarcalumenin knockout
SDH	Succinate dehydrogenase
SEPN1	Selenoprotein N
SERCA	Sarcoendoplasmatic reticulum Ca^{2+} transport ATPase
SIFs	Singly innervated fibers
SKF 96356	N,6-dimethyl-1-(2-methylphenyl)-2,3-dihydropyrrolo[3,2-c]quinolin-4-amine
SOCE	Store-operated calcium entry
SR	Sarcoplasmic reticulum
STIM1	Stromal interaction molecule 1
TPM3	Tropomyosin 3
TRDN	Triadin

CHAPTER 1: INTRODUCTION

1.1 Craniofacial muscles

More than 10% of the total number of muscles in the human body are found in the craniofacial region. The craniofacial muscles are involved in a number of crucial non-locomotor activities, and are critical for the most basic functions of life, including vision, taste, chewing and food manipulation, swallowing, respiration, speech, as well as regulating facial expression and controlling facial aperture patency. The biology of these small skeletal muscles is relatively unexplored. According to their developmental origin, they can be divided into extraocular muscles, branchiomeric muscles (facial, masticatory, pharyngeal and laryngeal muscles) and tongue muscles [1]. Their unique embryonic development and the genes that control it together with characteristic features that separate them from the skeletal muscle stereotype have started to be explored only recently [2].

Limb and trunk skeletal muscles are derived from the segmented paraxial mesoderm known as somites [2] while the origin of facial muscles is different and they do not follow the progression from mesoderm to segmented somites. The cranial mesoderm from which craniofacial muscles derive seems to be characterized more by molecular factors than for example, by anatomical ones [3], however, there is little information on the formation of facial muscles. The craniofacial muscles are highly heterogeneous as far as structure, function, anatomy and development are concerned. There are around 60 muscles in the head of vertebrates namely, those surrounding the eye - extraocular muscles (EOM) (derived from prechordal and paraxial mesoderm), those involved in mastication (derived from pharyngeal arch 1) and facial expression (derived from pharyngeal arch 2). The muscles of the 3rd pharyngeal arch (also known as branchial arch) control the larynx and pharynx. A number of head muscles (including the hypobranchial, tongue, posterior arch muscles) develop from the somites (Fig.1) [4].
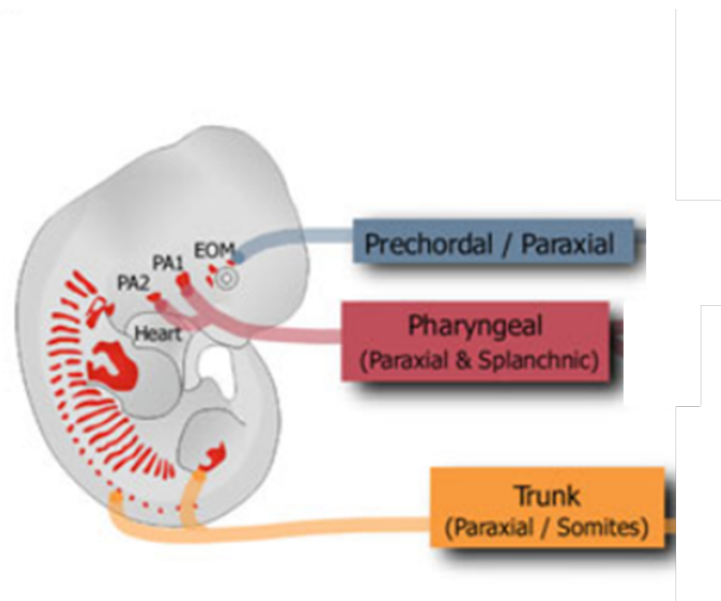
Figure 1: **Development of skeletal muscles.** Skeletal muscles and satellite cells in trunk and limb derive from somites (paraxial mesoderm). Pharyngeal arch (PA) muscles and their associated satellite cells derive from both cranial paraxial mesoderm and splanchnic mesoderm sources. Extraocular muscles derive from prechordal and paraxial mesoderm (somitomeres) [4].

1.1.1 Human extraocular muscles

Understanding the biology of skeletal muscles, does not necessarily mean understanding and knowing the physiology of extraocular muscles. They are among the fastest and most fatigue resistant muscles, but at the same time the presence of the slow, non-twitch muscles and some cardiac or embryonic skeletal muscle characteristics gives them a special place when it comes to classification [5, 6]. EOM are highly specialized muscles with six fiber types, high-frequency pattern of neuromuscular innervation as well as the singly and multiply innervated fibers which sets them in a distinctive group of muscles compared to the other skeletal muscles [7]. At early stages the development of extraocular muscles is dependent on the expression level of the transcription factor Pitx2. If the expression of Pitx2 is low, the formation of the oblique muscles does not occur, and the rectus muscles that develop are smaller. In case of Pitx2 absence the extraocular muscles do not develop at all [8, 9]. Extraocular muscles derive from prechordal and paraxial mesoderm (somitomeres) [4].

11

There are the six extraocular muscles, which act to turn or rotate an eye about its vertical, horizontal, and antero-posterior axes: superior rectus, inferior rectus, medial rectus, lateral rectus, superior oblique and inferior oblique (Fig. 2).
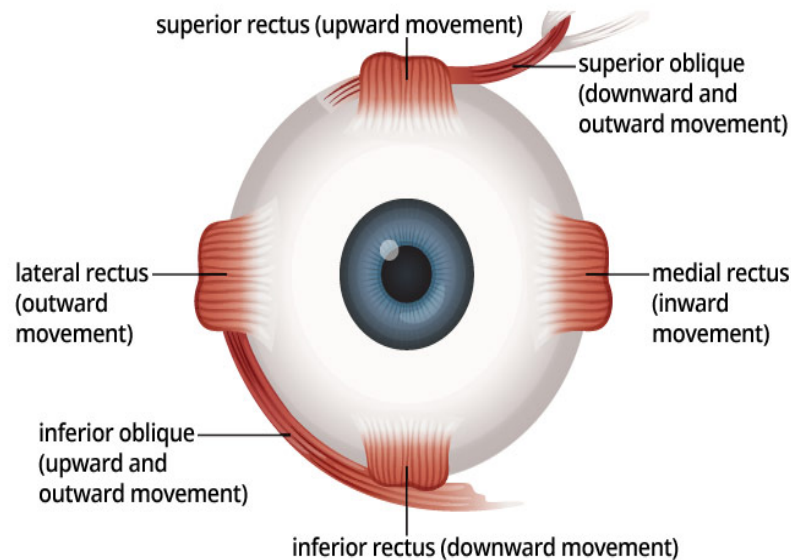
Figure 2: Human extraocular muscles.
(http://www.allaboutvision.com/conditions/strabismus-surgery.htm)

The histological structure of eye muscles differs in many aspects from that of other striated muscles. Extraocular muscles contain fibers of varying diameters and in general they are the finest fibers found in any striated muscle. They vary in diameter from 9 μm to 17 μm, with fibers as fine as 3 μm, but these muscles also contain coarse fibers up to 50 μm in width. As far as the literature goes there is no consensus as to whether each EOM fiber runs the entire length of the EOM or not. In general if each muscle would run the entire length, one would expect to find the same number of fibers in sections taken from the anterior, middle, or posterior portion of each EOM. But instead, it has been reported that the number of fibers in the central region of the muscle is higher than in proximal or distal areas [10, 11].

In extraocular muscles two layers can be distinguished: the orbital and global (Fig. 3) [12]. The orbital layer faces the orbital wall while the global layer faces the eyeball and is in part enclosed by the orbital layer. The orbital layer contains small-diameter fibers with many mitochondria and a dense vascular network. The global layer contains larger-diameter fibers with a variable content of mitochondria and fewer vessels.
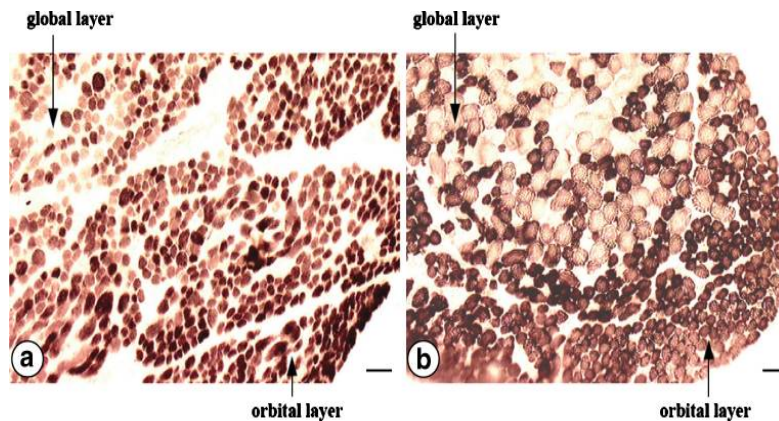
Figure 3: Cross section of (a) human and (b) rat ocular medial rectus muscle. Histochemical staining for succinate dehydrogenase (SDH) exhibits higher oxidative activity in the thinner orbital layer than in the thicker global layer. Human medial rectus muscle is much larger with a broad intermediate layer and a lot of connective tissue separating muscle fascicles. Scale bar 50μm [13].

In human EOM a third layer has been described and named marginal zone, located outside of the orbital layer, with fibers larger than the ones from the orbital layer and with a higher number of the multiply innervated fibers. It covers the whole length of the muscle except the very proximal and distal regions [10].

The EOM function could not be assigned to any particular layer. Predicting the function of any muscle without first establishing the mechanical connections between the fibers would be difficult and challenging. Elastic tissue is unusually abundant in extraocular muscles of adults and the elastic fibers are thick and arranged parallel to the muscle fibers. These longitudinal fibers are interconnected by transverse elastic fibers that form a very dense network around the muscle fibers. Recent anatomic studies have demonstrated that each rectus EOM passes through a pulley consisting of a surrounding ring or sleeve of collagen, located near the globe equator in Tenon's capsule (Fig. 4). Pulleys are connected to the orbital wall, adjacent EOMs, and

equatorial Tenon's capsule by bands containing collagen, elastin, and smooth muscles [14, 15]. Spindles are located in the peripheral layers of small diameter fibers and near their tendon. In general there are around 50 spindles in each EOM.
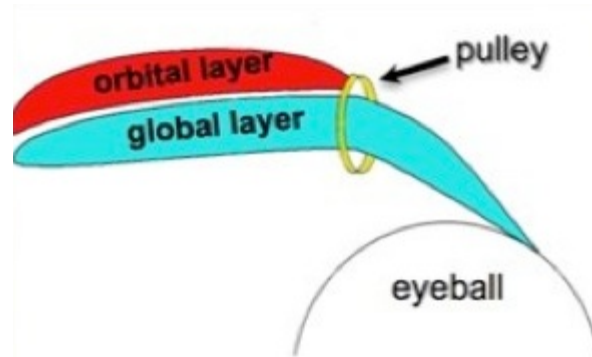
Figure 4: A pulley, that is supported by the orbital layer of the muscle guides the global layer that inserts in the globe. (http://www.efelder.de/eye_muscle_morphology.html)

Myosin Heavy Chain expression in human EOM

The highly specialized function of EOMs, that is to move the eyeball, is reflected in the specific Myosin Heavy Chain (MyHC) content and the complexity of fiber types. The MyHC expression pattern in adult EOM is different than that in adult skeletal muscle; in fact in single EOM fibers, developmental MyHC isoforms (neonatal and embryonic), are co-expressed together with adult MyHC isoforms, while normal adult skeletal muscle fibers only express adult MyHC isoforms [16-18]. The EOM specific MyHC13 isoform is also present in EOM [16] but additionally variations in MyHC isoform expression along single muscle fibers have been described [19]. Adult rabbit EOM also contain the cardiac MyHC isoforms [20].

In a study on the MyHC composition in human EOM, six isoforms were detected: MyHCemb/IIx, MyHCIIa, MyHCeom, MyHCI, and 2 unidentified forms. MyHCIIb was not detected. In the same study it was also shown that MyHC isoforms have a different pattern of expression in the human superior oblique muscle compared to the rectus muscles and inferior oblique muscles [21].

EOM fiber types

Human skeletal muscle fibers are usually divided into three major types based on their physiological, biochemical and histochemical characteristics: 1) slow twitch, fatigue resistant (type I fibers), 2) fast-twitch, fatigue resistant (type IIA fibers) and 3) fast-twitch fatigable (type IIB fibers - based on ATPase staining, IIX based on MyHC composition) [22]. EOM fiber classification can differ significantly based on the criteria taken for the fiber type characterization. The initial classification was based on the histological features and they were called "Feldenstruktur" or "Fibrilenstruktur" [23]. The slow fibers of the Felderstruktur type were described as clumped together in a more or less afibrillar appearing mass of myofilaments with large, partially fused fibers in sparse sarcoplasm with poorly developed sarcoplasmic reticulum. The Fibrillenstruktur type of the fast fiber system were characterized anatomically by small, well defined fibers, each surrounded by abundant sarcoplasm and having an even, punctate appearance when observed under the light microscope. Classification in "coarse", "granular" and "fine" came with the characterization of the amount and distribution of mitochondria [24]. This was followed by a more comprehensive description of rat EOM fiber types which included, location, diameter, innervation pattern, histochemical features and ultrastructure. Based on these criteria, six fiber types could be identified [25]. Later studies in different mammals confirmed the presence of the six different fiber types in EOM.

In human EOM fiber type classification, mitochondrial content was used to distinguish the different fiber types [26]. Studies based on ATPase staining together with the glycolytic and oxidative enzyme activity and MyHC isoform expression confirmed the higher complexity and fiber type diversity in EOM [27].

It is now generally agreed that in humans and higher mammals there are six fiber types in the EOMs and these can be classified on the basis of their location, innervation and color into: 1) orbital multiply innervated, 2) orbital singly innervated, 3) global multiply innervated, 4) global red singly innervated, 5) global intermediate singly innervated and 6) global pale singly innervated fibers [12]. None of the previously mentioned methods independently covers the full extent of differences present in EOM fibers [10].

Innervation of EOM

EOMs are innervated by lower motor neurons that form three cranial nerves: the abducens, the trochlear, and the oculomotor [28]. Compared to other skeletal muscles they are highly innervated and exist as both singly innervated fibers (SIFs) and multiply innervated fibers (MIFs), whereas trunk and limb skeletal muscles contain exclusively singly innervated fibers [29].

The motor neurons are very thick, due to the large number of fibers they contain. The ratio of nerve fibers to muscle fibers is nearly 1:12 in extraocular muscles, whereas in skeletal muscles it may be as high as 1:125. The abundance of nerve fibers has led to the conclusion that the all-or-none law could apply to eye muscles. According to this general principle, individual muscle fibers always respond with a maximum contraction to every stimulus that exceeds the threshold potential, otherwise there is no response. The amount of contraction of a muscle depends on the number of fibers taking part in a contraction [30].

Physiology of EOM

The physiological and pharmacological properties of extraocular muscles correspond to many unusual histological features. In an electromyographic study it was shown that responses of human extraocular muscles are considerably lower in amplitude (20 to 150 μV), of much shorter duration (1 and 2 ms), and much higher in frequency (up to 150 cps (contractions per second)), than those of peripheral skeletal muscles, in which the amplitude is 100 to 3000 μV, the duration, 5 to 10 ms and the frequency only up to 50 cps [30].

Extraocular muscles contract much more quickly than other voluntary muscles. As a measure of comparison, contraction times on cat muscles were: soleus muscle, 100 ms; gastrocnemius muscle, 40 ms; and medial rectus muscle, 8 ms. [31, 32]. The great speed of contraction of extraocular muscles is in keeping with the requirements of saccadic eye movements and with what is known of the structure and innervation of extraocular muscles.

Since the discovery that a dual motor system of slow and fast fibers exists in extraocular muscles, experiments have shown that acetylcholine, choline, and nicotine cause slow and tonic contraction of slow fibers, whereas fast fibers respond with a fast twitch. The response of extraocular muscles to neuromuscular blocking agents is of clinical interest, since these drugs are often used during general anesthesia [30].

1.1.2 Orbicularis oculi muscles (OO)

Orbicularis oculi (OO), together with the tarsal plate form the core of the eyelid. These are muscles important for facial expression and are innervated by the facial nerve (VII) [33]. OO are located directly under the surface of the skin around the eyes. Their function is to close the eyelid and to assist in passing and draining tears through the tear draining system. They are composed of three portions: the orbital portion, the palpebral portion and the lacrimal portion (Fig. 5). **The orbital portion** is involved in closing the eyelids firmly and is controlled by voluntary action. Coarse fibers surround the entire orbit. It has two origins: the frontal bone and the maxilla. The insertion circles around the orbit and it contracts to tightly close the eyes. **The palpebral portion** closes the eyelids gently as part of the involuntary or blinking reflex. This portion has three parts: the pretarsal, preseptal and ciliary part. It is made up of fine fibers and originates from the medial palpebral ligament and inserts into the zygomatic bone, specifically at the lateral palpebral ligament. **The lacrimal portion** compresses the lacrimal sac, which receives tears from the lacrimal ducts and transfers them into the nasolacrimal duct. Its origin is the lacrimal bone and its insertion is the lateral palpebral raphe. It has its own ciliary bundle [34].
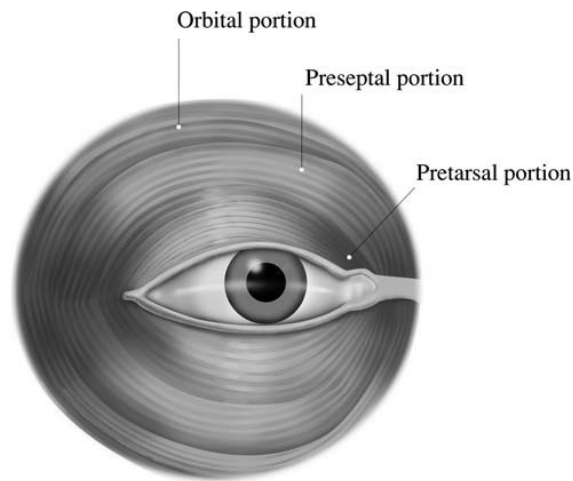
Figure 5: The three anatomical portions of human orbicularis oculi muscle [35].

The anatomy of the orbicularis oculi muscle is important in treating a number of conditions that require corrective eyelid surgery. It is also important in the physiology of blinking, corneal wetting, and lacrimal excretion through the lacrimal pump. The fibers in orbicularis oculi muscles have the smallest diameter of any skeletal muscle. There are differences in fiber cross-section and fiber type composition between different portions of the muscle. The pretarsal region has the smallest fiber cross-sectional areas and this region is composed almost entirely of type II fibers. The number of type I fibers increases when moving away from the eyelid margin towards the periphery, but the muscle in general is 80-90% composed of type II fibers [33].

The OO differ from both limb and extraocular muscles (EOM) in their histology and histochemistry. In OO there is a predominance of type IIB fibers, the fast fibers which are not able to sustain contraction for long periods of time due to fatigue and are ideally suited for blinking. Sustained squeezing of the eyelids can occur due to type IIA fibers which are fast but fatigue resistant. During sleep the OO are at rest, and the lid position is determined by the equilibrium between the state of relaxation of the levator muscles and OO [36].

The OO differ from some other facial muscles with regard to the ratio of type II muscle fiber subtypes. It was reported that type IIB fibers are present in the levator labii and OO. Type II fibers are more numerous in each of the facial muscles than in limb muscles [36].

Normal OO possess some features which, when present in limb or trunk muscles, would be considered consistent with a chronic myopathy or dystrophy. These include marked fiber size variation, rounded fiber shape, structural alterations such as lobulation and irregular coarseness of stainable sarcoplasmic network, absence of checkerboard pattern of fiber-type distribution, and an increase in endomysial and perimysial connective tissue. Although the OO do not appear to possess many of the characteristics of EOM, they are similar to them and to other facial muscles and can be placed somewhere between them with respect to histologic and histochemical parameters [36].

1.2 Excitation-contraction coupling (ECC)

1.2.1 ECC in skeletal muscle

Excitation-contraction coupling is the mechanism which involves a specific sequence of events starting from initiation and propagation of the action potential (AP) along the plasma membrane (sarcolemma), radial spreading of the potential along the transverse T-tubule system, DHPR (L-type Ca^{2+} channel)-mediated detection of changes in membrane potential, allosteric interaction of DHPR with RyR, release of Ca^{2+} from the SR and transient increase in cytoplasm Ca^{2+} concentration, transient activation of the cytoplasmic Ca^{2+} buffering system and contractile machinery, followed by a decrease of the cytoplasmic Ca^{2+} levels by the reuptake by SR through sarcoendoplasmatic reticulum Ca^{2+} transport ATPase (SERCA) and to a lesser extent by its transport by the Na^+/Ca^{2+} exchanger (NCX) and plasma membrane Ca^{2+}ATPase (PMCA) [37-39].

The release of divalent ions from the SR requires the expression of both the skeletal muscle L-type Ca^{2+} channel DHPR and the RyR1 since depolarization-induced Ca^{2+} entry is absent in myotubes lacking either the DHPR α_{1S} subunit (*dysgenic*) or RyR1 (*dyspedic*), respectively [40]. Skeletal ECC is practically exclusive for RyR1, since RyR2 and RyR3 are not able to recover the skeletal type of ECC when expressed in RyR1 deficient skeletal muscle cells [41].

T-tubules are invaginations of the plasma membrane that transversely expand into the muscle fiber allowing membrane depolarization to reach deep into the fiber to form the triad, i.e a region, where one T-tubule is surrounded by two terminal cisternae of the SR with their so called junctional regions [42, 43]. In the junctional region RyR1 face DHPR receptors located on the membrane of the T-tubule forming tetrads (Fig. 6 and 7) [44, 45].
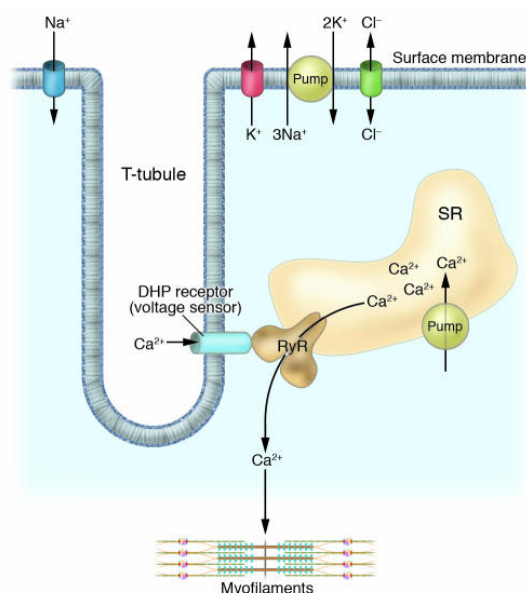
Figure 6: T-tubule DHPR and RyR localization. (https://www.premedhq.com/t-tubule-system)

Many proteins are engaged in the process of the ECC among them, calsequestrin, triadin, junctin, junctophilin, FKBP12, mitsugumin, sarcalumenin and JP45. Nevertheless RyR1s and DHPRs are considered the main players since in their absence no ECC occurs.

The DHPR is the physiological regulator of the RyR1 during ECC, but it is by no means the only regulator of RyR1 channel activity. Like RyR2 channels present in the heart, in the absence of the DHPR, RyR1 channels can be activated by cytosolic Ca^{2+} via a process called Ca^{2+} induced Ca^{2+} release (CICR). This is important because more than half of the RyR1 channels are not coupled to DHPRs [46, 47] and it is generally believed that CICR acts to amplify the signal that is generated by the DHPR-RyR1 interaction. Interestingly, the presence of "coupled" and "uncoupled" RyR1 channels indicates that RyR1 function can be heterogeneous. The amount of uncoupled RyR1 channels is not the same in all skeletal muscles. Slow-twitch skeletal

muscles may have three or more uncoupled RyR1 channels for each DHPR-linked RyR1 channel [46, 47]. Slow-twitch muscles have a slower rate of ECC and the number of uncoupled RyR1 may be partially responsible for this and in line with the fact that they have a more pronounced CICR [48, 49].
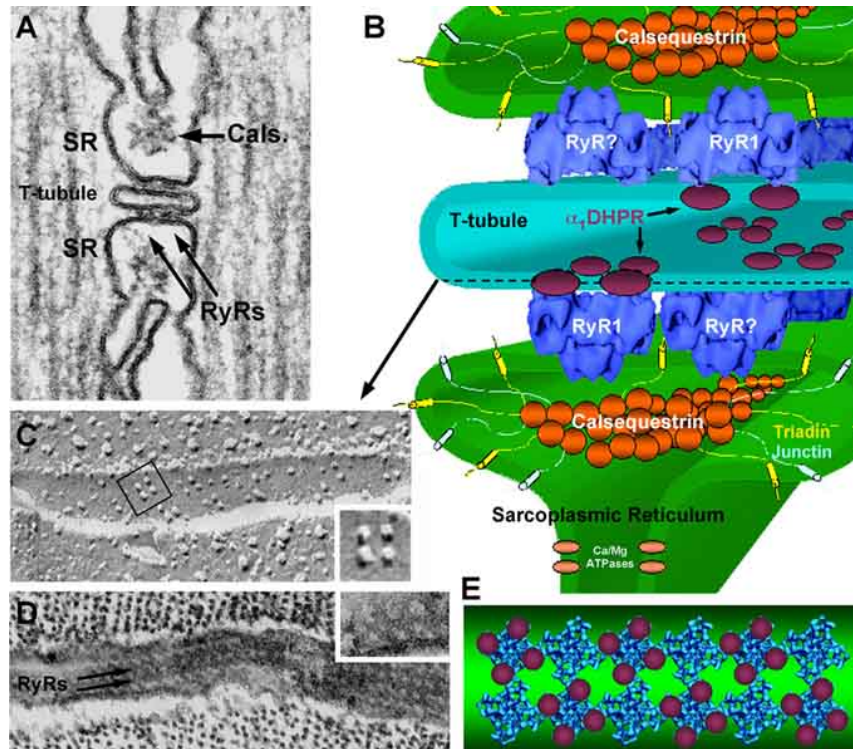
Figure 7: Structure of Calcium Release Units in adult skeletal muscle fibers. In adult skeletal muscle, junctions are mostly triads: two SR elements coupled to a central T-tubule. **(A)** A triad from the toadfish swim bladder muscle in thin section EM: the cytoplasmic domains of RyRs, or feet, and calsequestrin are well visible. **(B)** A tri-dimensional reconstruction of a skeletal muscle triad showing the ultrastructural localization of RyRs, DHPRs, Calsequestrin, Triadin, Junctin, and Ca^{2+}/Mg^{2+} ATPases. The DHPRs are intramembrane proteins that are not visible in thin section EM but can be visualized by freeze fracture replicas of T tubules (panel C). **(C)** DHPRs in skeletal muscle DHPRs form tetrads, group of four receptors (see enlarged detail), that are linked to subunit of alternate RyRs (smodels in B and E). **(D)** In sections parallel to the junctional plane, feet arrays are clearly visible (toadfish swimbladder muscle): feet touch each other close to the corner of the molecule (see enlarged detail). **(E)** Model that summarizes finding of panels C and D: RyRs form two (rarely three) rows and DHPRs form tetrads that are associated with alternate RyRs (RyRs in blue; DHPRs in purple; T-tubule in green). (EM courtesy of Clara Franzini-Armstrong; 3D reconstruction of RyRs courtesy of T. Wagenknecht) [50].

1.2.2 ECC in cardiac muscle

In cardiac muscle, ECC is dependent on a phenomenon called calcium-induced calcium release (CICR). Calcium induced calcium release is, as its name indicates, a process whereby an increase in Ca^{2+} concentration at the cytoplasmic surface of the intracellular Ca^{2+} store induces a release of Ca^{2+}. This process involves the conduction of calcium ions into the cell initiating further release of ions into the cytoplasm. This influx of Ca^{2+} occurs through the cardiac isoform of the alfa 1 subunit of the DHPR [51] and is initiated by an action potential which triggers the Ca^{2+} release from the SR which leads to cardiac contraction. The initial trigger is generated by depolarization of the plasma membrane, which allows Ca^{2+} entry through the L-type Ca^{2+} channels located on the transverse T-tubules. This influx of Ca^{2+} initiates a large intracellular Ca^{2+} release from the SR via RyR2s, which elevates cytosolic Ca^{2+} concentrations from 100 nM during diastole to about 1 μM during systole, and this Ca^{2+} elevation activates cardiac contraction.

There is about one DHPR for every 5 to 10 RyR2 channels in heart muscle and there is no finely defined alignment between these two proteins, as is the case in skeletal muscles (Fig. 8) [50, 52]. Long cardiac action potentials of about ~100ms give enough time for the DHPR to open and facilitate the influx of Ca^{2+} which will result in activation of the underlying RyR2 channels through the previously mentioned CICR mechanism. The fact that Ca^{2+} is the mediator of ECC in the heart makes signal transduction between cardiac DHPR and RyR2 much slower compared to that occurring between the skeletal isoforms of these proteins. This however, leaves more space for a higher level of regulation of DHPR-RyR2 interaction in cardiac muscle. [53, 54].

Procaine and tetracaine inhibit CICR and are used for investigating the physiology of this process. Ruthenium and high concentrations of ryanodine are inhibitors of RyR channels and also block CICR. In mature skeletal muscles CICR doesn`t play a primary role so its exact role remains elusive.
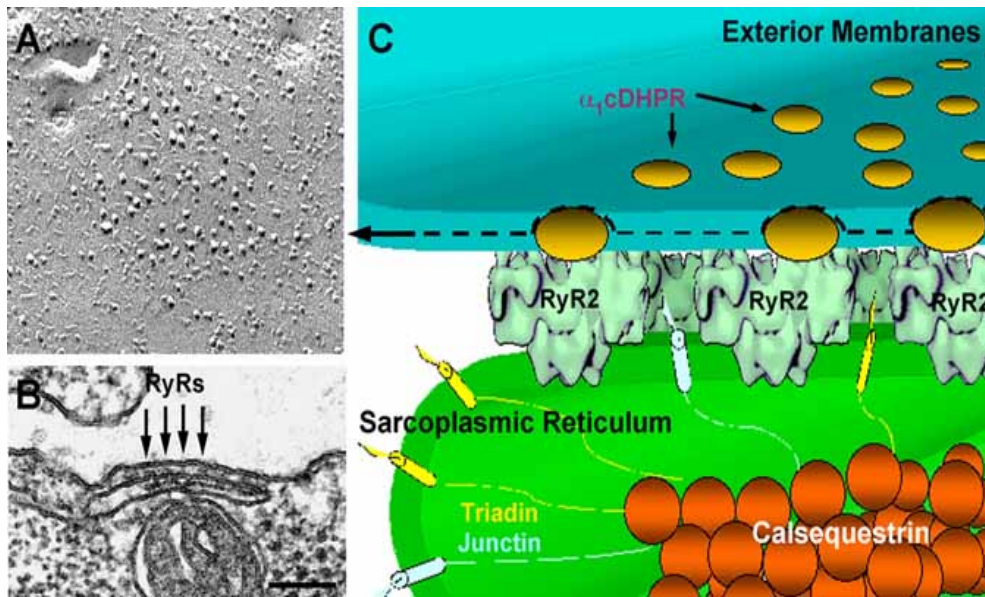
Figure 8: Structure of calcium release units in cardiac myocytes. Junctions in cardiac muscle cells are usually in the form of dyads or peripheral coupling formed by SR and either a T-tubule or the sarcolemma. **(A)** DHPRs in cardiac junctions do not form tetrads, but they are randomly arranged in exterior membrane domains that face arrays of feet. This observation implicates that DHPRs are not directly linked to RyRs in the heart. **(B)** RyRs, pointed by the arrow, usually form large clusters instead of the two rows described for skeletal muscle junctions. **(C)** Tri-dimensional reconstruction of a cardiac muscle dyad/peripheral coupling showing the ultrastructural localization of RyRs, DHPRs, Calsequestrin, Triadin, and Junctin. Bar, 0.1 mm (3D reconstruction of RyRs courtesy of T. Wagenknecht) [50].

1.2.3 Components of ECC

Ryanodine receptors (RyRs)

As mentioned in the previous sections, Ca^{2+} is an essential component for the process of excitation-contraction coupling. The biggest store of Ca^{2+} in striated muscles is the sarcoplasmic reticulum (SR). The major channels located on the membrane of the SR which are responsible for Ca^{2+} release are ryanodine receptors (RyRs) while inositol 1,4,5-triphosphate receptors (IP$_3$Rs) for Ca^{2+} channels are located on the endoplasmic reticulum and are not involved in ECC [55, 56]. There are three isoforms of RyR receptors in vertebrates (RyR1, RyR2 and RyR3) which are encoded by three different genes and which vary in their tissue distribution. RyR1 is predominantly expressed in skeletal muscle and to a minor extent in some areas of the CNS and in some immune cells; RyR2 is present in the heart and in the cerebellum and RyR3 was first identified in the brain, but later identified in developing tissues, including developing skeletal muscle [57, 58]. The three isoforms share 65% sequence identity, the biggest difference being detected in areas called "divergent regions"; D1 (from residue 4254-4631 in RyR1), D2 (from residue 1342-1403) and D3 (from residue 1872-1923) [58]. The name of the receptor comes from the alkaloid ryanodine isolated from the South American plant *Ryania speciosa*, which in nanomolar concentractions locks the channel in a subconductance state and in concentrations above 100μM induces inhibition of Ca^{2+} release [59-62].

Channel activity is modulated in a direct or indirect manner by dyhydropiridine receptors (DHPR) and a number of other proteins including protein kinase A, FKBP12 and FKBP12.6, calmodulin, S100, Ca^{2+}/calmodulin dependent protein kinase II (CaMKII), calsequestrin (CSQ), triadin, junction, as well as by ions like Ca^{2+}, Mg^{2+} [63-77].

RyR1

RyR1 is the biggest known ion channel with a homotetrameric structure, each subunit has an apparent molecular mass of ~565 kDa, and is made up of 5038 amino acids in human isoform ASI (-) and 5033 amino acids in isoform ASI (+). *RYR1* was originally cloned and sequenced from skeletal muscle by Takeshima et al. and Zorzato et al. [78, 79]. The gene encoding human *RyR1* is located on chromosome 19q13.2. The C terminal region contains the transmembrane domains and ion conducting pore, while the major part of the protein is the N-terminal cytoplasmic region which contains the domain interacting with the DHPR as well as domains involved in channel modulation [80].

Skeletal muscle is the tissue which is most enriched in RyR1 where it is located in the junctional region of the terminal SR [78, 79, 81] but other tissues including smooth muscle cells, stomach, kidney, thymus, Purkinje cells, adrenal glands, ovaries, and testis, dendritic cells and B-lymphocytes also express this protein but in lower amounts [78, 82-88].

The crystal structure of RyR is not yet fully resolved, but there are several cryo-EM studies which agree on the overall structure of the receptor (Fig. 9) [89-92]. The general structure can be presented as mushroom-like, with a big cap containing about 80% of the total volume located in the cytoplasmic region, facing the transverse tubules and the stalk which goes through the membrane into the SR lumen. The cytoplasmic region is about $270 \times 270 \times 100$Å and the trans-membrane region is $120 \times 120 \times 60$Å. The cytoplasmic cap is structured, contains many cavities and globular masses which may correspond to individual or groups of folded domains. The globular regions were numbered and are often called "subregions" [93, 94]. Most cryo-EM investigations have been preformed on RyR1, there are several on RyR2 and RyR3 but to a lower resolution. In general, the overall structural shape is similar for all three isoforms [95, 96].
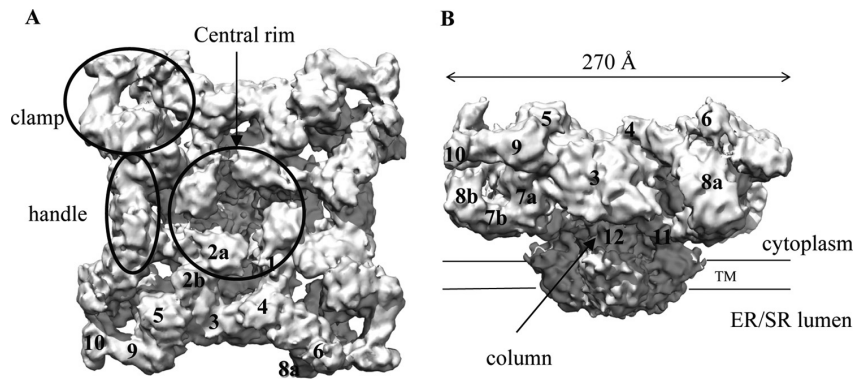
Figure 9: Cryo-EM structures of RyR. Shown are isocontour maps for cryo-EM reconstructions of RyR at 9.6Å (EMDB accession number 1275) [97] . **(A)** and **(B)** top (from the cytosol facing the ER/SR membrane) and side views of the RyR. The numbers indicate subregions, a nomenclature that has been used extensively in literature.

The number of the transmembrane helices is still under investigation, but the general consensus is that there are six or eight segments per subunit [98]. The inner helices create the pore-forming region. The purified protein can form a planar crystalline strucutre with a checkerboard pattern in the absence of any other protein [99]. Subregion 6 in the clamp region is responsible for the inter-protein interactions while the clamp region undergoes significant movement during opening and closing of the channel which can be also transmitted to the neighboring RyRs [89, 100]. This feature could be partly responsible for the phenomenon of coupled gating, where opening of one channel can induce opening of the neighboring channels through physical interactions [101].

Lack of *RYR1* in mice results in a lethal phenotype; knockout mice most likely die at birth because of breathing impairment, but they also exhibit skeletal abnormalities such as spinal curvature, arched vertebral column, thin limbs and a thick neck [102].

26

RyR2

RyR2 was first identified in cardiac muscle [84]. In humans, the gene encoding *RYR2* is located on chromosome 1q43 and spans 102 exons, *RYR2* is also expressed at high levels in Purkinje cells of the cerebellum and cerebral cortex [103] and to lower levels in the stomach, smooth muscle cells, adrenal glands, ovaries, thymus and lungs [104] [83].

RyR2 is the major SR Ca^{2+} release channel involved in cardiac excitation–contraction coupling, the process by which an electric depolarizing impulse is transduced into a cardiac contraction. The amount of released Ca^{2+} from the SR via RyR2 in great deal determines the Ca^{2+} transient amplitude, which correlates with the strength of systolic contraction [105]. The RyR2 channel consists of 4 pore-forming subunits that interact with numerous accessory proteins such as FKBP12.6, calmodulin, calsequestrin-2, junctin, triadin, and junctophilin-2. Each of these accessory proteins can regulate channel gating [106]. RyR2 is regulated at the post-translational level by S-nitrosylation, oxidation, and protein phosphorylation [107].

Mutations in *RYR2* are associated with catecholaminergic polymorphic ventricular tachycardia (CPVT) and arrhythmogenic right ventricular dysplasia type 2 (ARVD2) [108, 109].

RyR3

In humans, the *RYR3* gene is encoded by 103 exons and is located on chromosome 15q13.3-14. RyR*3* is expressed in hippocampal neurons, thalamus, Purkinje cells, corpus striatum, skeletal muscles with the highest expression in the diaphragm, smooth muscle cells of the coronary vasculature, lung, kidney, ileum, jejunum, spleen, stomach of mouse and aorta, uterus, ureter, urinary bladder, and esophagus of rabbit [58]. RyR3 is usually not the predominant RyR protein and it is often co-expressed with RyR1 or RyR2 in different tissues. In adult diaphragm muscle, RyR3 constitutes 1–4% of the total [^{3}H]ryanodine binding sites and the rest is due to RyR1 [110].

In mice, the RyR3 protein can be detected in skeletal muscles from the 18th day of the embryonic stage up to 15 days postnatal. Later, during development the levels decrease and almost completely disappear [111]. In *RYR3* KO mice, the isolated neonatal skeletal muscles show decreased tension development after stimulation with caffeine and contractile force after electrical stimulation. ECC is relatively normal in these mice compared to WT. Based on the available data, it seems that RyR3 have a role in both development and contraction of neonatal muscles [112], however, very little is known about its function. In fact, mice lacking RyR1 and RyR2 die early either at birth or during embryonic development [113, 114], while mice lacking RyR3 live normal lives and show no significant changes in muscle function or reproduction. [112, 115]. In toadfish and frog skeletal muscles, RyR3 is localized on the parajunctional membranes, immediately adjacent to the junctional region from [116].

There are strong suggestions that the activation of RyR3 is indirect, since it is not activated by DHPR. It can be assumed that activation of RyR1 by the DHPR occurs first and then activation of RyR3 occurs by CICR which then contributes to the amplification of ECC induced Ca^{2+} release. Since parajunctional RyR do not seem to be in close proximity to junctional RyR, then one can exclude the functional interaction of parajunctional RyR3 and junctional RyR1. The most likely possibility is that RyR3 is activated by the Ca^{2+} wave coming from the activated RyR1.

Regulators of RyR:

Ca^{2+} release via the RyR1 is finely controlled by number of proteins, small molecules and post-translational modifications that influence opening or closing of the channel (Fig. 10).

      (i)   **FK506-binding proteins (FKBPs)** 12 and 12.6 interact with all three RyR isoforms, more specifically FKPB12 co-purifies with RyR1 and FKBP12.6 with RyR2. FKBP12 is involved in stabilization of the closed state of the channels and prevents the occurrence of subconductance states [117]. Cryo-EM studies have shown that FKBPs bind to a site near subdomains 3, 5 and 9 [118, 119].

      (ii)   **Calmodulin (CaM)** is a 17kDa protein that binds to the cytoplasmic domain of the ryanodine receptor and affects its activity in a different manner depending on whether Ca^{2+} is bound or not. When it is in Ca^{2+} -free state or ApoCaM, it acts as a partial agonist, activating RyR1 and inhibiting RyR2, while at high Ca^{2+} concentrations in the Ca^{2+} -bound form known as CaCaM, it acts as an inhibitor of both RyR1 and RyR2 [73, 120]. ApoCaM and CaCaM bind to different RyR1 domains, but some regions contained within residues 3614-3643 and 2937-3225 can act as binding sites for both states of calmodulin [121, 122]. Cryo-EM studies have identified the binding domains of apo-CaM and Ca^{2+}/CaM on RyR1 [123]. According to this study the position of CaM on the 3D structure changes after Ca^{2+} binding.

      (iii)   **Calsequestrin** is Ca^{2+} buffering protein located in the lumen of the SR. Depending on the intraluminal Ca^{2+} levels, it can form oligomers and interact with junctin and triadin. It is believed that the calsequestrin-triadin-junctin complex can affect RyR activity, although the precise mechanism of action to achieve this effect has not been unraveled [124]. See the subsequent section for more information on calsequestrin.

      (iv)   **Phospohorylation:** Kinases such as PKA and CaMKII, as well as phosphatases such as PP1, PP2A and PDE4D3 target RyRs. Some of these enzymes are docked onto the RyRs through scaffolding proteins [125]. At least two residues in human RyRs are phosphorylated by PKA, namely Ser2843 in RyR1 and Ser2030, Ser2808 in RyR2.

(v) **CaMKII** is regulated by intracellular Ca^{2+} concentrations via CaM. It can phosphorylate Ser2843 in RyR1 and Ser2808 in RyR2 but also seems to have a unique phosphorylation site in RyR2 (Ser2814). CaMKII was found to increase the open probability and Ca^{2+} sensitivity of the channel and has also been shown to contribute to cardiac arrhythmia and contractile dysfunction [126].
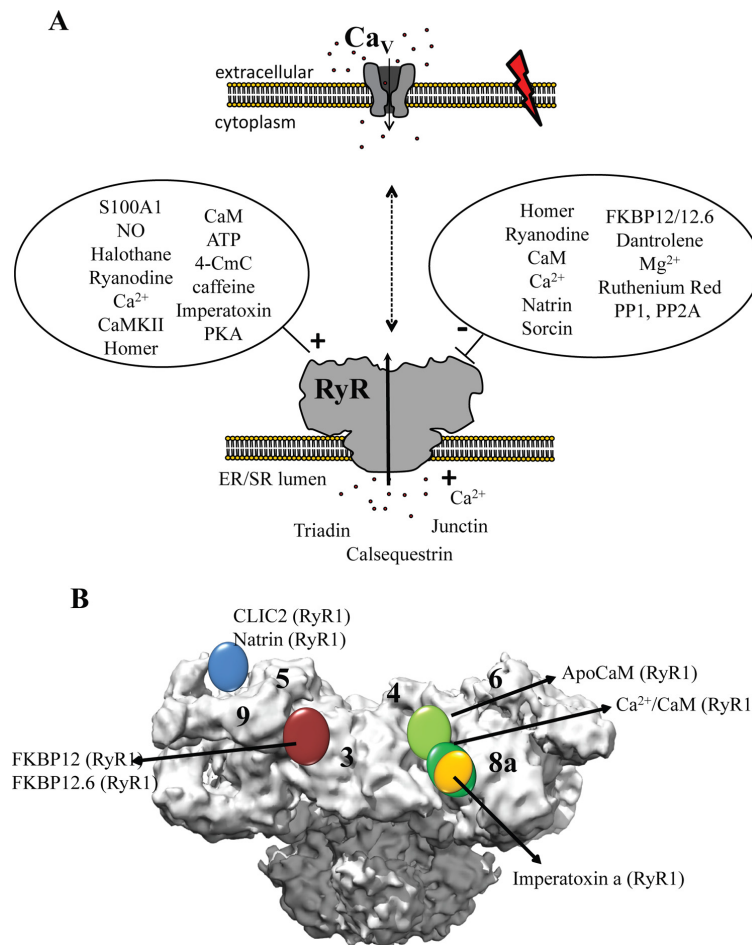
Figure 10: Binding partners and ligands of RyR. **(A)** Schematic overview of the RyR and voltage-gated calcium channel (Ca_v), present in two different membranes, along with several binding partners in the cytoplasmic and luminal areas. 4-CmC, 4-chloro-m-cresol. **(B)** Locations of several protein-binding partners based on difference cryo-EM [127].

DHPR skeletal (Ca$_v$1.1) and cardiac (Ca$_v$1.2) isoforms

Ca$_v$1.1 and Ca$_v$1.2 are the voltage gated calcium channels and together with the voltage-gated potassium and sodium channels, are members of the gene superfamily of transmembrane ion channel proteins. The α1 subunit having an approximate molecular mass of 190-250 KDa is the biggest subunit and acts as the voltage sensor and gate. The α1 subunit is organized in four homologous domains (I-IV) (Fig. 11) with six transmembrane segments in each domain (S1-S6). Channel regulation by second messengers, drugs and toxins occurs through known sites within the alpha 1 subunit. The S4 segment is responsible for voltage sensing, while the pore loop between S5 and S6 in each domain determines ion selectivity and conductance.
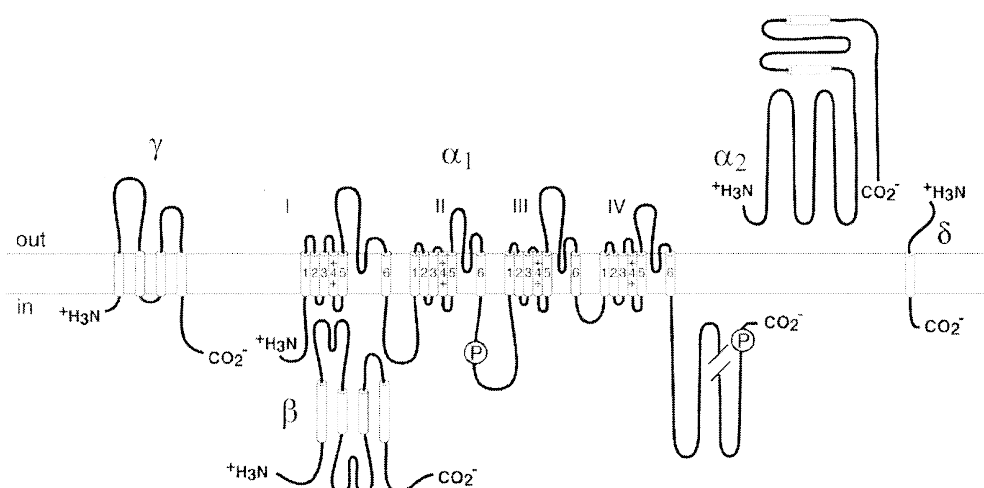
Figure 11: Illustrated model of Cav1.1 subunit composition of channels isolated from skeletal muscle. Model fits to the current available data for Ca$_v$2 channels as well.

The Ca$_v$1 subfamily (Ca$_v$1.1 to Ca$_v$1.4) includes channels with α_{1S}, α_{1C}, α_{1D} and α_{1F} which mediate L-type Ca^{2+} currents. The genes encoding the different α$_1$ subunits are not clustered on a single chromosome even for the close members of the family (Fig. 12) [128].
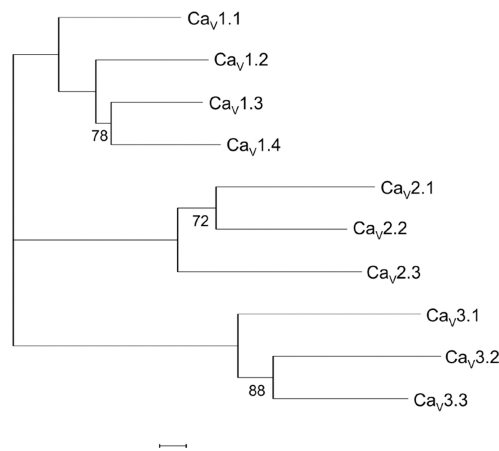
Figure 12: Ca$_v$α$_1$ subunit gene tree. Full-length amino acid sequences for all 10 human Ca$_v$α$_1$ genes were aligned using a branch and bound tree search with maximum parsimony (Genetic Computer Group, paupsearch and paupdisplay programs). Confidence values for each node were determined by bootstrap analysis. All unlabeled nodes represent 100% confidence [129].

It was shown that the cytoplasmic II-II loop of the skeletal DHPR α$_1$ subunit is necessary for the functional DHPR-RyR1 interaction (Fig. 13). Other regions may play a role in the interaction but this area seems to be essential. The nature of the DHPR-RyR interaction is tissue specific, in skeletal muscle the physical interaction occurs through direct contact of the two proteins, while in cardiac muscle DHPR acts as a mediator of a small influx of Ca^{2+} which leads to the RyR2 channel activation [39].
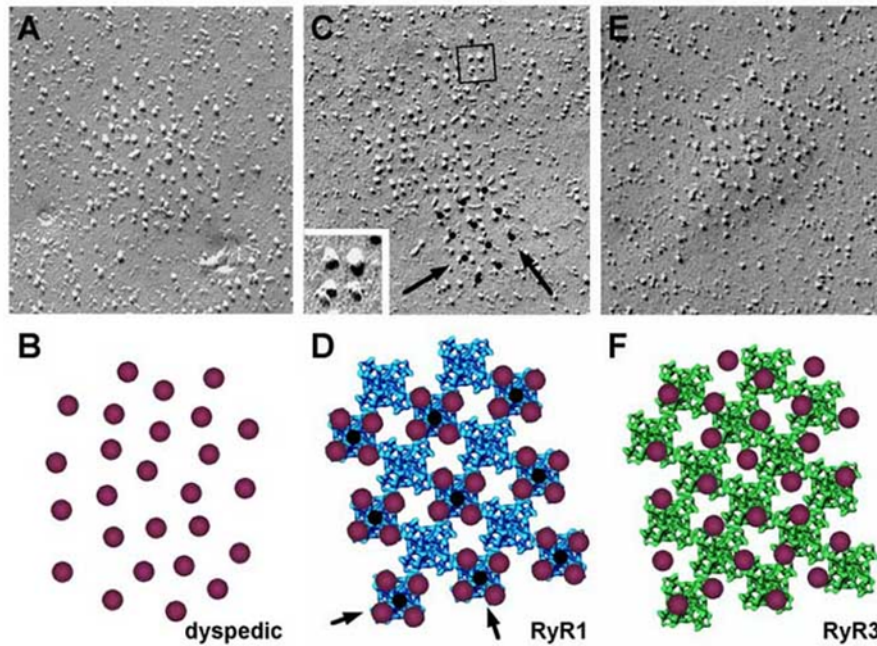
Figure 13: Interaction of RyR1 and RyR3 with skeletal DHPRs. (A) and **(B)** In dyspedic 1B5 cells (RyR1 -/-), DHPRs are clustered in correspondence of CRUs, but they are not grouped in tetrads as in normal skeletal muscle cells because of lack of RyR type 1 in the SR junctional domains. **(C)** and **(D)** DHPR tetrad arrangement is restored by transfection with cDNA encoding for RyR1. Dotting the center of tetrads in the array (C, bottom) results in an ordered pattern that is related to the arrays of feet in the SR. **(E)** and **(F)** RyR3 expression does not restore DHPR tetrad arrays suggesting that RyR3 in skeletal muscle cells does not interact directly with DHPRs as RyR1 does. Bar, 0.1 μm (3D reconstruction of RyRs courtesy of T. Wagenknecht) [50].

The $Ca_V1.2$ gene (α_{1C}) is expressed in a variety of cells including ventricular cardiac muscle, smooth muscle, pancreatic cells, fibroblasts, and neurons his channel opens as the membrane potential depolarizes beyond about −30 mV. $Ca_V1.2$ channels help define the shape of the action potential in cardiac and smooth muscle. These channels function primarily as calcium ion channels and, unlike $Ca_V1.1$ of skeletal muscle, calcium flow through $Ca_V1.2$ is an essential step in initiating the signaling cascade that leads to cardiac and smooth muscle contraction [39].

Sarcoendoplasmic reticulum Ca^{2+}-ATPase SERCA

SERCAs are members of the P-type ATPases; they are a made up of a single polypeptide of 110KDa and can be found in the ER and SR membrane. This group of ATPases is characterized by the transfer of the terminal phosphate from ATP to an aspartate residue in the catalytic domain inducing a reversible conformational change. SERCA uses the energy obtained from ATP hydrolysis to transport Ca^{2+} across the ER/SR membrane. For every hydrolyzed ATP molecule, two Ca^{2+} ions are transported. The activity of SERCA pumps is regulated by phospholamban and sarcolipin in a tissue specific manner.

There are three genes encoding SERCA 1, 2 and 3. SERCA1 is found in fast-twitch skeletal muscle and has two isoforms SERCA1a adult and SERCA1b fetal. SERCA2a is found mostly in cardiac and slow-twitch skeletal muscles, while SERCA2b is expressed to low extent in all tissues. Recently a new isoform has been reported in cardiac muscle named SERCA2c. SERCA3 isoforms are found in non-muscle tissues mainly in hematopoietic cell lineages, platelets, epithelial cells, fibroblasts and endothelial cells. Low levels of this isoform have been detected in muscle tissue as well. The primary structure of SERCA isoforms is highly conserved. Thapsigargin inhibits all SERCA isoforms, and shows no effect on Na^{+}/K^{+} or other ATPases [130].

Sarcalumenin

In the longitudinal section of skeletal and cardiac sarcoplasmic reticulum two alternative splice products of the same gene known as 160 kDa sarcalumenin and 53 kDa glycoprotein are present at low levels. Sarcalumenins are high capacity low affinity Ca^{2+} binding proteins while the 53 kDa glycoprotein does not bind Ca^{2+} as it lacks the NH$_2$ terminus [131]. Sarcalumenin knockout (SARKO) mice exhibit mild cardiac dysfunction and show reduced SERCA activity and SERCA protein content [132], however sarcalumenin deficiency leads to progressive heart failure in response to pressure overload [133].

Triadin

The single triadin gene *TRDN* gives rise to different isoforms formed by alternative splicing. In rat skeletal muscle three isoforms of triadin have been found, namely Trisk 95, Trisk 51 and Trisk 32. Trisk 95 and Trisk 51 are expressed only in skeletal muscle where they localize to the triads and in association with RyR1 and CSQ1. Trisk 32 is the main cardiac isoform found in skeletal muscle it is expressed at low levels in the whole SR [134]. Triadin KO mice show cardiac and skeletal muscle impairments, with moderate muscle weakness and reduction in the amplitude of the Ca^{2+} transient. Isoproterenol induced arrhythmias were observed at the level of cardiac muscle [134].

Junctin

Junctin was first identified as a 26-kDa calsequestrin-binding protein in cardiac and skeletal muscle junctional SR membranes. It was originally proposed that junctin is responsible for anchoring calsequestrin to the SR membrane in proximity to the ryanodine receptor and indeed it was later shown that junctin binds to both calsequestrin and the ryanodine receptor as well as triadin. Results from our laboratoy provide strong support for a model in which a quaternary protein complex exists between junctin, triadin, calsequestrin, and the ryanodine receptor at the junctional SR membrane. This complex may be important for operation of Ca^{2+} release during excitation-contraction coupling in cardiac and skeletal muscle [135]. The close structural similarities between junctin and triadin suggest that both proteins have related functions.

Mitsugumin 29

According to its name mitsugumin29 is a 29kDa protein found in SR/ER membrane. It is localized in the triad junction of the skeletal muscle. It shares close to 45% homology with synaptophysin, a family of proteins with a role in secretion and release of the neurotransmitters. Mice lacking Mg29 showed reduced contractile force, altered structure of the triadic junction and are prone to fatigue indicating that this protein has a role in ECC [131, 136].

Junctophilin-1

There are at least three junctophillin isoforms encoded by distinct genes: junctophillin-1 is expressed in skeletal muscle, while junctophillin-2 and -3 are expressed in heart and brain. Junctophillin-1 a 72 kDa protein whose function is to physically link the T-tubules with the SR membrane via a probable phospholipid mediated interaction. KO mice for this gene die within 20h after birth [131].

JP-45

This protein is a 45 kDa transmembrane protein found in the skeletal muscle junctional face membrane, with highest expression levels during the second postnatal month. It was originally identified as a protein which is weakly phosphorylated by cAMP-dependent protein kinase and co-elutes with the DHPR from a heparin-agarose column [137]. Co-immunoprecipitation experiments showed that JP-45 is not part of the RyR1 macromolecular complex but rather it interacts with calsequestrin via its luminal carboxy-terminal domain and with $Ca_v1.1$, through its cytoplasmic amino terminus. Skeletal muscles of young JP-45 KO mice exhibit characteristics of muscles from aged mice such as decreased levels of $Ca_v1.1$ content/density in the SR membrane [138].

Parvalbumin

Parvalbumin is a high-affinity calcium-binding protein found in a limited number of vertebrate tissues, including skeletal muscle and specific nerve cells. The highest levels of parvalbumin are found in the fast-contracting and fast-relaxing skeletal muscles, while in slow-twitch skeletal muscles, cardiac and smooth muscles, little or no parvalbumin is expressed. Parvalbumin contains two high-affinity Ca^{2+}-binding sites that are occupied by Mg^{2+} under resting conditions. Upon cell activation, $[Ca^{2+}]_i$ rises to micromolar levels, and Mg^{2+} ions are replaced by calcium ions. The Ca^{2+} association rate of parvalbumin is slower than the rate of Ca^{2+} binding to troponin C. For that reason, Ca^{2+} binds preferentially to troponin C during muscle activation, and the parvalbumin-buffering activity is delayed. On the basis of these observations, parvalbumin is expected to promote the relaxation of fast-contracting skeletal muscles [139].

1.2.4 Ryanodine receptor related neuromuscular disorders

Mutations in both receptors *RYR1* and *RYR2* have been linked to a number of genetic diseases [140, 141]. So far there is no described disease phenotype associated with mutations in *RYR3*.

Most of the mutations in *RYR1* and *RYR2* are found at domain-domain boundaries, either in between the three domains or at interfaces with neighboring RyR domains. This indicates that some domain interactions may be disrupted during channel opening and that mutations facilitate the opening of the channel by weakening these contacts. Most of the mutations are at interfaces with other N-terminal hot spot domains, either within or across subunits. The zipper hypothesis, involving interactions with the central hot spot region, can apply to only less than one-third of the N-terminal mutations [127]

In the section below I will only discuss disorders relating to mutations in *RYR1*, where both dominant and recessive mutations have been identified and are associated with several muscle disorders, including Malignant hyperthermia (MH), central core disease (CCD), multi-minicore disease (MmD), Centronuclear myopathy (CNM), core-rod myopathy and congenital fiber type disproportion (CFTD) [142-144].

Malignant Hyperthermia

Malignant hyperthermia (MH) is a pharmacogenetic disorder induced by volatile anesthetics or depolarizing muscle agents, characterized by muscle rigidity, rhabdomyolysis, tachycardia, metabolic acidosis and a fatal rise in body temperature [80, 145, 146]. It is typically triggered by the combination of a *RYR1* mutation and an external compound such as a volatile anesthetic or the muscle relaxant succinylcholine. In some cases, stress may serve as an alternative external trigger [147] . In general, most MH susceptible individuals have unaffected muscle function as long as they are not exposed to triggering agents. Patients with congenital myopathies with mutations in *RYR1* receptors can be at risk of an MH reaction during general anesthesia.

During an MH event, an excessive leak of Ca^{2+} from the SR results in a hypermetabolic state, depleting the ATP pool and leading to acidosis. Dantrolene is a clinically approved drug to treat MH and acts by decreasing the SR Ca^{2+} release [148]. According to several studies there is a direct interaction between dantrolene and RyR1 [149]. Dantrolene inhibits RyR1 Ca^{2+} release from HEK 293 cells transfected with *RYR1* cDNA and appears to inhibit store overload-induced calcium release (SOICR) [150]. On the other hand, the single-channel behavior of RyR1 incorporated in planar lipid bilayers appears to be unaffected by dantrolene.

Central core disease (CCD)

Central core disease is a dominantly inherited neuromuscular disorder characterized histologically by centrally located areas of reduced oxidative activity and spanning the entire longitudinal axis of the muscle fiber and with clinical features of congenital myopathy (Fig. 14) [151].
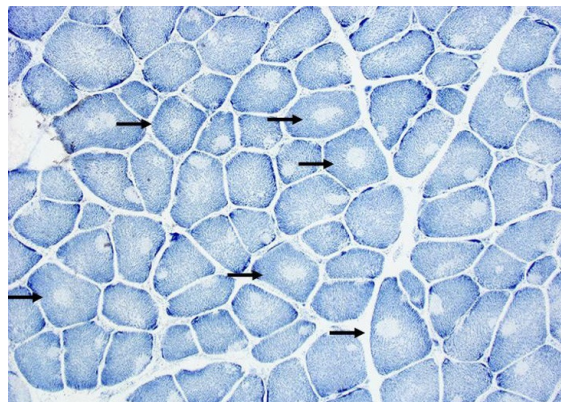
Figure 14: Histopathologic appearance of typical central core disease. NADH-TR, transverse section from the rectus femoris. Marked predominance of dark staining, high oxidative type 1 fibres with cores affecting the majority of fibres. Cores are typically well demarcated and centrally located (→), but may occasionally be multiple and of eccentric location [151].

The symptoms include hypotonia appearing in infancy or in early childhood with a delay in motor development. Stiffness and weakness of the muscles are a feature of CCD and distribution of the weakness is usually proximal with the involvement of the hip girdle and axial muscles; in rare cases facial wasting is present as well. As part of the weak facial involvement, inability to bury eyelashes fully appears, while the extraocular muscle involvement was proposed to be an exclusive indicator for the presence of the recessive *RYR1* mutations [151]. Cardiomyopathies in general are not associated with CCD. Scoliosis, congenital dislocation of the hips, foot deformities are also part of the phenotype of this disorder. So far, there has been no association between the number of cores in muscle biopsy and the severity of the muscle weakness. Many patients with CCD are positive for the malignant hyperthermia susceptibility (MHS) in vitro contracture test (IVCT) and should be considered at risk for malignant hyperthermia during general anesthesia [151].

Around 40 different missense mutations and small deletions in the human *RYR1* gene have been associated with CCD [152]. There are three regions of the RyR1 protein where MH and CCD causing mutations were identified. The first domain is from residue 1-614, the second from 2101-2458 and the third from 3916-4973 [153]. According to recent studies patients with CCD predominantly have point mutations and in-frame deletions in the C-terminal region of the *RYR1* [154] [155].

The functional effects of *RYR1* mutations associated with CCD have been primarily investigated by expressing the mutated RYR1 channel in myotubes derived from *RYR1*-KO mice, in primary myotube cultures and lymphoblastoid cell lines derived from patients. According to these studies, there are two mechanisms by which missense mutations affect Ca^{2+} release during ECC. The first mechanism is by enhancing Ca^{2+} leak from the SR into the cytosol leading to depleted SR stores [156] [157]. The second mechanism is the "uncoupling model" where the mutations affect the capacity of channels to transport Ca^{2+} from the SR following depolarization or direct ligand activation [156]. It seems that RYR1 mutations linked to CCD located in the first and second domain are associated with Ca^{2+} leak from the SR, while mutations in the third domain are responsible for EC uncoupling, though this might not be exclusive, as some leak-inducing mutations have been identified in the third domain as well [152].

Multi-minicore disease (MmD)

Multi-minicore Disease (MmD) is an inherited neuromuscular disorder which is characterized by the presence of multiple areas with reduced oxidative activity (called minicores) running along a limited area of the longitudinal axis of the muscle fiber.Symptoms of MmD appear in infancy or in early childhood and the most prominent ones are hypotonia with delayed motor development. Other symptoms associated with the presence of minicores include spinal rigidity, scoliosis and respiratory impairment. These are usually indicators of a classical MmD phenotype. Since it appears in life, feeding problems can be present and slow the rate of growth and weight gain. Axial muscle weakness in the neck and trunk area are common and indicative of MmD.

Clinical characteristics:

Multiminicore disease (MmD) is broadly classified into four groups:

- Classic form (75% of individuals)
- Moderate form, with hand involvement (<10%)
- Antenatal form, with arthrogryposis multiplex congenita (<10%)
- Ophthalmoplegic form (<10%)

In general, the diagnosis of MmD is based on the presence of multiple "minicores" visible on muscle biopsy using oxidative stains, identification of static or slowly progressive weakness, and absence of findings diagnostic of other neuromuscular disorders. 50% of MmD patients have causative mutations in *SEPN1* and *RYR1* (Fig. 15).

The severe, classic form of multiminicore disease is usually caused by mutations in the *SEPN1* gene. This gene encodes a protein called selenoprotein N. Although its function is unknown, researchers suspect that it may play a role in the formation of muscle tissue before birth but it must also be important for normal muscle function. It is unclear, however, how mutations in the *SEPN1* gene lead to muscle weakness and other features of multiminicore disease [158]. The so called ophthalmoplegic form encompasses patients with weakness and wasting of muscles similar to the classic phenotype, however such patients also exhibit specific weakness of the extraocular muscles or external ophthalmoplegia that is pronounced on abduction and upward gaze. In this group respiratory impairment is not so pronounced as in the classic form [159].

Predominant hip girdle weakness with relative sparing of respiratory and bulbar muscles similar to the pattern in patients with CCD is observed in another subgroup of MmD; some patients may show additional marked distal weakness and wasting, predominantly affecting the hands in the so called moderate form of MmD with hand involvement. [160]. The pattern of selective involvement on muscle imaging is similar to that observed in classic CCD caused by dominant *RYR1* mutations and distinct from the selective muscle involvement described in myopathies due to recessive mutations in the *SEPN1* gene. The latter two groups may form part of a clinical spectrum rather than distinct entities, as suggested by the observation of extra-ocular muscle involvement evolving over time in patients with the moderate form of MmD. Few severely affected cases have been reported with antenatal onset, generalized arthrogryposis, dysmorphic features and mild to moderate reduction of respiratory function.
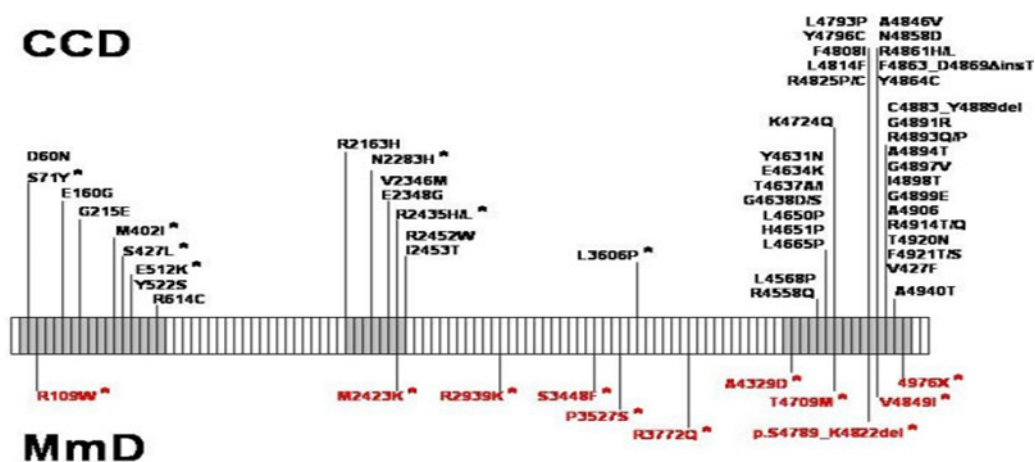
Figure 15: Schematic representation of the skeletal muscle ryanodine receptor *(RYR1)* gene and distribution of dominant and recessive (*) mutations associated with central core disease (CCD, in black) and Multi-minicore Disease (MmD, in red). Dominant mutations associated with a CCD phenotype predominantly affect the *RYR1* C-terminal domain encoding the calcium release channel pore of the ryanodine receptor protein, whereas recessive mutations predominantly associated with a MmD phenotype are distributed evenly throughout the gene. N-terminal, central and C-terminal mutational hotspots within the *RYR1* gene are highlighted in grey. (Figure courtesy of Dr Haiyan Zhou) [158].

Centronuclear myopathy (CNM)

Centronuclear myopathy (CNM) is a genetically heterogeneous condition characterized by the prominence of centrally located nuclei on muscle biopsy and clinical features of a congenital myopathy (Fig. 16). The severe X-linked recessive form is associated with mutations in the myotubularin1 (*MTM1*) gene. Dominant mutations in dynamin 2 gene (*DNM2*) and *RYR1* and recessive in amphiphysin 2 (*BIN1*) mutations have been associated with a milder phenotype. Extraocular muscle involvement is common in all forms of CNM. The *MTM1*, *DNM2*, and *BIN1* genes all encode proteins with a role in different aspects of membrane trafficking and remodeling [144].

The most severe X-linked form of the disease is caused by mutation in the Xq28 region which encodes *MTM1* or the protein called myotubularin.1. Most mutations cause very low levels of expression if any of myotubularin in the muscle fibres. This protein plays a role in phospholipid signaling as it regulates the levels of PI3phosphate and PI3,5P by dephosphorylating these phospholipids. Affected muscle fibers have a phenotype of a fetal/immature muscle. Boys with the X-linked recessive form, show very early symptoms, with poor muscle tone and severe weakness, including breathing difficulties. Other symptoms include undescended testicles (testes retention), weak eye musculature and a larger head than normal, with or without hydrocephalus. In the most severe form, myotubular myopathy, muscle weakness and respiratory problems are often so severe that the child dies during the first year of life.

The *DNM2* mutation on chromosome 19p13.2 is the cause of the autosomal dominant form of the disease. The dynamin 2 protein is involved in the formation of muscles cell membranes and formation of T tubules. The symptoms of the disease are mild and they appear in late childhood or in adult age. Mutations in *RYR1* cause the dominant form of the disease and symptoms appear in the neonatal period or later. Mutations in *MTMR14* and *MYF6* have been discovered in rare cases causing the dominant form of CNM. The phenotypes of the patients are very similar and slightly milder than those caused by *DNM2* or *RYR1* mutations and can include respiratory difficulties to stiff joints and scoliosis

The recessive form of the disease is caused by mutations in *BIN1* which is responsible for the expression of the amphiphysin 2, a protein enabling dynamin 2 regulation of T tubule formation and transport of membrane proteins within muscle cells. In this form of the disease, muscle weakness appears in childhood and initially is most apparent in the upper arms, thighs, face and eye muscles. The latter causes squinting and drooping of the upper eyelids known as ptosis [151]. All three major forms of centronuclear myopathy are rare occurring in less than 10 individuals per 100 000.
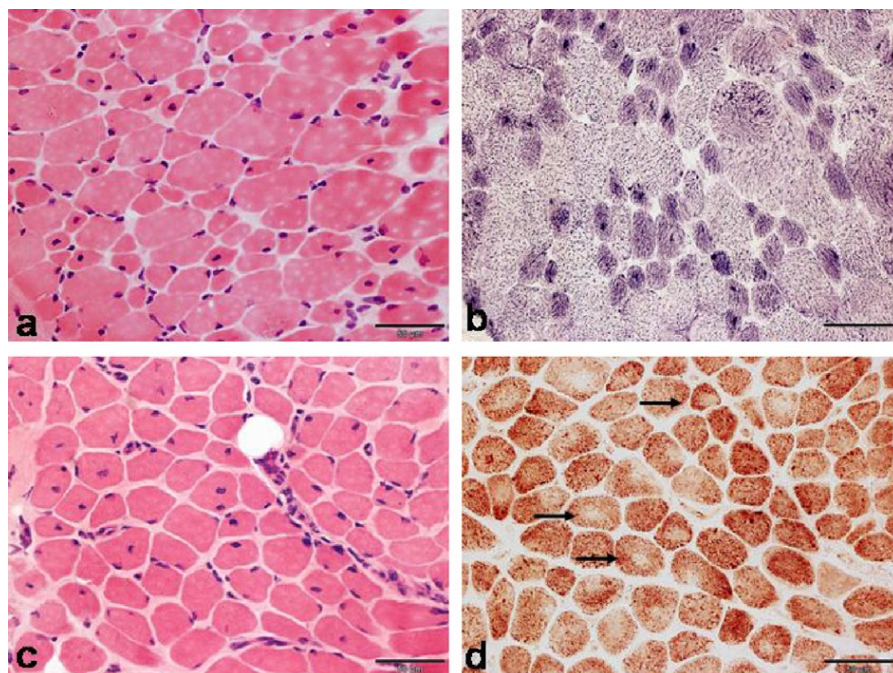
Figure 16: Histopathological features of RYR1-related centronuclear myopathy. Haematoxylin and eosin (H&E) (a and c), NADH-tetrazolium reductase (NADH-TR) (b) and cytochrome oxidase (COX) (d), stains from muscle biopsies taken from the left quadriceps at 1 year (a and b) and the right tibialis anterior at 9 years of age (c and d). With H&E stain at 1 year of age (a), there is hypotrophy and hypertrophy of two populations of fibres with numerous central nuclei mainly in smaller fibres. The smaller fibres are darker with NADH-TR and show central accumulation of stain (b). With H&E stain at 9 years of age (c), in addition to central nuclei there is a mild increase in connective tissue and staining for COX shows core-like areas devoid of activity that are often central (d, arrows) . Bars = 50 nm. [161].

Congenital fiber type disproportion (CFTD)

Congenital fiber type disproportion is a rare muscle disease with first symptoms appearing at birth or within the first five years of life. Most apparent symptoms include loss of muscle tone (hypotonia) and generalized muscle weakness (myopathy) particularly in the muscles of the shoulders, upper arms, hips and thighs. Weakness can also affect muscles of the face and muscles controlling eye movement (EOM) and in some cases causing droopy eyelid (ptosis). If the muscle weakness is pronounced scoliosis appears, in addition to dislocated hips and the permanent fixation of joints in a flexed position (contracture). Delays in motor development are present in the majority of cases.

Establishing the correct diagnosis for this disease can be quite demanding, as the changes occurring in the muscle tissue can appear in association with other disorders such as congenital muscle disorders, spinal muscular dystrophy, metabolic conditions, etc. In some cases CFTD is inherited as autosomal recessive or dominant trait [162]. Approximately 30% of patients have mild to severe respiratory involvement and feeding difficulties. It is estimated that up to 25 percent of affected individuals experience severe muscle weakness at birth and die in infancy or childhood. Muscle weakness generally does not worsen over time, and in some cases may improve. The histochemical pattern of muscle biopsies includes predominance of the type 1 fibers, which are around 12% or more smaller than type 2 fibers. Type 2 fibers remain normal or hypertrophic [162].

Mutations in the *TPM3* have been identified as common cause of CFTD. Mutations in the α-skeletal actin (*ACTA1*) gene have been identified in severe cases of CFTD, but the molecular mechanisms leading to disproportion in fiber size are unknown [163], it is still unknown if the *ACTA1* mutations are involved in the milder cases of CFTD. Causative mutations have been identified in *TPM2* and *SEPN1* as well. The genetic cause is still not known for approximately 50% of the cases.

Recently in a study of Clarke at al. mutations in *RYR1* were identified in 4 families with typical CFTD in whom no other genetic cause was found. From the cohort of patients used in this study it was estimated that 10-20% of CFTD cases are due to mutations in *RYR1* [143]. The pathophysiological effect of the *RYR1* mutations is not known, though reduced channel activity as a consequence of the low expression of RyR1 in the muscle of some patients with recessive form of the disease has been postulated [164].The presence of

ophtalmoplegia could be a specific clinical indicator for the presence of mutations in *RYR1* in the CFTD patients, since this symptom is not present in patients with other genetic causes. The difficulty however is that in milder cases, ophthalmoplegia might not be apparent and therefore hard to detect [165].

Although there was no family history of MH in any of the reported families with *RYR1* mutations the novel missense mutations may translate into susceptibility to MH in heterozygous mutation carriers. Since mutation of *RYR1* appears to be a common cause of CFTD, it should be recommended that MH precautions are taken for anesthetics in CFTD patients who do not have a genetic diagnosis [143]. To date molecular testing is clinically available for all genes and completes the diagnosis.

1.3 Calcium influx and spontaneous calcium events in muscle cells

1.3.1 Excitation-coupled calcium entry (ECCE)

Calcium influx in muscle cells is operated by two main mechanisms: excitation-coupled Ca^{2+} entry (ECCE) and store-operated Ca^{2+} entry (SOCE). ECCE is a form of Ca^{2+} entry from the extracellular environment into the myoplasm, which requires the interaction between DHPR and RyR1 as it was shown that in dyspedic and dysgenic myotubes ECCE does not occur. ECCE is activated in muscle cells following prolonged membrane depolarization.

ECCE is enhanced in myotubes expressing *RYR1* constructs that carry mutations causing malignant hyperthermia in humans. This increase in ECCE may contribute to the pathophysiological increase in intracellular Ca^{2+} that occurs during episodes of malignant hyperthermia. It appears that ECCE may be important in normal skeletal muscle as well, to help maintain force generation during tetanic stimulation. ECCE is blocked by 2-aminoethyl diphenylborate (2-APB), SKF 96356, La^{3+}, Gd^{3+} and 50μM nifedipine. ECCE can occur without any store depletion or in cells in which stores are fully depleted [40].

1.3.2 Store-operated calcium entry (SOCE)

SOCE was originally characterized in non-excitable cells but was studied in skeletal muscles following the discovery of stromal interaction molecule 1 (STIM1) and Orai1. SOCE is a process whereby Ca^{2+} influx across the plasma membrane is activated in response to depletion of intracellular Ca^{2+} stores in the ER/SR, thus it is an important process involved in maintaining intracellular calcium stores.

STIM1 is a transmembrane phosphoprotein containing several domains which include an EF-hand domain, a sterile-α-motif (SAM) domain at the N-terminus, and two coiled-coil regions and a proline-rich region at the C-terminus. The EF-hand domain of STIM1 has a high affinity for calcium and is located in the lumen of the endoplasmic reticulum (ER), where it is thought to sense changes in calcium store content. The coiled-coil domains are located in the cytosolic C-terminus and are important for oligomerization and punctae formation which occur during the activation of store-operated calcium (SOC) channels. The Orai channel family consists of three family members that form a highly selective calcium channel by tetramerization. STIM1 and Orai1 are both expressed in skeletal muscle, and mice lacking STIM1 and Orai1 display reduced muscle mass.

Three basic models for SOCE have been proposed in recent years: two of these involve conformational coupling between the Transient Receptor Potential channels (TRPC) and either the inositol trisphosphate receptor (IP3R) and/or RYR1 and a third that involves the physical interaction of STIM1 and Orai1 [166].

1.3.3 Sparks

The term Ca^{2+} spark was used for the first time by Chen and Lederer to describe spontaneous subcellular Ca^{2+} release events [167]. Ca^{2+} sparks are small, brief and very localized releases of Ca^{2+} and were originally described in cardiac myocytes and later in amphibian skeletal muscles. They appear spontaneously in frog skeletal muscle fibers at rest and at higher frequency during depolarization [168]. In general, sparks and other local Ca^{2+} events are described and quantified by their amplitude expressed in $[Ca^{2+}]$ or as normalized

increase of fluorescence, $\Delta F/F_0$, by the duration measured as full duration at half maximal amplitude (FDHM) and by their width measured as full width at half maximal amplitude (FWHM). The decay of the sparks occurs through diffusional dissipation of the Ca^{2+} signal away from its source [169].

Ca^{2+} sparks were also discovered in smooth muscle cells two years after their initial report in cardiomyocytes [170]. In unstimulated single cardiac myocytes, a Ca^{2+} spark appears suddenly, reaches its peak of about a two-fold increase in fluorescence intensity within 10 ms, and disappears in a matter of 20 ms. It is defined by an area of ~2.0 μm in diameter. Spontaneous Ca^{2+} sparks do not require Ca^{2+} entry into the myocyte through DHPR or by other channels on the plasma membrane. At a resting membrane potential of -80mV spontaneous sparks appear even when extracellular Ca^{2+} is removed for a short period [53].

Ca^{2+} sparks also occur even after the L-type calcium channels have been blocked pharmacologically. Saponin-permeabilised myocytes also exhibit sparks indicating that the membrane integrity is not a prerequisite for these events. It is now accepted that spontaneous Ca^{2+} sparks are due to the small but limited opening of RyRs that depends on many factors including $[Ca^{2+}]_i$ and $[Ca^{2+}]_{SR}$, the free Ca^{2+} concentration in the cytosol and in the SR lumen, respectively. At supramicromolar concentrations, ryanodine abolishes sparks altogether.

Ca^{2+} sparks occur in skeletal and smooth muscles, cardiac myocytes, neuroendocrine cells and neurons containing different isoforms of RyRs. Localized Ca^{2+} release events with characteristics similar to sparks have also been observed in some non-excitable cells, including endothelial cells [167].

In vertebrate skeletal muscles, type 1 RyRs form a "double checkerboard" arrangement where unconnected RyRs are in direct contact with those that are engaged with DHPRs. Under normal conditions in mammalian skeletal muscles sparks do not occur as the highly ordered checkerboard conformation is thought to inhibit sparks as the DHPR blocks RyR1 Ca^{2+} release. Experimentally under non-physiological conditions and under hypo-osmotic stress, Ca^{2+} sparks were induced in isolated mouse skeletal muscle fibers [167].

CHAPTER 2: RESULTS

2.1 Excitation-contraction coupling and Ca^{2+} homeostasis in human craniofacial muscles

2.1.1 Introduction

There are approximately 60 distinct skeletal muscles in the vertebrate head that control food intake, facial expression and eye movement. These muscles develop in a manner that is tightly coordinated with other craniofacial tissues. In recent years, interest in this unique group of skeletal muscles has significantly increased, with the accumulation of new information in terms of molecular profiling and gene targeting studies. From a clinical point of view they are coming into the spotlight, especially when it comes to diseases that affect them (strabismus, laryngeal dystonias, facial paralysis and others), but more intriguing is their selective and non-uniform response in different neuromuscular disorders, where some of them are spared and others heavily affected [4]. For this reason we were interested to resolve some of the questions regarding the similarities and differences between different groups of head muscles in the context of neuromuscular disorders.

Keeping this in mind, we investigated human extraocular muscle samples at different points of maturity, either in mature muscles isolated during corrective eye surgery or in myotubes derived in culture from the muscle biopsies. Our aim was to define the Ca^{2+} handling properties of these muscles. Defining the characteristics of EOM as well as those of the distinct but spatially close muscles known as orbicularis oculi was also one of the our aims, Indeed, we found significant differences between human EOM, OO and LM in terms of protein levels of different ECC components as well as in the regulation of Ca^{2+} homeostasis.

2.1.2 Publication – Characterization of the excitation contraction coupling in human extraocular muscles

Marijana Sekulic-Jablanovic[*], Anja Palmowski-Wolfe[†], Francesco Zorzato[*,‡] and Susan Treves[*,‡]

[*]Departments of Anesthesia and Biomedizin, Basel University Hospital, Hebelstrasse 20, 4031 Basel, Switzerland. [†]Eye Hospital, Basel University Hospital, Mittlere Strasse 91, 4031Basel, Switzerland. [‡]Department of Life Sciences and Biotechnology, General Pathology section, University of Ferrara, Via Borsari 46, 44100 Ferrara, Italy.

Short Title: Calcium regulation in human extraocular muscles

To whom correspondence should be addressed: Susan Treves, Departments of Anaesthesia and Biomedicine, Basel University Hospital, Hebelstrasse 20, 4031 Basel, Switzerland. Tel. +41-61-2652373; Fax:+41-61-2653702; E-mail: susan.treves@unibas.ch

Key words: excitation-contraction coupling, calcium homeostasis, gene expression.

Characterization of excitation–contraction coupling components in human extraocular muscles

Marijana Sekulic-Jablanovic*, Anja Palmowski-Wolfe†, Francesco Zorzato*‡ and Susan Treves*‡[1]

*Departments of Anesthesia and Biomedizin, Basel University Hospital, Hebelstrasse 20, 4031 Basel, Switzerland
†Eye Hospital, Basel University Hospital, Mittlere Strasse 91, 4031Basel, Switzerland
‡Department of Life Sciences and Biotechnology, General Pathology section, University of Ferrara, Via Borsari 46, 44100 Ferrara, Italy

Excitation–contraction coupling (ECC) is the physiological mechanism whereby an electrical signal detected by the dihydropyridine receptor, is converted into an increase in $[Ca^{2+}]$, via activation of ryanodine receptors (RyRs). Mutations in *RYR1*, the gene encoding RyR1, are the underlying cause of various congenital myopathies including central core disease, multiminicore disease (MmD), some forms of centronuclear myopathy (CNM) and congenital fibre-type disproportion. Interestingly, patients with recessive, but not dominant, *RYR1* mutations show a significant reduction in RyR protein in muscle biopsies as well as ophthalmoplegia. This specific involvement of the extraocular muscles (EOMs) indicates that this group of muscles may express different amounts of proteins involved in ECC compared with limb muscles. In the present paper, we report that this is indeed the case; in particular the transcripts encoding RyR3, cardiac calsequestrin (CSQ2) and the $\alpha 1$ subunit of the cardiac dihydropyridine receptor are up-regulated by at least 100-fold, whereas excitation-coupled Ca^{2+} entry is 3-fold higher. These findings support the hypothesis that EOMs have a unique mode of calcium handling.

Key words: calcium homoeostasis, excitation–contraction coupling, gene expression.

INTRODUCTION

Extraocular muscles (EOMs) are among the fastest and most fatigue-resistant skeletal muscles [1]. More than 20 years ago, they were categorized as a separate group of muscles or 'allotype' since they represent a unique group of highly specialized muscles, anatomically and physiologically different from other skeletal muscles [2]. Indeed, their embryonic origin is distinct from that of limb muscles: the former, together with the striated muscles of the face, jaw and throat, develop from the first seven somitomeres whereas the latter derive from somites [3]. In humans, there are six types of EOMs and they are characterized by the presence of two layers: the inner global layer and the outer orbital layer [4]. The fibre type classification of limb muscles does not fit the six fibre types described in EOMs [1] and the innervation of EOMs is also different, as they are innervated by cranial nerves and contain both singly innervated muscle fibres (SIFs) and multiply innervated fibres (MIFs), whereas mammalian limb muscle fibres are singly innervated by motoneurons originating from the spinal cord [5]. The distinct origin and innervation of EOMs are probably responsible for the differences in gene and protein expression that have been described in mammalian EOMs [6].

The ryanodine receptor 1 (RyR1) is the calcium channel of striated skeletal muscle responsible for releasing Ca^{2+} from the sarcoplasmic reticulum leading to muscle contraction [7,8]. Over the last two decades, more than 200 mutations in *RYR1* (the gene encoding RyR1) have been identified in the human population and linked to neuromuscular disorders and/or the pharmacogenetic disorder malignant hyperthermia [9,10]. Whereas the dominant *RYR1* mutations are predominantly associated with central core disease and/or a susceptibility to malignant hyperthermia,

recessive mutations are found in patients with multiminicore disease (MmD), centronuclear myopathy (CNM) and congenital fibre-type disproportion [10–15]. Interestingly, patients with recessive, but not dominant, *RYR1* mutations show a decreased amount of RyR1 protein in biopsied muscles, as well as specific involvement of EOM (ophthalmoplegia) [11–14,16]. Selective involvement of EOM or lack thereof, also characterizes particular neuromuscular diseases: in myasthenia gravis and mitochondrial myopathies they are the first and most affected muscle group [17] whereas they are characteristically spared from pathology in aging, Duchenne muscular dystrophy and congenital muscular dystrophy [18–20]. Such sparing of EOM in muscular dystrophies has been attributed to constitutive differences between EOM and other skeletal muscles [20] but the factors controlling these differences remain largely unknown.

In order to help clarify the cause(s) for the specific involvement of EOM in patients with recessive *RYR1* mutations, we investigated their excitation–contraction coupling (ECC) machinery and calcium homoeostasis. Our results show that there are significant differences between leg muscles (LMs) and EOM; in particular the latter have developed a chimaeric configuration in that they express significantly lower levels of RyR1, the $\alpha 1$ subunit of the dihydropyridine receptor ($Ca_v 1.1$) and calsequestrin-1 (CSQ1), whereas the cardiac isoforms of the $Ca_v 1.2$ and CSQ2 are highly expressed as is RyR3. Such changes result in different characteristics of calcium homoeostasis, as myotubes explanted from EOM exhibit a large component of excitation coupled Ca^{2+} entry (ECCE). The results of the present study shed light on the underlying causes leading to EOM involvement in congenital muscle disorders due to *RYR1* mutations causing a decrease in RyR1 protein.

EXPERIMENTAL PROCEDURES

Human muscle cell cultures

Primary muscle cell cultures were established from fragments of quadriceps muscles obtained from biopsies of healthy donors (five donors) and EOM samples obtained from patients undergoing squint corrective surgery (four donors), as described previously [21,22]. Cells were cultured on laminin-coated 0.17-mm-thick glass coverslips in growth medium (Skeletal Muscle Cell Growth medium; Promo Cell) and induced to differentiate into myotubes by culturing them in differentiation medium (Skeletal Muscle Cell Differentiation medium; Promo Cell) for 7–14 days. This research was carried out in accordance with the Declaration of Helsinki (2013) of the World Medical Association and was approved by the Ethikkommission beider Basel (permit number EK64/12); all subjects gave written informed consent to carry out this work.

Calcium measurements

Myotubes were loaded with fura-2 (Calbiochem) or fluo-4 (Life Technologies) (final concentration 5 μM) in differentiation medium for 30 min at 37°C, after which the coverslips were mounted on to a 37°C thermostatically-controlled chamber which was continuously perfused with Krebs–Ringer medium; individual cells were stimulated by means of a 12- or 8-way 100 mm diameter quartz micro-manifold computer-controlled microperfuser (ALA Scientific Instruments), as described previously [22]. For global changes in the intracellular Ca^{2+} concentration, the fluorescent ratiometric Ca^{2+} indicator fura-2 was used. Online measurements were recorded using a fluorescent Axiovert S100 TV inverted microscope (Carl Zeiss) equipped with a 20× water-immersion FLUAR objective [0.17 numerical aperture (NA)] and filters (BP 340/380, FT 425, BP 500/530) and attached to a Cascade 128 + CCD (charge-coupled device) camera. Changes in fluorescence were analysed using Metamorph imaging software (Molecular Devices) and the average pixel value for each cell was measured at excitation wavelengths of 340 nm and 380 nm as described previously [21,22]. Fura-2 fluorescent ratio signals were converted into $[Ca^{2+}]$ using the fura-2 Ca^{2+} imaging calibration kit from Molecular Probes/Invitrogen following the manufacturer's instructions, as previously described [23]. The dynamics of $[Ca^{2+}]$ influx were investigated by TIRF (total internal reflection fluorescence) microscopy using the fast Ca^{2+} indicator fluo-4, as described previously [24]. Briefly, differentiated human myotubes were mounted on a thermostatically controlled perfusion chamber, bathed continuously in Krebs–Ringer containing 2 mM Ca^{2+}. ECCE was measured after the application of 60 mM KCl to myotubes pre-treated with 50 μM ryanodine (Calbiochem) to block RyR1-mediated Ca^{2+} release. Nifedipine (50 μM) (Calbiochem) was used to block the dihydropyridine receptor or 0.5 mM EGTA to chelate Ca^{2+}. Online fluorescence images were acquired using an inverted Nikon TE2000 TIRF microscope equipped with an oil immersion CFI Plan Apochromat 60× TIRF objective (1.49 NA) and an electron multiplier Hamamatsu CCD camera C9100–13. Data were analysed using Metamorph imaging software (Molecular Devices).

Quantitative real-time PCR

Total RNA was extracted from muscle biopsies using TRIzol® (Invitrogen) and following the manufacturer's protocol. The RNA was first treated with DNase I (Invitrogen) and then 1000 ng were reverse-transcribed using the high-capacity cDNA reverse transcription kit (Applied Biosystems); cDNA was amplified by quantitative real-time PCR (qPCR) using SYBR Green technology (Fast SYBR Green Master Mix, Applied Biosystems) as described previously [25]. The sequence of the primers used to amplify and quantify the different genes is given in Supplementary Table S1. qPCR was performed on a 7500 Fast Real-Time PCR machine from Applied Biosystems using the 7500 software v2.3. The standard protocol was selected and the running method consisted of a holding stage at 50°C for 20 s and a denaturing step at 95°C for 10 min, followed by 40 cycles of denaturing at 95°C for 15 s and an extension step at 60°C for 1 min. Gene expression was normalized to expression *ACTN2*, which is present in all muscle fibre types. Results are expressed as fold change compared with expression of the gene in LMs.

Immunofluorescence

Glass coverslip grown and differentiated myotubes were fixed with 4 % paraformaldehyde (made in Phosphate buffered saline (PBS)), permeabilized with 1 % Triton in PBS for 20 min and processed as previously described [24]. The following antibodies were used: mouse anti-RyR1 (Thermo Scientific; MA3–925), goat anti-Ca$_v$1.1 (Santa Cruz Biotechnology, sc-8160), rabbit anti-Ca$_v$1.2 (Santa Cruz Biotechnology, sc-25686), Alexa Fluor® 488-conjugated chicken anti-rabbit, Alexa Fluor®-conjugated donkey anti-goat IgG (Life Technologies) and Alexa Fluor®-conjugated goat anti-mouse IgG (Life Technologies). Cells were stained with DAPI (Life Technologies) to visualize nuclei and observed using a Nikon A1R confocal microscope with a CFI Apo TIRF 100× (1.49 NA) objective.

Electrophoresis and immunoblotting

The total sarcoplasmic reticulum fraction was isolated from flash-frozen muscle samples (human EOM, quadriceps muscles and mouse heart) stored in liquid nitrogen as previously described [26]. Protein concentration was determined using Protein Assay Kit II (Bio-Rad Laboratories) using BSA as a standard. SDS/PAGE, protein transfer on to nitrocellulose membranes and immunostaining were performed as described previously [26]. The following primary antibodies were used: mouse anti-RyR1 (Thermo Scientific, MA3–925), goat anti-Ca$_v$1.1 (Santa Cruz Biotechnology, sc-8160), rabbit anti-Ca$_v$1.2 (Santa Cruz Biotechnology, sc-25686), rabbit anti-CSQ-1 (Sigma, C-0743) and CSQ2 (Abcam, ab-3516), goat anti-SERCA1 (sarcoplasmic/endoplasmic reticulum Ca^{2+}-ATPase 1) (Santa Cruz Biotechnology, sc-8093), goat anti-SERCA2 (Santa Cruz Biotechnology, sc-8095), mouse anti-sarcalumenin (Thermo Scientific, MA3-932), goat anti-junctophilin1 (Santa Cruz Biotechnology, sc-51308). Secondary horseradish peroxidase conjugates were Protein G–horseradish peroxidase (Sigma, P8170) and horseradish peroxidase-conjugated goat anti-mouse IgG (Sigma, A2304). The immunopositive bands were visualized by chemiluminescence using the Super Signal West Dura kit (Thermo Scientific) or the chemiluminescence kit from Roche.

Statistical analysis

Statistical analysis was performed using Student's *t* test for two populations. Values were considered significant when $P < 0.05$. When more than two groups were compared, analysis was performed by the ANOVA test followed by the Bonferroni post-hoc test, using the GraphPad Prism 4.0 software. The Origin Pro
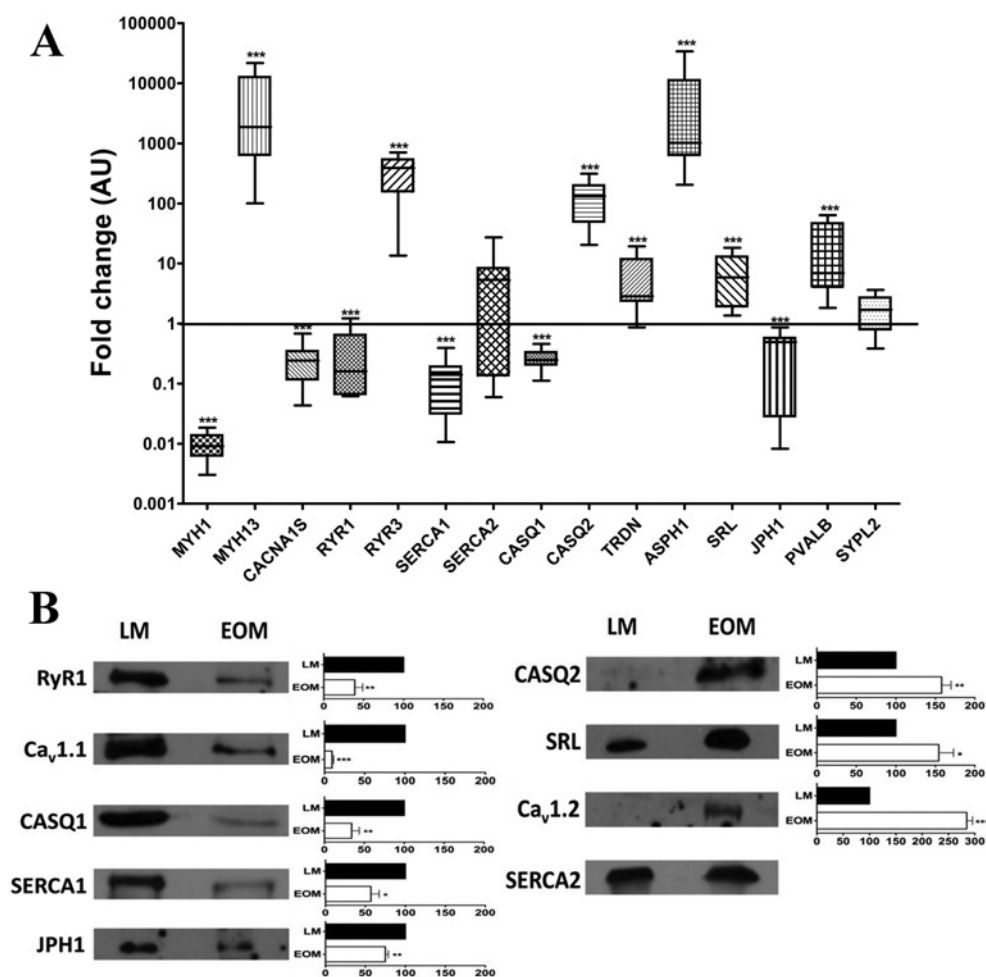
Figure 1   Expression of ECC transcripts and proteins in human EOM biopsies

(**A**) Gene expression was carried out by qPCR as described in the 'Experimental Procedures' section. Each reaction was carried out in triplicate, in pooled muscle samples from 4–5 biopsies from different individuals. Expression levels were normalized to *ACTN2* expression. Results are expressed as mean fold change (AU, arbitrary units) of transcripts in EOM compared with LMs, the latter were set as 1. Results were analysed using Student's *t* test (***$P < 0.0001$). (**B**) Western blot analysis of total sarcoplasmic reticulum proteins in human EOM and LMs. Twenty micrograms of protein were loaded per lane and separated on SDS/6 % PAGE or SDS/10 % PAGE. Blots were probed with the indicated antibodies. Histograms represent the mean $\pm$ S.E.M. band intensity normalized to SERCA2 content (*$P < 0.05$; **$P < 0.005$; ***$P < 0.0001$).

8.6 software was used for generating dose–response curves and calculating EC_{50} values.

RESULTS

Excitation–contraction coupling gene and protein expression levels in human EOM

Figure 1(A) shows the expression level as assessed by qPCR, of the main genes involved in skeletal muscle ECC in EOM biopsies, compared with quadriceps biopsies from healthy donors; the latter were taken as the reference tissue and the expression of the different set of muscle-specific genes in human quadriceps was set as 1. The results represent the mean expression levels of samples pooled from four to five biopsies and are expressed on a logarithmic scale. The most interesting finding is that the expression levels of major genes involved in skeletal muscle ECC, namely *RYR1*, *CACNA1S*, *SERCA1* and *CASQ1* were $\sim$10-fold lower ($P < 0.0001$) than in LM biopsies. Intriguingly, the transcript level of *RYR3* was $\sim$800-fold higher in EOM ($P < 0.0001$). A second interesting result was that the expression

level of *CASQ2* was found to be $\sim$100-fold higher in EOM ($P < 0.0001$) as was that of the structural proteins *TRDN* and *ASPH1* ($\sim$10-fold and $\sim$1000-fold respectively; $P < 0.0001$) and of the calcium buffering and binding proteins *SRL* and *PVALB* (10-fold; $P < 0.0001$) As expected, the *MYH1* transcript level was significantly lower in EOM (100-fold; $P < 0.0001$) than in LMs, since this isoform is mainly expressed in slow-twitch muscles. In contrast, the transcript of *MYH13,* which is the isoform characteristically expressed in eye muscles, was $\sim$5000-fold higher in EOM ($P < 0.0001$), corroborating the validity of our assay. Taken together, these results indicate that the gene expression pattern of the main components involved in ECC of human EOM is specific and distinct from that of other striated skeletal muscles.

In order to confirm the changes in gene expression on the protein level, we prepared the total sarcoplasmic reticulum fractions and probed them with a panel of antibodies against skeletal and cardiac ECC protein components. The protein expression levels were then normalized for SERCA2 whose content was similar in LM and EOM as assessed by real time PCR (Figure 1A) and immunoblotting. Figure 1(B) shows the representative Western
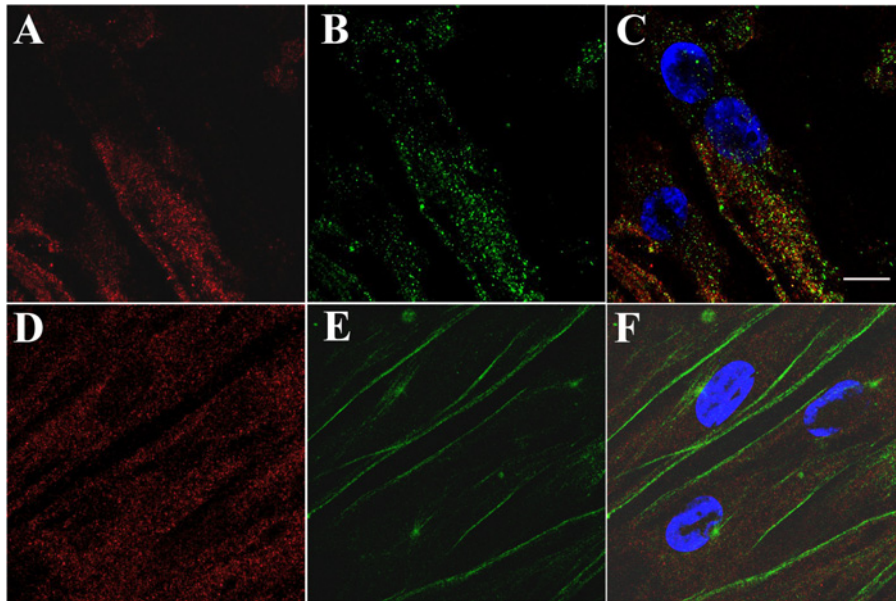
Figure 2   Cellular localization of RyR1, Ca$_v$1.1 and Ca$_v$1.2 in differentiated EOM-derived myotubes

Human myotubes were stained as described in the 'Experimental Procedures' section and visualized with a Nikon A1R confocal microscope equipped with a CFI Apo TIRF 100× objective (1.49 NA). (**A**) anti-RyR1 (red), (**B**) anti-Ca$_v$1.1 (green), (**C**) merged image of anti-RyR1, anti-Ca$_v$1.1 and DAPI (blue); orange pixels show co-localization between RyR1 and Ca$_v$1.1. (**D**) anti-RyR1 (red), (**E**) anti-Ca$_v$1.2 (green), (**F**) merged image of anti-RyR1, anti-Ca$_v$1.2 and DAPI (blue). Scale bar, 20 μm.

blots and quantitative histograms, as can be seen, for RyR1, Ca$_v$1.1, SERCA1 and CSQ1 the protein levels are decreased by more than 50 % in EOM compared with LM samples. The cardiac isoform of the RyR2 was not detectable in EOM (Supplementary Figure S1) whereas Ca$_v$1.2, the cardiac isoform of the Ca$_v$ CSQ2, as well as sarcalumenin, were significantly up-regulated in EOM (2-fold for Ca$_v$1.2 and by 50 % for CSQ2 and sarcalumenin); qPCR could not be used reliably to compare the expression levels of the Ca$_v$1.2 transcript because of its extremely low level of expression in leg skeletal muscles (the reference tissue in the qPCR); its level of expression is comparable with that found in mouse heart microsomes (Supplementary Figure S1).

Ca^{2+} homoeostasis in EOM cultured myotubes

Muscle biopsies have been used as a starting material to obtain primary muscle cultures from patients with different neuromuscular disorders and the myotubes that have been obtained have been a useful model to study ECC under normal and pathological conditions [21,22,24,25]. In the present study, we successfully used a protocol similar to that used for LM biopsies, in order to obtain EOM-derived myotubes (Figure 3A). Once a sufficient number of myoblasts grew out of the biopsy, they were further expanded and then induced to differentiate into myotubes. Figure 2 shows photomicrographs of myotubes stained with anti-RyR1 (red, Figure 2A), anti-Ca$_v$1.1 (green, Figure 2B) merged plus DAPI (Figure 2C) and anti-RyR1 (red, Figure 2D), anti-Ca$_v$1.2 (green, Figure 2E) and merged plus DAPI (Figure 2F) and observed by confocal microscopy. As can be seen, the myotubes are positive for RyR1 and Ca$_v$1.1 and the two proteins co-localize within an intracellular membrane compartment, but as previously established [25] their distribution is punctuated, not highly regular and lacks the distinct structure observed in mature fibres. The localization of Ca$_v$1.2, however, is clearly different

from that of Ca$_v$1.1 (compare Figures 2B and 2E); indeed the Ca$_v$1.2 appears to be almost exclusively localized on the plasma membrane. These results point to a potential alternative form of ECC in EOM-derived myotubes and we next studied calcium homoeostasis in these cells. Results from LM-derived myotubes from five donors and EOM-derived myotubes from four donors were pooled and averaged. Figure 3(B) shows that the KCl-induced Ca^{2+} release from intracellular stores (in the presence of 100 μM La^{3+} and therefore reflecting skeletal ECC) was similar in LM and EOM-derived myotubes. However, in EOM-derived myotubes the EC$_{50}$ for 4-chloro-m-cresol-induced Ca^{2+} release was increased (332 ± 26 and 234 ± 58 μM for EOM and LM respectively). Additionally, Figure 3(C) shows that the resting [Ca^{2+}] in EOM-derived myotubes is significantly lower than that of LM-derived myotubes ($P < 0.0001$; Student's t test), whereas the size of the rapidly releasable intracellular Ca^{2+} stores is more than 2-fold larger in EOM-derived myotubes compared with LM-derived myotubes (Figure 3D).

Plasma membrane depolarization of skeletal muscle cells is accompanied by Ca^{2+} influx through the dihydropyridine receptor and this phenomenon is defined as ECCE [24,27,28]. We next studied ECCE in EOM-derived myotubes using a TIRF microscope [24]. The top panels in Figure 4(A) show a representative myotube pre-treated with 50 μM ryanodine and stimulated with 60 mM KCl; Figure 4(B) shows a representative Ca^{2+} influx trace initiated by the application of 60 mM KCl in EOM-derived myotubes (continuous line) and LM-derived myotubes (dotted line). The change in fluo-4 fluorescence represents Ca^{2+} influx via the dihydropyridine receptor and not release from stores as: (i) myotubes were incubated with 50 μM ryanodine in order to block Ca^{2+} release via RyR; (ii) pre-incubation of myotubes with ryanodine plus 50 μM nifedipine blocked the Ca^{2+} increase (Figure 4C); and (iii) Ca^{2+} influx was inhibited when the experiment was performed in Krebs–Ringer solution containing 0.5 mM EGTA (Figure 4C). Thus, compared
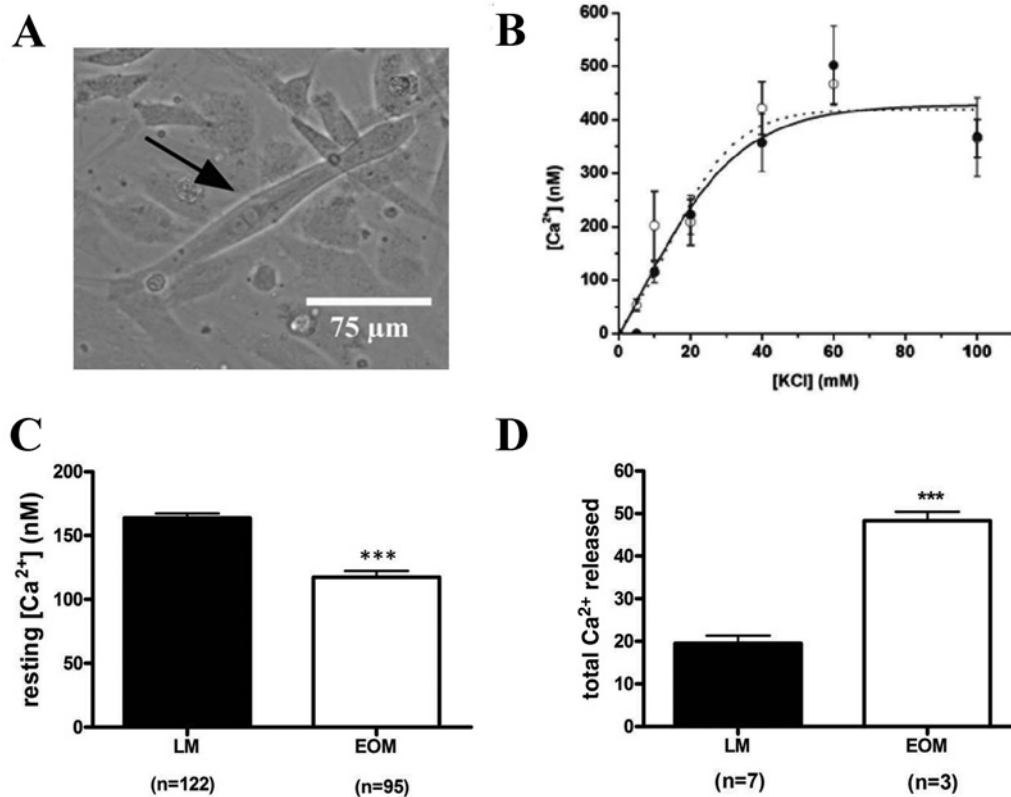
Figure 3   Global calcium homoeostasis of EOM-derived myotubes

Myotubes were loaded with 5 μM fura-2 and perfused with Krebs–Ringer medium containing 2 mM $CaCl_2$. For KCl-induced Ca^{2+} release, individual cells were perfused with Krebs–Ringer plus 100 μM La^{3+} and the indicated concentration of KCl was applied using a microperfusion system. (**A**) Brightfield photomicrograph of a fully-differentiated myotube 5 days after differentiation. (**B**) KCl dose–response curve of EOM-derived myotubes (filled circles, continuous line) and LM-derived myotubes (empty circles, dotted line). Curves show the changes in peak calcium, expressed as $[Ca^{2+}]$ in nM. Each point represents the mean $\pm$ S.E.M. of a minimum of four to ten different cells. (**C**) Mean $\pm$ S.E.M. resting $[Ca^{2+}]$ in EOM and LM-derived myotubes. (**D**) Total amount of Ca^{2+} in the sarcoplasmic reticulum. The total amount of rapidly releasable Ca^{2+} in the stores was determined by calculating the area under the curve of the transient induced by the application of 1 μM ionomycin plus 500 nM thapsigargin in Krebs–Ringer containing 0.5 mM EGTA. Values represent the mean $\pm$ S.E.M. of the indicated number of cells. ***$P < 0.0001$. Experiments were performed on LM-derived myotubes from five donors and EOM-derived myotubes from four donors. The values represent mean intracellular calcium measurements from coverslips measured on different days.

with LM-derived myotubes, depolarization-induced Ca^{2+} influx in EOM myotubes was 3-fold higher (Figure 4D).

DISCUSSION

In the present study, we characterized the ECC machinery of human EOM and report that these muscles are particular in as much as they express important components of the cardiac ECC machinery; in addition, we report for the first time that primary muscle cell cultures can be obtained from biopsies of patients undergoing squint or corrective surgery. Such myotubes maintain their phenotypic characteristics since they exhibit intracellular calcium regulation that is enhanced compared with primary cultures of LM-derived myotubes. The present study is important as it shows the feasibility of performing such experiments not only in biopsies obtained from normal individuals, but also can be extended to patients suffering from neuromuscular disorders causing ophthalmoplegia.

In a previous study, Porter et al. [29] used a bioinformatic gene profiling approach to identify key differences between murine EOM, LMs and jaw muscles. In their study, they scanned the expression pattern for transcripts encoding proteins involved in transcriptional regulation, signal transduction, intermediary metabolism and sarcomeric ECC. As far as the ECC coupling machinery is concerned, our results do not support their findings as we found significant changes between leg and EOM expression of CSQ1 and CSQ2, RyR1, SERCA1 and $Ca_v 1.1$, triadin, sarcalumenin and parvalbumin and no change in mitsugumin-29. Such inconsistencies may be due to the fact that (i) they used mouse skeletal muscle and we used human biopsies, (ii) we used qPCR on pooled samples; (iii) the biopsies we analysed were derived from patients with strabismus and therefore not 'normal' muscles. Indeed the pattern of expression of transcripts in strabismic and normal EOMs has been reported to be different [30]; and (iv) we normalized all qPCR results for the content of the muscle-specific gene *ACTN2*. In support of our findings, it was shown that there are important differences between human EOM and those of other species [31].

An interesting observation of the present report is that EOM express low levels of RyR1 but high levels of RyR3, a finding that may explain why patients with recessive ryanodinopathies leading to decreased expression of RyR1 characteristically show extraocular involvement [11,15] whereas those with dominant *RYR1* mutations do not. It is plausible that since the levels of expression of RyR1 are low in EOM, mutations leading to a further decrease in its level of expression will severely affect muscle function, leading to ophthalmoplegia. In this context, it should be mentioned that the higher levels of RyR3 expressed in EOM do not compensate for the decrease in RyR1, indicating that the RyR3
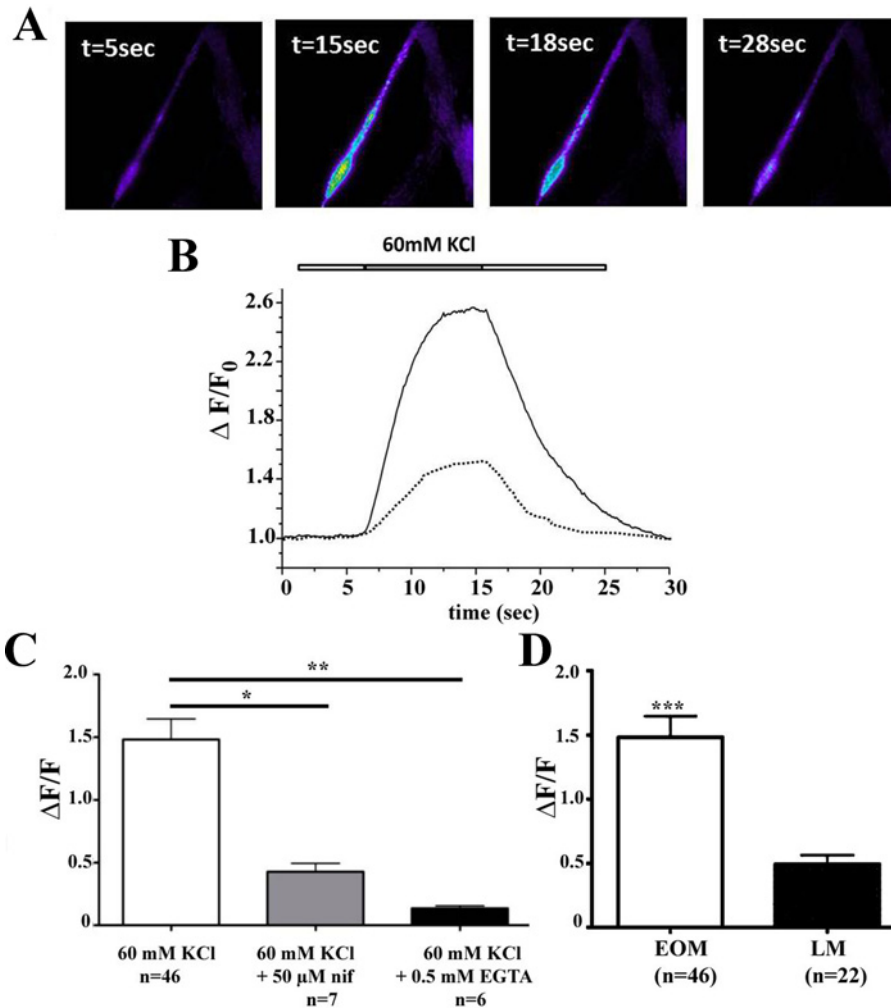
Figure 4   EOM-derived myotubes exhibit a larger depolarization-induced Ca^{2+} influx compared with LM-derived myotubes

Ca^{2+} influx induced by addition of 60 mM KCl was monitored using a TIRF microscope in myotubes pre-incubated with 50 μM ryanodine to block RyR1-mediated Ca^{2+} release and loaded with 5 μM fluo-4. (**A**) Top panels, pseudocoloured ratiometric images (peak fluorescence after addition of KCl/resting fluorescence) of fluo-4 fluorescence changes after application of KCl to EOM-derived myotubes. (**B**) Representative ECCE trace showing changes in fluo-4 fluorescence in a EOM-derived myotube (continuous line) and LM-derived myotube (dotted line). (**C**) Histogram depicting mean $\pm$ S.E.M. peak increase of fluo-4 fluorescence induced in EOM-derived myotubes by 60 mM KCl alone (white bar), in cells pre-incubated with 50 μM nifedipine (grey bar) or in cells stimulated with Krebs–Ringer containing 0.5 mM EGTA (black bar). Statistical analysis performed by the ANOVA test followed by the Bonferroni post-hoc test; *$P < 0.02$, **$P < 0.005$. (**D**) Mean $\pm$ S.E.M. peak increase of fluo-4 fluorescence induced by 60 mM KCl in human EOM-derived myotubes (white bar) compared with LM-derived myotubes (black bar). Experiments were performed on cells grown from three different biopsies on three different days and results were pooled and averaged. Statistical analysis was performed using Student's t test; ***$P < 0.0001$.

isoform must be involved in other aspects of calcium release, cannot be directly activated by the Ca$_v$1.1 voltage sensor and cannot functionally replace RyR1. On the other hand, EOM also express high levels of the Ca$_v$1.2 and of CSQ [32]; as far as CSQ2 is concerned, it has half the calcium-binding capacity of CSQ1 [33], it is phosphorylated to a higher stoichiometry and at least 50-fold more rapidly [34]. Though the role of phosphorylation is unclear, it is thought to increase the Ca^{2+}-binding affinity and to assure that the levels of Ca^{2+} near the Ca^{2+} release sites are elevated [35]. The observed up-regulation of Ca$_v$1.2 is both novel and intriguing as this isoform is mainly expressed in the heart, where it functions as a voltage sensor and Ca^{2+} channel, activating RyR2 via a Ca^{2+}-induced Ca^{2+} release mechanism [36]. In EOM-derived myotubes, this isoform was clearly distributed on the plasma membrane and since RyR2 was not detectable in EOM, either these muscles have evolved a chimaeric cardiac/skeletal ECC, with Ca$_v$1.2 activating RyR1, or Ca$_v$1.2 may be coupled to RyR3 or it may be involved in Ca^{2+} influx following plasma membrane depolarization. Such chimaeric expressions of RyR isoforms are not uncommon in smooth muscle cells that are reported to express different combinations of calcium channels and L-type voltage sensors, depending on their tissue of origin and physiological requirements [37].

Zeiger et al. [38] showed that rat eye muscle-derived myotubes exhibit superior calcium homoeostasis compared with leg tibialis anterior-derived myotubes and release double the amount of calcium after treatment with ionomycin than LM-derived myotubes. The results of the present study support and extend these findings; indeed human EOMs not only have larger intracellular Ca^{2+} stores and express different calcium-buffering proteins, but also show lower resting [Ca^{2+}] and enhanced depolarization-induced calcium influx (or ECCE). The enhanced calcium-handling capacity may be due to the higher expression levels of CSQ2 and of the calcium-binding proteins parvalbumin and sarcalumenin. Parvalbumin is a cytosolic high-affinity Ca^{2+}-binding protein preferentially expressed in fast

twitch muscles whose function is to promote muscle relaxation [39,40], whereas sarcalumenin is localized on the longitudinal sarcoplasmic reticulum where it is involved in stabilizing the Ca^{2+} pump and in maintaining rapid contraction and relaxation rates [41]. The physiological function of depolarization-induced calcium influx is far from clear but it is postulated to be important for refilling of intracellular Ca^{2+} stores, which is essential during repetitive stimulation [42,43]. Interestingly EOM-derived myotubes have significantly larger intracellular calcium stores and enhanced Ca^{2+} influx and the latter is probably due to the high levels of expression of $Ca_v1.2$.

A final observation resulting from the present study and from a previous study [25] concerns the phenotype of satellite cells; depending on their muscle of origin, be it fast or slow twitch or EOM, the satellite subpopulations are intrinsically different [44] and they maintain the specific characteristics particular to the muscle from which they originated even after explantation and culture.

In conclusion, the present study provides insights into the ECC characteristics of human EOM. Reduced expression of RyR1, CSQ1 and SERCA1 is a feature of great significance in the context of ophthalmoplegia and neuromuscular disorders. Taking into account the importance of exquisitely efficient calcium management in order to achieve the demanding physiological properties of the EOMs, the increased levels of CSQ2, parvalbumin and sarcalumenin together with reported higher depolarization-induced calcium influx and particular high expression of $Ca_v1.2$ indicate that this group of muscles which is in constant use, relies on a chimaeric skeletal/cardiac ECC configuration.

AUTHOR CONTRIBUTION

Marijana Sekulic-Jablanovic performed the experiments, analysed the data and drafted the article. Anja Palmowski-Wolfe performed surgeries, provided the biopsies and critically revised the paper for important intellectual content. Francesco Zorzato was responsible for conception and design of the experiments, interpretation of data and critically revised the paper for important intellectual content. Susan Treves was responsible for conception and design of the experiments, collection, analysis and interpretation of data and drafted the article.

ACKNOWLEDGEMENTS

FUNDING

REFERENCES

1   Porter, J.D., Baker, R.S., Ragusa, R.J. and Brueckner, J.K. (1995) Extraocular muscles: basic and clinical aspects of structure and function. Surv. Ophthalmol. **39**, 451–484 CrossRef PubMed

2   Hoh, J.F.Y., Hughes, S., Hugh, G. and Pozgaj, I. (1989) Three hierarchies in skeletal muscle fibre classification: allotype, isotype and phenotype. In UCLA Symposia on Molecular and Cellular Biology (Stockdale, F. and Kedes, L., eds), pp. 15–26, Alan R. Liss, New York

3   Hauschka, S.D. (1994) The embryonic origin of muscle. In Myology (Engel, A.G. and Franzini-Armstrong, C., eds), pp. 3–73, McGraw Hill, New York

4   Spencer, R.F. and Porter, J.D. (2006) Structural organization of the extraocular muscles. In Neuroanatomy of the Oculomotor System (Reviews in Oculomotor Research Vol. 2) (Buttner-Ennever, J.A., ed.), pp. 33–73, Elsevier, New York

5   Ketterer, C., Zeiger, U., Budak, M.T., Rubinstein, N.A. and Khurana, T.S. (2010) Identification of the neuromuscular junction transcriptome of extraocular muscle by laser capture microdissection. Invest. Ophthalmol. Vis. Sci. **51**, 4589–4599 CrossRef PubMed

6   Fischer, M.D., Budak, M.T., Bakay, M., Gorospe, J.R., Kjellgren, D., Pedrosa-Domellof, F., Hoffman, E.P. and Khurana, T.S. (2005) Definition of the unique human extraocular muscle allotype by expression profiling. Physiol. Genomics **22**, 283–291 CrossRef PubMed

7   Fleischer, S. and Inui, M. (1989) Biochemistry and biophysics of excitation–contraction coupling. Annu. Rev. Biophys. Biophys. Chem. **18**, 333–364 CrossRef PubMed

8   Van Petegem, F. (2011) Ryanodine receptors: structure and function. J. Biol. Chem. **287**, 31624–31632 CrossRef

9   Robinson, R., Carpenter, D., Shaw, M.A., Halsall, J. and Hopkins, P. (2006) Mutations in RYR1 in malignant hyperthermia and central core disease. Hum. Mutat. **27**, 977–989 CrossRef PubMed

10 Hwang, J.H., Zorzato, F., Clarke, N.F. and Treves, S. (2012) Mapping domains and mutations on the skeletal muscle ryanodine receptor channel. Trends Mol. Med. **18**, 644–657 CrossRef PubMed

11 Jungbluth, H. (2007) Multi-minicore disease. Orphanet J. Rare Dis. **2**, 31 CrossRef PubMed

12 Jungbluth, H., Zhou, H., Hartley, L., Halliger-Keller, B., Messina, S., Longman, C., Brockington, M., Robb, S.A., Straub, V., Voit, T. et al. (2005) Minicore myopathy with ophthalmoplegia caused by mutations in the ryanodine receptor type 1 gene. Neurology **65**, 1930–1935 CrossRef PubMed

13 Clarke, N.F., Waddell, L.B., Cooper, S.T., Perry, M., Smith, R.L., Kornberg, A.J., Muntoni, F., Lillis, S., Straub, V., Bushby, K. et al. (2010) Recessive mutations in RYR1 are a common cause of congenital fiber type disproportion. Hum. Mutat. **31**, E1544–E1550 CrossRef PubMed

14 Wilmshurst, J.M., Lillis, S., Zhou, H., Pillay, K., Henderson, H., Kress, W., Müller, C.R., Ndondo, A., Cloke, V., Cullup, T. et al. (2010) RYR1 mutations are a common cause of congenital myopathies with central nuclei. Ann. Neurol. **68**, 717–726 CrossRef PubMed

15 Treves, S., Jungbluth, H., Muntoni, F. and Zorzato, F. (2008) Congenital muscle disorders with cores: the ryanodine receptor calcium channel paradigm. Curr. Opin. Pharmacol. **8**, 319–326 CrossRef PubMed

16 Shaaban, S., Ramos-Platt, L., Gilles, F.H., Chan, W.M., Andrews, C., De Girolami, U., Derner, J. and Engle, E.C. (2013) RYR1 mutations as a cause of ophthalmoplegia, facial weakness, and malignant hyperthermia. JAMA Ophthalmol. **131**, 1532–1540 CrossRef PubMed

17 Kaminski, H.J. and Ruff, R.L. (1997) Ocular muscle involvement by myasthenia gravis. Ann. Neurol. **41**, 419–420 CrossRef PubMed

18 Kaminski, H.J., Al-Hakim, M., Leigh, R.J., Katirji, M.B. and Ruff, R.L. (1992) Extraocular muscles are spared in advanced Duchenne dystrophy. Ann. Neurol. **32**, 586–588 CrossRef PubMed

19 Khurana, T.S., Prendergast, R.A., Alameddine, H.S., Tome, F.M., Fardeau, M., Arahata, K., Sugita, H. and Kunkel, L.M. (1995) Absence of extraocular muscle pathology in Duchenne's muscular dystrophy: role for calcium homeostasis in extraocular muscle sparing. J. Exp. Med. **182**, 467–475 CrossRef PubMed

20 Kallestad, K.M., Hebert, S.L., McDonald, A.A., Daniel, M.L., Cu, S.R. and McLoon, L. K. (2011) Sparing of extraocular muscle in aging and muscular distrophies: a myogenig precursor cell hypothesis. Exp. Cell Res. **317**, 873–885 CrossRef PubMed

21 Censier, K., Urwyler, A., Zorzato, F. and Treves, S. (1998) Intracellular calcium homeostasis in human primary muscle cells from malignant hyperthermia-susceptible and normal individuals: effect of overexpression of recombinant wild-type and Arg163Cys mutated ryanodine receptors. J. Clin. Invest. **101**, 1233–1242 CrossRef PubMed

22 Ducreux, S., Zorzato, F., Müller, C., Sewry, C., Muntoni, F., Quinlivan, R., Restagno, G., Girard, T. and Treves, S. (2004) Effect of ryanodine receptor mutations on IL-6 release and intracellular calcium homeostasis in human myotubes from malignant hyperthermia susceptible individuals and patients affected by central core disease. J. Biol. Chem. **279**, 43838–43846 CrossRef PubMed

23 Vukcevic, M., Zorzato, F., Keck, S., Tsakiris, D.A., Keiser, J., Maizels, R.M. and Treves, S. (2013) Gain of function in the immune system caused by a ryanodine receptor 1 mutation. J. Cell Sci. **126**, 3485–3492 CrossRef PubMed

24 Treves, S., Vukcevic, M., Jeannet, P.Y., Levano, S., Girard, T., Urwyler, A., Fischer, D., Voit, T., Jungbluth, H., Lillis, S. et al. (2011) Enhanced excitation-coupled Ca^{2+} entry induces nuclear translocation of NFAT and contributes to IL-6 release from myotubes from patients with central core disease. Hum. Mol. Genet. **20**, 589–600 CrossRef PubMed

25 Rokach, O., Ullrich, N.D., Rausch, M., Mouly, V., Zhou, H., Muntoni, F., Zorzato, F. and Treves, S. (2013) Establishment of a human skeletal muscle-derived cell line: biochemical, cellular and electrophysiological characterization. Biochem. J. **455**, 169–177 CrossRef PubMed

26 Anderson, A.A., Treves, S., Biral, D., Betto, R., Sandon'a, D., Ronjat, M. and Zorzato, F. (2003) The novel skeletal muscle sarcoplasmic reticulum JP-45 protein: molecular cloning, tissue distribution, developmental expression, and interaction with α1.1 subunit of the voltage-gated calcium channel. J. Biol. Chem. **278**, 39987–39992 CrossRef PubMed

27 Cherednichenko, G., Hurne, A.M., Fessenden, J.D., Lee, E.H., Allen, P.D., Beam, K.G. and Pessah, I.N. (2004) Conformational activation of calcium entry by depolarisation of skeletal muscle myotubes. Proc. Natl. Acad. Sci. U.S.A. **101**, 15793–15798 CrossRef PubMed

28 Bannister, R.A., Pessah, I.N. and Beam, K.G. (2008) The skeletal L-type Ca^{2+} current is a major contributor to excitation-coupled Ca^{2+} entry. J. Gen. Physiol. **133**, 79–91 CrossRef

29 Porter, J.D., Khanna, S., Kaminski, H.J., Rao, J.S., Merriam, A.P., Richmonds, C.R., Leahy, P., Li, J. and Andrade, P.H. (2001) Extraocular muscle is defined by a fundamentally distinct gene expression profile. Proc. Natl. Acad. Sci. U.S.A. **98**, 12062–12067 CrossRef PubMed

30 Altick, A.L., Feng, C.Y., Schlauch, K., Johnson, L.A. and von Barthold, C.S. (2012) Differences in gene expression between expression between strabismic and normal human extraocular muscles. Invest. Ophthalmol. Vis. **53**, 5168–5177 CrossRef

31 Kjellgren, D., Ryan, M., Ohlendieck, K., Thornell, L.E. and Pedrosa-Domellöf, F. (2003) Sarco(endo)plasmic reticulum Ca^{2+} ATPases (SERCA1 and-2) in human extraocular muscles. Invest. Ophthalmol. Vis. Sci. **44**, 5057–5062 CrossRef PubMed

32 Wescombe, L., Lahooti, H., Gopinath, B. and Wall, J.R. (2010) The cardiac calsequestrin gene (*CASQ2*) is up-regulated in the thyroid in patients with Grave's ophthalmopathy: support for a role of autoimmunity against calsequestrin as the triggering event. Clin. Endocrinol. **73**, 522–528

33 Slupsky, J.R., Ohnishi, M., Carpenter, M.R. and Reithemier, R.A. (1987) Characterization of cardiac calsequestrin. Biochemistry **26**, 6539–6544 CrossRef PubMed

34 Cala, S.E. and Jones, L.R. (1991) Phosphorylation of cardiac and skeletal muscle calsequestrin isoforms by casein kinase II. J. Biol. Chem. **266**, 391–398 PubMed

35 Sanchez, E.J., Muske, G.R., Criswell, A., Milting, H., Dunker, A.K. and Kang, C. (2011) Phosphorylation of human calsequestin: implications for calcium regulation. Mol. Cell. Biochem. **353**, 195–204 CrossRef PubMed

36 Nabauer, M., Callewaert, G., Cleemann, L. and Morad, M. (1989) Regulation of calcium release is gated by calcium current, not gating charge, in cardiac myocytes. Science **244**, 800–803 CrossRef PubMed

37 Berridge, M.J. (2008) Smooth muscle cell activation mechanisms. J. Physiol. **586**, 5047–5061 CrossRef PubMed

38 Zeiger, U., Mitchell, C.H. and Khurana, T.S. (2010) Superior calcium homeostasis of extraocular muscles. Exp. Eye Res. **91**, 613–622 CrossRef PubMed

39 Heizmann, C.W., Berchtold, M.W. and Rowlerson, A.M. (1982) Correlation of parvalbumin concentration with relaxation speed in mammalian muscles. Proc. Natl. Acad. Sci. U.S.A. **79**, 7243–7247 CrossRef PubMed

40 Stuhlfauth, I., Reininghaus, J., Jockusch, H. and Heizmann, C.W. (1984) Calcium-binding protein, parvalbumin, is reduced in mutant mammalian muscle with abnormal contractile properties. Proc. Natl. Acad. Sci. U.S.A. **81**, 4814–4818 CrossRef PubMed

41 Yoshida, M., Minamisawa, S., Shimura, M., Komazaki, S., Kume, H., Zhang, M., Matsumura, K., Nishi, M., Saito, M., Saeki, Y. et al. (2005) Impaired Ca^{2+} store functions in skeletal and cardiac muscle cells from sarcalumenin-deficient mice. J. Biol. Chem. **280**, 3500–3506 CrossRef PubMed

42 Cherednichenko, G., Hurne, A.M., Fessenden, J., Lee, E.H., Allen, P.D., Beam, K.G. and Pessah, I.N. (2004) Conformational activation of Ca^{2+} entry by depolarization of skeletal myotubes. Proc. Natl. Acad. Sci. U.S.A. **101**, 15793–15798 CrossRef PubMed

43 Mosca, B., Delbono, O., Messi, M.L., Bergamelli, L., Wang, Z.M., Vukcevic, M., Lopez, R., Treves, S., Nishi, M., Takeshima, H. et al. (2103) Enhanced dihydropyridine receptor channel activity restores muscle strength in JP45/CASQ1 double knockout mice. Nat. Commun. **4**, 1541 CrossRef

44 Kalhovde, J.M., Jerkovic, R., Sefland, I., Cordonnier, C., Calantibodiesria, E., Schiaffino, S. and Lømo, T. (2005) "Fast" and "slow" muscle fibres in hindlimb muscles of adult rats regenerate from intrinsically different satellite cells. J. Physiol. **562**, 847–857 CrossRef PubMed

2.1.3 Publication – Structural and functional characterization of human orbicularis oculi and extraocular muscles: so close, but yet so far

Marijana Sekulic-Jablanovic[*], David Goldblum[†], Anja Palmowski-Wolfe[†], Francesco Zorzato[*,‡] and Susan Treves[*,‡]

[*]Departments of Anesthesia and Biomedizin, Basel University Hospital, Hebelstrasse 20, 4031 Basel, Switzerland. [†]Eye Hospital, Basel University Hospital, Mittlere Strasse 91, 4031Basel, Switzerland. [‡]Department of Life Sciences and Biotechnology, General Pathology section, University of Ferrara, Via Borsari 46, 44100 Ferrara, Italy.

Short Title: Subspecialisation of calcium regulation in ocular muscles

To whom correspondence should be addressed: Susan Treves, Departments of Anaesthesia and Biomedicine, Basel University Hospital, Hebelstrasse 20, 4031 Basel, Switzerland. Tel. +41-61-2652373; Fax:+41-61-2653702; E-mail: susan.treves@unibas.ch

Key words: eye muscles, excitation-contraction coupling, calcium homeostasis, gene expression.

Structural and functional characterization of orbicularis oculi and extraocular muscles: so close, but yet so far

Marijana Sekulic-Jablanovic[1], David Goldblum[2], Anja Palmowski-Wolfe[2], Francesco Zorzato[1,3] and Susan Treves[1,3]

[1]Departments of Anesthesia and Biomedizin, Basel University Hospital, Hebelstrasse 20, 4031 Basel, Switzerland.

[2]Eye Hospital, Basel University and Basel University Hospital, Mittlere Strasse 91, 4031Basel, Switzerland.

[3]Department of Life Sciences and Biotechnology, General Pathology section, University of Ferrara, Via Borsari 46, 44100 Ferrara, Italy.

Short Title: Subspecialisation of human ocular muscles

Key words: eye muscles, excitation-contraction coupling, calcium homeostasis, gene expression, utrophin, dystrophin.

To whom correspondence should be addressed: Susan Treves, Departments of Anaesthesia and Biomedicine, Basel University Hospital, Hebelstrasse 20, 4031 Basel, Switzerland. Tel. +41-61-2652373; Fax:+41-61-2653702; E-mail: susan.treves@unibas.ch

ABSTRACT

The *orbicularis oculi* are the sphincter muscles of the eyelids and are involved in modulating facial expression. They differ from both limb and extraocular muscles in their histology and biochemistry. Normal *orbicularis oculi* possess some features which, when present in limb or trunk muscles, would be considered consistent with a chronic myopathy or dystrophy. Weakness of the *orbicularis oculi* muscles is present in neuromuscular disorders affecting the neuromuscular junction and weakness of facial muscles and ptosis have also been described in patients with mutations in *RYR1*. In the present paper, we investigated human *orbicularis oculi* muscles and found that they are functionally more similar to quadriceps than to extraocular muscles in terms of skeletal muscle excitation-contraction coupling components. In fact, they do not express the cardiac isoform of the dihydropyridine receptor, which was found to be highly expressed in extraocular muscles and is most likely responsible for the large depolarization induced calcium influx in the latter muscles. On the other hand, human *orbicularis oculi* and extraocular muscles express high levels of utrophin and very low levels of dystrophin, while quadriceps express dystrophin and low levels of utrophin. The results of the present study highlight the notion that myotubes obtained by explanting satellite cells from different muscles are not functionally identical and retain the physiological characteristics of their muscle of origin. Furthermore our results indicate that sparing of facial and extraocular muscles in patients with Duchenne is the result of the higher levels of utrophin expression.

INTRODUCTION

Excitation-contraction coupling (ECC) is the process whereby an electrical signal, depolarization of the plasma membrane, is converted into a chemical signal, Ca^{2+} release from the sarcoplasmic reticulum, leading to muscle contraction (Caputo 2010). ECC relies on the function of two main Ca^{2+} channels, the voltage sensing dihydropyridine receptor (DHPR) an L-type Ca^{2+} channel present on the transverse tubules and the ryanodine receptor Ca^{2+} channel (RyR) present on the sarcoplasmic reticulum terminal cisternae. In mammalian skeletal muscle ECC is mechanically coupled, that is membrane depolarization causes the α1 subunit ($Ca_v1.1$) of the DHPR to undergo a conformational change causing it to come in direct contact with the RyR1 and leading to release of Ca^{2+} from the sarcoplasmic reticulum (Rios and Pizarro 1991). In mammalian cardiac muscles on the other hand, ECC does not rely on mechanical coupling, but rather influx of Ca^{2+} through the cardiac α1 subunit of the DHPR ($Ca_v1.2$) activates the cardiac RyR2 leading to release of Ca^{2+} from the sarcoplasmic reticulum (Bers 2002). Thus the functional requirements of heart and skeletal muscle are assured by the exquisite specificity of protein isoform expression. This general configuration of skeletal and cardiac ECC protein expression was thought to underlie the function of most striated muscles; however, in a recent study on the protein composition of human extraocular muscles (EOM), we found that hybrid skeletal/cardiac muscle configurations of the ECC machinery can exist. Indeed EOM express both the skeletal and cardiac isoforms of α1 subunit of the DHPR, rely on influx of Ca^{2+} from the extracellular environment and express not only RyR1 but also RyR3 (Sekulic-Jablanovic, Palmowski-Wolfe et al. 2015).

Extraocular muscles (EOM), the fastest muscles in the body, derive from somitomeres (preotic mesodermal segments) (Wright, Hengst et al. 2007). There are six extraocular muscles distributed in three antagonistic pairs of muscles that finely control eye movements (Spencer and Porter 1988); they are innervated by three cranial nerves (III, IV and VI) (Sadeh and Stern 1984). EOM are highly specialized and can be either singly innervated or multiply innervated. These characteristics together with the unique expression of Myosin Heavy Chain-EO (MyHC13) (Schiaffino and Reggiani 2011), sets them apart from all other skeletal muscles, as a distinctive group of highly specialized muscles (Spencer and Porter 1988). The *orbicularis oculi* muscles on the other hand, comprise the sphincter muscles of the eyelids; they are classified as facial muscles and functionally antagonize the *levator palpebrae superior* muscles which are accessory extraocular muscles (Porter, Rafael et al. 1998). The *orbicularis oculi* muscles can be subdivided into orbital, palpebral and lacrimal portions. The orbital portion firmly closes the eyelids and is controlled by voluntary

action; the palpebral portion closes the eyelids gently in involuntary or reflex blinking; the palpebral portion can be further divided into pretarsal, preseptal portion, and ciliary. The lacrimal portion compresses the lacrimal sac, which receives tears from the lacrimal ducts and conveys them into the nasolacrimal duct (Gray and Lewis 1918). The *orbicularis oculi* muscles derive from the mesenchyme in the second pharyngeal arch (Moore, Persaud et al. 2015) and are innervated by the VII cranial nerve (Ouattara, Vacher et al. 2004).

Weakness of the *orbicularis oculi* muscles is often apparent in neuromuscular disorders affecting the neuromuscular junction (Walsh, Newman et al. 2008). Similar to extraocular muscles, they are also one of the first targets of mitochondrial myopathies and Myasthenia gravis, resulting in weakness of eyelid closure usually and ptosis (Walsh, Newman et al. 2008). Facial weakness and ptosis have also been described in patients with recessive *RYR1* mutations (the gene encoding the RyR1) (Taylor, Lachlan et al. 2012), affected by Multi Minicore Disease, Congenital Fiber Type Disproportion and Centronuclear Disease (Jungbluth, Zhou et al. 2005, Treves, Jungbluth et al. 2008, Clarke, Waddell et al. 2010, Wilmshurst, Lillis et al. 2010). On the other hand, EOM are spared in aging, Duchenne muscular dystrophy and Congenital muscular dystrophy when all other skeletal muscles are affected (Kaminski, al-Hakim et al. 1992, Khurana, Prendergast et al. 1995, Kallestad, Hebert et al. 2011). Weakness of the facial musculature caused by any disease is almost certainly accompanied by weakness of the *orbicularis oculi* muscles as well (Walsh, Newman et al. 2008). The present investigation was undertaken in order to identify similarities and differences in ECC and calcium homeostasis in human extraocular muscles, *orbicularis oculi* and quadriceps, in order to identify factors that might contribute to the selective involvement in different neuromuscular disorders. The results of the present investigation show that that the ECC machinery and calcium regulation of human *orbicularis oculi* are more similar to those of quadriceps than of EOM; on the other hand *orbicularis oculi* and EOM are similar in that they both express high levels of utrophin, while quadriceps express dystrophin. This findings explains the sparing of facial and EOM muscles in Duchenne patients; since the ECC machinery between *orbicularis oculi* and quadriceps appears to be similar, our study points to a potential use of autologous facial muscle-derived satellite cells for muscle re-implantation in patients with muscular dystrophy.

MATERIALS AND METHODS

Human muscle cell cultures

Primary muscle cell cultures were established from fragments of quadriceps muscles obtained from biopsies of healthy donors (6 donors), orbicularis oculi muscle samples from patients undergoing eyelid cosmetic procedure or blepharoplasty (5 donors) and extraocular muscle samples obtained from patients undergoing squint corrective surgery (4 donors), as described previously (Censier, Urwyler et al. 1998, Ducreux, Zorzato et al. 2004). Laminin-coated 0.17 mm thick glass coverslips were used for calcium imaging; briefly cells were plated on the coated glass coverslips and allowed to grow in growth medium (Skeletal Muscle Cell Growth Medium, Promo Cell Cat N° C-23080) until cells were approximately 80% confluent at which point they were induced to differentiate into myotubes by switching the medium to differentiation medium (Skeletal Muscle Cell Differentiation medium, Promo Cell, Cat N° C-23061) for 7–14 days. This research was carried out in accordance with the Declaration of Helsinki (2013) of the World Medical Association, and was approved by the Ethikkommission beider Basel (permit N° EK64/12); all subjects gave written informed consent to carry out this work.

Calcium measurements

Fura-2 (Calbiochem) or fluo-4 (Life Technologies, Ltd) at final concentrations of 5 μM were used to load myotubes for 30 min at 37°C, after which the coverslips were mounted onto a 37° C thermostatically controlled chamber that was continuously perfused with Krebs–Ringer medium; individual cells were stimulated by means of a 12- or 8-way 100 mm diameter quartz micromanifold computer-controlled microperfuser (ALA Scientific Instruments, Westbury, NY, USA), as described previously (Ducreux, Zorzato et al. 2004).

The fluorescent ratiometric Ca^{2+} indicator fura-2 was used for monitoring the global changes in the intracellular Ca^{2+} concentration. Online measurements were recorded using a fluorescent Axiovert S100 TV inverted microscope (Carl Zeiss GmbH, Jena, Germany) equipped with a 20× water-immersion FLUAR objective (0.17 N.A.) and filters (BP 340/380, FT 425, BP 500/530) attached to a Cascade 128+ CCD camera Average pixel value for each cell was measured at excitation wavelengths of 340 nm and 380 nm as previously described (Censier, Urwyler et al. 1998, Ducreux, Zorzato et al. 2004). Fura-2 fluorescent ratio signals were converted into $[Ca^{2+}]$ using the curve generated using the fura-2 Ca^{2+} imaging calibration kit from Molecular Probes (Invitrogen) following the manufacturer's instructions and as previously described (Vukcevic, Zorzato et al. 2013). The

dynamics of [Ca^{2+}] influx were investigated by TIRF microscopy using the fast Ca^{2+} indicator Fluo-4 as previously described (Treves, Vukcevic et al. 2011). Myotubes were pre-treated with 50 μM ryanodine (Calbiochem) in order to block Ca^{2+} release through the RyR1 receptor and excitation coupled Ca^{2+} entry (ECCE) was stimulated by the application of 60 mM KCl. Online fluorescence images were acquired using an inverted Nikon TE2000 TIRF microscope equipped with an oil immersion CFI Plan Apochromat 60× TIRF objective (1.49 N.A.) and an electron multiplier Hamamatsu CCD camera C9100–13. Metamorph imaging software from Molecular Devices was used for analysis of the fluorescence changes.

Quantitative Real-time PCR

Total RNA was extracted from muscle biopsies using Trizol (Invitrogen) and following the manufacturer's instructions. RNA was first treated with deoxyribonuclease I (Invitrogen) and then 1000 ng were reverse transcribed using the high-capacity cDNA reverse transcription kit (Applied Biosystems). cDNA was amplified by quantitative real-time PCR using SYBR Green technology (Fast SYBR Green Master Mix, Applied Biosystems) as previously described (Rokach, Ullrich et al. 2013). The sequences of the primers used for gene amplification and quantification is given in Supplementary Table 1. qPCR was performed on a 7500 Fast Real-Time PCR machine from Applied Biosystems using the 7500 software v2.3. Running method for qPCR was including a standard protocol consisted of holding stage at 50°C for 20 seconds and a denaturing step at 95°C for 10 minutes, followed by 40 cycles of denaturing at 95°C for 15 seconds and an extension step at 60°C for 1 min. Gene expression was normalized to expression *ACTN2,* which is present in all muscle fiber types. Results are expressed as fold change compared to expression of the gene in quadriceps muscles.

Immunofluorescence

Differentiated human myotubes grown on a glass coverslip coated with laminin were fixed with 4% paraformaldehyde (made in Phosphate Buffered Saline, PBS), permeabilized with 1% Triton in PBS for 20 min and processed as previously described (Treves, Vukcevic et al. 2011). The following antibodies were used: mouse anti-RyR1 (Thermo Scientific; MA3-925), goat anti-Ca$_v$1.1 (Santa Cruz; sc-8160), rabbit anti-Ca$_v$1.2 (Santa Cruz, sc-25686), AlexaFluor 488 conjugated-chicken anti-rabbit, AlexaFluor 555 conjugated-donkey anti-goat IgG (Life Technologies, Ltd) and AlexaFluor 647 conjugated-goat anti-mouse IgG (Life Technologies, Ltd). Cells were stained with 4',6-diamidino-2-

phenylindole (DAPI) (Life Technologies, Ltd) to visualize nuclei and observed using a Nikon A1R confocal microscope with a CFI Apo TIRF 100X (1.49 N.A.) objective.

Electrophoresis and Immunoblotting

The total sarcoplasmic reticulum fraction was isolated from flash frozen muscle samples (human *orbicularis oculi*, EOM, quadriceps muscles and mouse heart) as previously described (Anderson, Treves et al. 2003) and stored in liquid nitrogen. The protein concentration was determined using the Protein Assay Kit II (Bio-Rad Laboratories) and BSA as a standard. SDS-PAGE, protein transfer on to nitrocellulose membranes and immunostaining were performed as previously described (Anderson, Treves et al. 2003). The following primary antibodies were used: mouse anti-RyR1 (Thermo Scientific, MA3-925), goat anti-Ca$_v$1.1 (Santa Cruz sc-8160), rabbit anti-Ca$_v$1.2 (Santa Cruz, sc-25686) rabbit anti-calsequestrin-1 (Sigma, C-0743), goat anti-SERCA1 (Santa Cruz, sc-8093) and mouse anti-sarcalumenin (Thermo Scientific, MA3-932) anti-dystrophin (Abcam, ab-7164), anti-utrophin (Santa Cruz, sc-15377) and mouse anti-myosin heavy chain (Millipore, 05-716). Secondary peroxidase conjugates were protein G-peroxidase (Sigma, P8170) and peroxidase-conjugated goat anti-mouse IgG) (Sigma, A2304). The immunopositive bands were visualized by chemiluminescence using the Super Signal West Dura kit (Thermo Scientific) or the Chemiluminescence kit from Roche.

For Myosin Heavy Chain, gels were performed as described by Talmadge and Roy (Talmadge and Roy 1993) except that 30 μg total protein extracts were separated and the final acrylamide concentration was 6.5%. Gels were stained with Coomassie Brilliant Blue.

Statistical analysis

Statistical analysis was performed using the Student's t-test for two populations. Values were considered significant when $P < 0.05$. When more than two groups were compared, analysis was performed by the ANOVA test followed by the Bonferroni post hoc test, using the GraphPad Prism 4.0 software. The Origin Pro 8.6 software was used for generating dose-response curves.

RESULTS

Gene and protein expression levels in human orbicularis oculi, EOM and quadriceps muscles

The expression levels of the major gene products involved in skeletal ECC is shown in figure 1A; the values obtained from *orbicularis oculi* were compared to those obtained from quadriceps of healthy donors. The latter muscles were used as reference and the expression level of different genes therein was set to 1. The results show the mean (±SEM) expression level of genes from five pooled biopsy samples normalized to *ACTN2*. The expression of *RYR1* and *SERCA1* transcripts was slightly elevated (approximately 2 fold; *$P<0.05$ Student's *t* test), as was that of *RYR3* and *CACNA1C* (5 and 10 fold, respectively; ***$P<0.0001$ Student's *t* test) while *CACNA1S* expression was similar in *orbicularis oculi* and quadriceps muscles. Interesting, the expression levels of *UTRN* and *DMD* showed ~ a 13 and 16-fold increase, respectively compared to quadriceps muscles (***$P<0.0001$ Student's *t* test). Although it was reported that *MYH13* isoform is exclusively expressed in EOM (Wieczorek, Periasamy et al. 1985), we also found that it is expressed in *orbicularis oculi* (Fig. 1B). *JP45* levels remained unchanged.

Total sarcoplasmic reticulum fractions were prepared and probed with antibodies against the major skeletal ECC proteins as well as $Ca_v1.2$; the intensities of the immunoreactive bands were normalized to sarcalumenin content and are expressed as % expression of that of quadriceps muscles. Surprisingly, at the protein level the content of RyR1, $Ca_v1.1$, SERCA1, and CASQ1 were not changed between *orbicularis oculi* and quadriceps (Fig. 1C). We chose to normalize to SRL content and not to SERCA1 or calsequestrin 1, since by qPCR both SERCA1 and CSQ1 transcripts were significantly increased in *orbicularis oculi*. $Ca_v1.2$, the cardiac isoform of the DHPR could not be detected in western blots of *orbicularis oculi* and quadriceps, but it is clearly present in human EOM and mouse heart which served as positive control (Fig. 1D). Utrophin was highly expressed in both EOM and *orbicularis oculi* but less so in quadriceps (4-fold in OO vs QU *$P< 0.05$), while the opposite was true for dystrophin (OO expressed approximately 50% compared to QU *$P<0.05$) (Fig. 1E).

Ca^{2+} homeostasis in human myotubes derived from *orbicularis oculi*, EOM and quadriceps

Since in a previous study we showed that primary cultures of myotubes explanted from human EOM muscle biopsies had different Ca^{2+} handling properties, in the next series of experiments we compared Ca^{2+} homeostasis in myotubes derived from the three types of muscles. In the first set of experiments cells were perfused with Krebs-Ringer containing 100 μM La^{3+} to prevent influx of extracellular Ca^{2+} and to ensure that the measurements represent skeletal ECC. As shown the KCl-induced Ca^{2+} release was not different in *orbicularis oculi* -derived myotubes compared to quadriceps-derived myotubes (Fig. 2A). Similar results were reported for EOM (Sekulic-Jablanovic, Palmowski-Wolfe et al. 2015) and the curves are not shown in the figure for simplicity. The 4-cmc induced Ca^{2+} release curve was also similar between *orbicularis oculi* - and quadriceps-derived myotubes (Fig. 2B). There were small differences in the resting [Ca^{2+}]$_i$ in the three populations of myotubes while the size of the intracellular Ca^{2+} stores of *orbicularis oculi* -derived myotubes were similar to those of quadriceps -derived myotubes, but significantly lower than those of EOM-derived myotubes (Fig. 2C and D; Student's *t* test ***P<0.0001).

We next investigated excitation-coupled Ca^{2+} entry (ECCE), the process by which membrane depolarisation activates Ca^{2+} influx through the dyhydropiridine receptor (Bannister, Pessah et al. 2009). The top panels of figure 3A show pseudocoloured fluo-4 fluorescent changes in a representative myotube pre-treated with 50 μM ryanodine and stimulated with 60 mM KCl; the pre-treatment with high concentrations of ryanodine is necessary to block Ca^{2+} release through RyR, ensuring that the change in fluo-4 fluorescence is not due to Ca^{2+} release from the SR, but rather from Ca^{2+} influx through the dyhydropiridine receptor. Figure 3B shows a representative Ca^{2+} influx trace initiated by the application of 60 mM KCl in *orbicularis oculi* -derived myotubes (____), quadriceps-derived myotubes (-.-.-.) and EOM-derived myotubes (……). Figure 3C summarizes the results confirming that ECCE in *orbicularis oculi* myotubes is not significantly different from quadriceps myotubes, but almost 3 fold lower compared to EOM derived myotubes.

The difference in Ca^{2+} influx between EOM and *orbicularis oculi* muscles most likely reflects the differential expression of Ca$_v$ isoforms in these groups of muscles. Figure 4 (top panels) shows the subcellular distribution of Ca$_v$1.1 and RyR1 in *orbicularis oculi* myotubes; as seen the distribution of Ca$_v$1.1 (panel A, green) and RyR1 (panel B, red) is

punctuated and unstructured, within an intracellular membrane compartment. Though they lack a mature organization, RyR1 and $Ca_v1.1$ co-localize within the myotube (Fig. 4C). A similar subcellular punctuated distribution of $Ca_v1.1$ (Fig. 4E) and RyR1 (Fig. 4F) is found in EOM myotubes however, there are major differences in the expression and distribution of $Ca_v1.2$, that is, this isoform is exclusively distributed on the plasma membrane of EOM-derived myotubes (Fig. 4H) and could not be detected in *orbicularis oculi* myotubes (Fig. 4D).

DISCUSSION

In the present study we investigated the biochemical and physiological characteristics of *orbicularis oculi* muscles a group of facial muscles that are selectively spared or involved in different neuromuscular disorders. As far as the expression of proteins involved in ECC is concerned, it appears that *orbicularis oculi* muscles are closer to quadriceps than to EOM. Indeed, the content of skeletal muscle sarcoplasmic reticulum proteins was similar between quadriceps and *orbicularis oculi* muscles and differed from that of EOM, as only the latter express proteins characteristic of both cardiac and skeletal muscle ECC (Sekulic-Jablanovic, Palmowski-Wolfe et al. 2015). Surprisingly however, the expression of transcripts did not always match the actual protein content, highlighting the importance of validating arrays or qPCR experiments whenever possible. This was particularly relevant for the difference between the expression of $Ca_v1.2$ and dystrophin whose transcripts were increased >8-10 fold in *orbicularis oculi*, but at the protein level they were barely detectable. The reason for this discrepancy is at present unclear, but agreement between mRNA and protein content occurs only approximately 40% of the time and is influenced by different factors, including mRNA and protein stability, presence of microRNAs, posttranscriptional modifications, with the key role in determining protein abundance being played at the level of translation (Tian, Stepaniants et al. 2004, Vogel, Abreu Rde et al. 2010, Schwanhausser, Busse et al. 2011). A limited overlap in genomic and proteomic data was also reported by Khanna et al. while profiling EOM and leg muscles (Khanna, Merriam et al. 2003).

From a point of view of calcium homeostasis it appears that *orbicularis oculi* muscles are closer to quadriceps than to EOM, since the Ca^{2+}-release dose response curves, the resting $[Ca^{2+}]$, and ionomycin/thapsigargin sensitive intracellular stores, in myotubes derived from the two muscle types were functionally undistinguishable and were clearly different from EOM-derived myotubes. The latter have significantly larger ionomycin/thapsigargin sensitive intracellular stores, express $Ca_v1.2$ and exhibit a 3- fold

larger ECCE. One of the physiological characteristics of EOM muscles is that they are fatigue resistant (Fuchs and Binder 1983) and this may be functionally related to the high levels of expression of $Ca_v1.2$ and consequent large Ca^{2+} influx. The Ca^{2+} influx may be used as a means (i) to activate ECC more rapidly by enhancing Ca^{2+} induced Ca^{2+} release, or (ii) to rapidly replenish intracellular stores. ECCE is less pronounced in myotubes derived from other skeletal muscles, most likely because they lack the cardiac isoform of the alfa1 DHPR subunit.

Though *orbicularis oculi* express a typical skeletal muscle ECC, they also show similarities with EOM in that they express MyHC13 and high levels of RYR3. In humans, *Orbicularis oculi* are composed of 90% type II fibers and 10% type I fibers (Wirtschafter, Lander et al. 1994, Campbell, Williams et al. 1999) but our results show that they also express MyH13. In a study on levator palpebrae and retractor bulbi muscles from different species, it was shown that the latter muscles also express MyHC13 and that this is probably responsible for their rapid contracture times (<10 msec), in fact limb muscles do not express the superfast myosin isoforms and their contracture time is about 5 times longer (Lucas and Hoh 1997). As far as RYR3 expression is concerned, our results are enigmatic since in general RYR3 transcripts are expressed at low levels, if at all, in adult skeletal muscle (Martin, Chapman et al. 1998) and the role of RyR3 is unclear. RYR3KO mice are viable, their muscles show no obvious physiological differences compared to their wild type littermates including no changes in electrically induced Ca^{2+} release and contractile properties of adult muscle fibers, though skeletal muscles from neonatal RYR3 KO mice show decreased tension development (Takeshima, Ikemoto et al. 1996). Although for the time being the function of RyR3s is speculative, it is possible that these channels act as amplifiers of the Ca^{2+} signals; compatibly, RYR3KO mice were reported to have a mild cognitive impairment when tested on a water maize (Balschun, Wolfer et al. 1999), but retrospectively, this may have also been related to a visual impairment. Studies aimed at understanding the role of RyR3 in EOM are currently under way.

Our results concerning the expression of utrophin are interesting and most likely explain why in patients with Duchenne muscular dystrophy ocular and facial muscles are spared. Furthermore the observation that EOM are spared in Duchenne muscular dystrophy even though they exhibit a large Ca^{2+} influx, provides strong evidence that controlled Ca^{2+} influx *per se*, is not deleterious to skeletal muscles as recently proposed (Millay, Goonasekera et al. 2009), but is actually a physiological mechanism used by some skeletal muscles.

Utrophin and dystrophin share considerable sequence and structural homology (Tinsley, Blake et al. 1992, Winder, Gibson et al. 1995) and utrophin can associate with the dystrophin associated complex serving as a link between actin and the extracellular matrix (Matsumura, Ervasti et al. 1992). In mdx mice it is believed that utrophin compensates for the lack of dystrophin (Wakefield, Tinsley et al. 2000). Based on our results and on the fact that mdx knocked out also for utrophin show EOM involvement (Baker, Kearney et al. 2006), it appears that utrophin can functionally compensate *in vivo* for the lack of dystrophin, supporting the current strategies aimed at modulating utrophin expression in the therapy for Duchenne muscular dystrophy (Perkins and Davies 2002, Chakkalakal, Thompson et al. 2005, Guiraud, Squire et al. 2015).

Taken together these studies show that subspecialization of skeletal muscles occurs through multiple factors; while it is true that muscle innervation plays a prominent role, the distribution of a specific muscle within a niche devoted to a precise physiological function is also important. Indeed the term muscle allotype was proposed to describe the different capacities of myogenic cells of different lineages to express a different subset of myofibrillar genes. Since EOM, *Orbicularis oculi* and levator palpebrae (and the retractor bulbi which is present in some mammals but not in humans) are derived from cells from different lineage than those giving rise to limb muscles, their myogenic precursors must be programmed to express different subsets of proteins. The present study substantiates the validity of the muscle allotype hypothesis since we show that satellite cells derived from different muscles are primed and will follow the developmental characteristics of their muscle of origin, a property that can be exploited in laboratories devoted to tissue engineering.

AUTHOR CONTRIBUTION

Marijana Sekulic-Jablanovic performed the experiments, analysed the data and drafted the article. Anja Palmowski-Wolfe and David Goldblum performed surgeries, provided the biopsies and critically revised the paper for important intellectual content. Francesco Zorzato was responsible for conception and design of the experiments, interpretation of data and critically revised the paper for important intellectual content. Susan Treves was responsible for conception and design of the experiments, collection, analysis and interpretation of data and drafted the article.

ACKNOWLEDGEMENTS

FOOTNOTES: Ca_v, α1 subunit of the dihydropyridine receptor; CSQ, calsequestrin; DHPR, dihydropyridine receptor; ECC, excitation–contraction coupling; ECCE, excitation-coupled Ca^{2+} entry; EOM, extraocular muscle; OO, *orbicularis oculi*; QU, quadriceps muscle; qPCR, quantitative real-time PCR; RyR, ryanodine receptor; SERCA, sarcoplasmic/endoplasmic reticulum Ca^{2+} -ATPase; TIRF, total internal reflection fluorescence

REFERENCES

Anderson, A. A., S. Treves, D. Biral, R. Betto, D. Sandona, M. Ronjat and F. Zorzato. 2003. The novel skeletal muscle sarcoplasmic reticulum JP-45 protein. Molecular cloning, tissue distribution, developmental expression, and interaction with alpha 1.1 subunit of the voltage-gated calcium channel. *J. Biol. Chem.* 278: 39987-39992.

Baker, P. E., J. A. Kearney, B. Gong, A. P. Merriam, D. E. Kuhn, J. D. Porter and J. A. Rafael-Fortney. 2006. Analysis of gene expression differences between utrophin/dystrophin-deficient vs mdx skeletal muscles reveals a specific upregulation of slow muscle genes in limb muscles. *Neurogenetics* 7: 81-91.

Balschun, D., D. P. Wolfer, F. Bertocchini, V. Barone, A. Conti, W. Zuschratter, L. Missiaen, H. P. Lipp, J. U. Frey and V. Sorrentino. 1999. Deletion of the ryanodine receptor type 3 (RyR3) impairs forms of synaptic plasticity and spatial learning. *EMBO J.* 18: 5264-5273.

Bannister, R. A., I. N. Pessah and K. G. Beam. 2009. The skeletal L-type Ca(2+) current is a major contributor to excitation-coupled Ca(2+) entry. *J. Gen. Physiol.* 133: 79-91.

Bers, D. M. 2002. Cardiac excitation-contraction coupling. *Nature* 415: 198-205.

Campbell, S. P., D. A. Williams, B. R. Frueh and G. S. Lynch. 1999. Contractile activation characteristics of single permeabilized fibres from levator palpebrae superioris, orbicularis oculi and vastus lateralis muscles from humans. *J. Physiol.* 519 : 615-622.

Caputo, C. 2010. Pharmacological Investigations of Excitation-Contraction Coupling. *Comprehensive Physiology*, John Wiley & Sons, Inc.

Censier, K., A. Urwyler, F. Zorzato and S. Treves. 1998. Intracellular calcium homeostasis in human primary muscle cells from malignant hyperthermia-susceptible and normal individuals. Effect Of overexpression of recombinant wild-type and Arg163Cys mutated ryanodine receptors. *J. Clin. Invest.* 101: 1233-1242.

Chakkalakal, J. V., J. Thompson, R. J. Parks and B. J. Jasmin. 2005. Molecular, cellular, and pharmacological therapies for Duchenne/Becker muscular dystrophies. *FASEB. J.* 19: 880-891.

Clarke, N. F., L. B. Waddell, S. T. Cooper, M. Perry, R. L. Smith, A. J. Kornberg, F. Muntoni, S. Lillis, V. Straub, K. Bushby, M. Guglieri, M. D. King, M. A. Farrell, I. Marty, J. Lunardi, N. Monnier and K. N. North. 2010. Recessive mutations in RYR1 are a common cause of congenital fiber type disproportion. *Hum. Mutat.* 31: E1544-1550.

Ducreux, S., F. Zorzato, C. Muller, C. Sewry, F. Muntoni, R. Quinlivan, G. Restagno, T. Girard and S. Treves. 2004. Effect of ryanodine receptor mutations on interleukin-6 release and intracellular calcium homeostasis in human myotubes from malignant hyperthermia-susceptible individuals and patients affected by central core disease. *J. Biol. Chem.* 279: 43838-43846.

Fuchs, A. F. and M. D. Binder. 1983. Fatigue resistance of human extraocular muscles. *J. Neurophysiol.* 49: 28-34.

Gray, H. and W. H. Lewis. 1918. *Anatomy of the Human Body*, Lea & Febiger.

Guiraud, S., S. E. Squire, B. Edwards, H. Chen, D. T. Burns, N. Shah, A. Babbs, S. G. Davies, G. M. Wynne, A. J. Russell, D. Elsey, F. X. Wilson, J. M. Tinsley and K. E. Davies. 2015. Second-generation compound for the modulation of utrophin in the therapy of DMD. *Hum. Mol. Genet.* 24: 4212-4224.

Jungbluth, H., H. Zhou, L. Hartley, B. Halliger-Keller, S. Messina, C. Longman, M. Brockington, S. A. Robb, V. Straub, T. Voit, M. Swash, A. Ferreiro, G. Bydder, C. A. Sewry, C. Muller and F. Muntoni. 2005. Minicore myopathy with ophthalmoplegia caused by mutations in the ryanodine receptor type 1 gene. *Neurology* 65: 1930-1935.

Kallestad, K. M., S. L. Hebert, A. A. McDonald, M. L. Daniel, S. R. Cu and L. K. McLoon. 2011. Sparing of extraocular muscle in aging and muscular dystrophies: a myogenic precursor cell hypothesis. *Exp. Cell. Res.* 317: 873-885.

Kaminski, H. J., M. al-Hakim, R. J. Leigh, M. B. Katirji and R. L. Ruff. 1992. Extraocular muscles are spared in advanced Duchenne dystrophy. *Ann. Neurol.* 32: 586-588.

Khanna, S., A. P. Merriam, B. Gong, P. Leahy and J. D. Porter. 2003. Comprehensive expression profiling by muscle tissue class and identification of the molecular niche of extraocular muscle. *FASEB. J.* 17: 1370-1372.

Khurana, T. S., R. A. Prendergast, H. S. Alameddine, F. M. Tome, M. Fardeau, K. Arahata, H. Sugita and L. M. Kunkel. 1995. Absence of extraocular muscle pathology in Duchenne's muscular dystrophy: role for calcium homeostasis in extraocular muscle sparing. *J. Exp. Med.* 182: 467-475.

Lucas, C. A. and J. F. Hoh. 1997. Extraocular fast myosin heavy chain expression in the levator palpebrae and retractor bulbi muscles. *Invest. Ophthalmol. Vis. Sci.* 38: 2817-2825.

Martin, C., K. E. Chapman, J. R. Seckl and R. H. Ashley. 1998. Partial cloning and differential expression of ryanodine receptor/calcium-release channel genes in human tissues including the hippocampus and cerebellum. *Neuroscience* 85: 205-216.

Matsumura, K., J. M. Ervasti, K. Ohlendieck, S. D. Kahl and K. P. Campbell. 1992. Association of dystrophin-related protein with dystrophin-associated proteins in mdx mouse muscle. *Nature* 360: 588-591.

Millay, D. P., S. A. Goonasekera, M. A. Sargent, M. Maillet, B. J. Aronow and J. D. Molkentin. 2009. Calcium influx is sufficient to induce muscular dystrophy through a TRPC-dependent mechanism. *Proc. Natl. Acad. Sci. U. S. A.* 106: 19023-19028.

Moore, K. L., T. V. N. Persaud and M. G. Torchia. 2015. The Developing Human: Clinically Oriented Embryology. *Elsevier Health Sciences.*

Ouattara, D., C. Vacher, J. J. A. de Vasconcellos, S. Kassanyou, G. Gnanazan and B. N'Guessan. 2004. Anatomical study of the variations in innervation of the orbicularis oculi by the facial nerve. *Surg. Radiol. Anat.* 26: 51-53.

Perkins, K. J. and K. E. Davies. 2002. The role of utrophin in the potential therapy of Duchenne muscular dystrophy. *Neuromuscul. Disord.* 12 Suppl 1: S78-89.

Porter, J. D., J. A. Rafael, R. J. Ragusa, J. K. Brueckner, J. I. Trickett and K. E. Davies. 1998. The sparing of extraocular muscle in dystrophinopathy is lost in mice lacking utrophin and dystrophin. *J. Cell Sci.* 111: 1801-1811.

Rios, E. and G. Pizarro. 1991. Voltage sensor of excitation-contraction coupling in skeletal muscle. *Physiol. Rev.* 71: 849-908.

Rokach, O., N. D. Ullrich, M. Rausch, V. Mouly, H. Zhou, F. Muntoni, F. Zorzato and S. Treves. 2013. Establishment of a human skeletal muscle-derived cell line: biochemical, cellular and electrophysiological characterization. *Biochem. J.* 455: 169-177.

Sadeh, M. and L. Z. Stern. 1984. Observations on the innervation of human extraocular muscles. *J. Neurol. Sci.* 66: 295-305.

Schiaffino, S. and C. Reggiani. 2011. Fiber types in mammalian skeletal muscles. *Physiol. Rev.* 91: 1447-1531.

Schwanhausser, B., D. Busse, N. Li, G. Dittmar, J. Schuchhardt, J. Wolf, W. Chen and M. Selbach. 2011. Global quantification of mammalian gene expression control. *Nature* 473: 337-342.

Sekulic-Jablanovic, M., A. Palmowski-Wolfe, F. Zorzato and S. Treves. 2015. Characterization of excitation-contraction coupling components in human extraocular muscles. *Biochem. J.* 466: 29-36.

Spencer, R. F. and J. D. Porter. 1988. Structural organization of the extraocular muscles. *Rev. Oculomot. Res.* 2: 33-79.

Takeshima, H., T. Ikemoto, M. Nishi, N. Nishiyama, M. Shimuta, Y. Sugitani, J. Kuno, I. Saito, H. Saito, M. Endo, M. Iino and T. Noda. 1996. Generation and characterization of mutant mice lacking ryanodine receptor type 3. *J. Biol. Chem.* 271: 19649-19652.

Talmadge, R. J. and R. R. Roy. 1993. Electrophoretic separation of rat skeletal muscle myosin heavy-chain isoforms. *J. Appl. Physiol.* **75**: 2337-2340.

Taylor, A., K. Lachlan, R. M. Manners and A. J. Lotery. 2012. A study of a family with the skeletal muscle RYR1 mutation (c.7354C>T) associated with central core myopathy and malignant hyperthermia susceptibility. *J. Clin. Neurosi.* 19: 65-70.

Tian, Q., S. B. Stepaniants, M. Mao, L. Weng, M. C. Feetham, M. J. Doyle, E. C. Yi, H. Dai, V. Thorsson, J. Eng, D. Goodlett, J. P. Berger, B. Gunter, P. S. Linseley, R. B. Stoughton, R. Aebersold, S. J. Collins, W. A. Hanlon and L. E. Hood. 2004. Integrated genomic and proteomic analyses of gene expression in Mammalian cells. *Mol. Cell Proteomics* 3: 960-969.

Tinsley, J. M., D. J. Blake, A. Roche, U. Fairbrother, J. Riss, B. C. Byth, A. E. Knight, J. Kendrick-Jones, G. K. Suthers, D. R. Love. 1992. Primary structure of dystrophin-related protein. *Nature* 360: 591-593.

Treves, S., H. Jungbluth, F. Muntoni and F. Zorzato. 2008. Congenital muscle disorders with cores: the ryanodine receptor calcium channel paradigm. *Curr. Opin. Pharmacol.* 8: 319-326.

Treves, S., M. Vukcevic, P. Y. Jeannet, S. Levano, T. Girard, A. Urwyler, D. Fischer, T. Voit, H. Jungbluth, S. Lillis, F. Muntoni, R. Quinlivan, A. Sarkozy, K. Bushby and F. Zorzato. 2011. Enhanced excitation-coupled Ca(2+) entry induces nuclear translocation of NFAT and contributes to IL-6 release from myotubes from patients with central core disease. *Hum. Mol. Genet.* 20: 589-600.

Vogel, C., S. Abreu Rde, D. Ko, S. Y. Le, B. A. Shapiro, S. C. Burns, D. Sandhu, D. R. Boutz, E. M. Marcotte and L. O. Penalva. 2010. Sequence signatures and mRNA concentration can explain two-thirds of protein abundance variation in a human cell line. *Mol. Syst. Biol.* 6: 400.

Vukcevic, M., F. Zorzato, S. Keck, D. A. Tsakiris, J. Keiser, R. M. Maizels and S. Treves. 2013. Gain of function in the immune system caused by a ryanodine receptor 1 mutation. *J. Cell Sci.* 126: 3485-3492.

Wakefield, P. M., J. M. Tinsley, M. J. Wood, R. Gilbert, G. Karpati and K. E. Davies. 2000. Prevention of the dystrophic phenotype in dystrophin/utrophin-deficient muscle following adenovirus-mediated transfer of a utrophin minigene. *Gene Ther.* 7: 201-204.

Walsh, F. B., N. J. Newman, W. F. Hoyt, N. R. Miller and V. Biousse. 2008. Walsh and Hoyt's Clinical Neuro-ophthalmology: The Essentials. *Wolters Kluwer Health/Lippincott Williams & Wilkins.*

Wieczorek, D. F., M. Periasamy, G. S. Butler-Browne, R. G. Whalen and B. Nadal-Ginard. 1985. Co-expression of multiple myosin heavy chain genes, in addition to a tissue-specific one, in extraocular musculature. *J. Cell Biol.* 101: 618-629.

Wilmshurst, J. M., S. Lillis, H. Zhou, K. Pillay, H. Henderson, W. Kress, C. R. Muller, A. Ndondo, V. Cloke, T. Cullup, E. Bertini, C. Boennemann, V. Straub, R. Quinlivan, J. J. Dowling, S. Al-Sarraj, S. Treves, S. Abbs, A. Y. Manzur, C. A. Sewry, F. Muntoni and H. Jungbluth. 2010. RYR1 mutations are a common cause of congenital myopathies with central nuclei. *Ann. Neurol.* 68: 717-726.

Winder, S. J., T. J. Gibson and J. Kendrick-Jones. 1995. Dystrophin and utrophin: the missing links! *FEBS Lett.* 369: 27-33.

Wirtschafter, J. D., T. Lander, R. H. Baker, M. Stevanovic, J. Kirsch and L. K. McLoon. 1994. Heterogeneous length and in-series arrangement of orbicularis oculi muscle:

individual myofibers do not extend the length of the eyelid. *Trans. Am. Ophthalmol. Soc.* 92: 71-88.

Wright, K. W., T. C. Hengst, S. Gilbert, P. H. Spiegel, F. Cogswell and L. S. Thompson. 2007. Handbook of Pediatric Neuro-Ophthalmology. *Springer New York.*

FIGURE LEGENDS

Figure 1: Expression of major excitation-contraction coupling transcripts and proteins in human _orbicularis oculi_ muscle biopsies. (A) Gene expression was carried out by qPCR as described in the Materials and Methods section. Each reaction was carried out in triplicate, in pooled muscle samples from 5 biopsies from different individuals. Expression levels were normalized to _ACTN2_ expression. Results are expressed as mean fold change of transcripts in _orbicularis oculi_ compared to quadriceps, the latter was set as 1. Results were analyzed using the Student's _t_-test (*p<0.05; ***P<0.0001). **(B)** _MYH13_ gene expression was carried out by qPCR as described in Materials and Methods section. Each reaction was carried out in triplicate, in pooled muscle samples from 5 biopsies from different individuals. Expression levels were normalized to _ACTN2_ expression. Results are expressed as mean fold change of transcripts in _orbicularis oculi_ compared to quadriceps, the latter were set as 1. Results were analyzed using the Student's _t_-test (***p<0.0001). Insert shows MyHC protein expression in EOM and _orbicularis oculi_ muscle homogenates; 10 and 30 μg protein were loaded per lane, respectively. Gels and conditions were as described in the Materials and Methods section. **(C)** Western blot analysis of total sarcoplasmic reticulum proteins in human _orbicularis oculi_ and quadriceps muscles. Thirty micrograms of protein were loaded per lane and separated on 6% SDS-PAGE or 10% SDS-PAGE. Blots were probed with the indicated antibodies. Bar histograms represent the mean (± SEM) band intensity normalized to sarcalumenin content. **(D)** Western blot of human quadriceps, EOM, _orbicularis oculi_ and mouse heart (positive control) total sarcoplasmic reticulum proteins, probed with $Ca_v1.2$ antibody. Thirty micrograms of protein was loaded per lane and separated on 6% SDS-PAGE. **(E)** Western blot of total muscle extracts; 30 μg of protein were loaded per lane, separated on 6% SDS-PAGE and probed with anti-utrophin (top) and anti-dystrophin (bottom) antibodies. Bar histograms represent the mean (± SEM) band intensity normalized to MyHC content (* P<0.05 Student's _t_ test).

Figure 2: Calcium homeostasis of _orbicularis oculi_-derived myotubes compared to lquadriceps and EOM muscle-derived myotubes. Myotubes were loaded with 5 μM fura-2 and perfused with Krebs–Ringer medium containing 2 mM $CaCl_2$. For KCl- and 4-cmc induced Ca^{2+} release, individual cells were perfused with Krebs–Ringer plus 100 μM La^{3+} and the indicated concentration of agonist was applied using a microperfusion system. **(A)** KCl dose response curve **(B)** 4-cmc dose response curve- _Orbicularis oculi_-derived myotubes filled circles, continuous line and quadriceps derived myotubes empty circles, dotted line. Curves show the changes in peak calcium, expressed as $[Ca^{2+}]$ in nM. Each point

represents the mean (±SEM) of minimum 5-12 different cells. **(C)** Mean (±SEM) resting [Ca^{2+}]. *P<0.05; **P<0.001. **(D)** Total amount of Ca^{2+} in the sarcoplasmic reticulum. The total amount of rapidly releasable Ca^{2+} in the stores was determined by calculating the area under the curve of the transient induced by the application of 1 μM ionomycin, plus 1 μM thapsigargin in Krebs-Ringer containing 0.5 mM EGTA. Values represent the mean (± SEM) calculated area under the curve. Student's *t* test ***p<0.0001. For quadriceps-derived myotubes cells from 6 donors were measured, for *orbicularis oculi*-derived myotubes cells from 5 donors and for EOM-derived myotubes cells from 4 donors.

Figure 3: Depolarization-induced Ca^{2+} influx in *orbicularis oculi*, EOM and quadriceps derived myotubes. Ca^{2+} influx induced by the addition of 60 mM KCl was monitored using a TIRF microscope in myotubes pre-incubated with 50 μM ryanodine to block RyR1 mediated Ca^{2+} release and loaded with 5 μM fluo-4. **(A)** Top panels, pseudocolored ratiometric images (peak fluorescence after addition of KCl/resting fluorescence) of fluo-4 fluorescence changes after application of 60 KCl to *orbicularis oculi*-derived myotubes (**A1** EpiSRIC image, **A2-5** pseudocolored ratiometric images at 2, 5, 11 and 20 sec after the addition of KCl). **(B)** Representative excitation-coupled Ca^{2+} entry (ECCE) trace showing changes in fluo-4 fluorescence in a EOM-derived myotube (. . . . .), quadriceps derived myotube (._._.) and *orbicularis oculi* (_____). **(C)** Mean (±SEM) peak increase of fluo-4 fluorescence induced by 60 mM KCl in human *orbicularis oculi*-derived myotubes (white bar), EOM derived-myotubes (gray bar) compared quadriceps-derived myotubes (black bar). Experiments were performed on cells obtained from at least 4 different biopsies and results were averaged. Statistical analysis was performed using the ANOVA test; *** P<0.0001.

Figure 4: Cellular localization of RyR1 and $Ca_v1.1$ in differentiated *orbicularis oculi* - derived myotubes. Human myotubes were visualized with a Nikon A1R confocal microscope equipped with a CFI Apo TIRF 100X objective (1.49 N.A.) and stained as described in the Materials and Methods section. Top panels *orbicularis oculi*, bottom panels EOM. Panels **A** and **E** anti-$Ca_v1.1$ (green), **B** and **F** anti-RyR1 (red), **C and G**, merged image of anti-RyR1, anti-$Ca_v1.1$ and DAPI (blue); orange pixels show co-localization between RyR1 and $Ca_v1.1$. Panels **D** and **H**, anti-$Ca_v1.2$ (green). Bar indicates 20 μm.

Figure 1

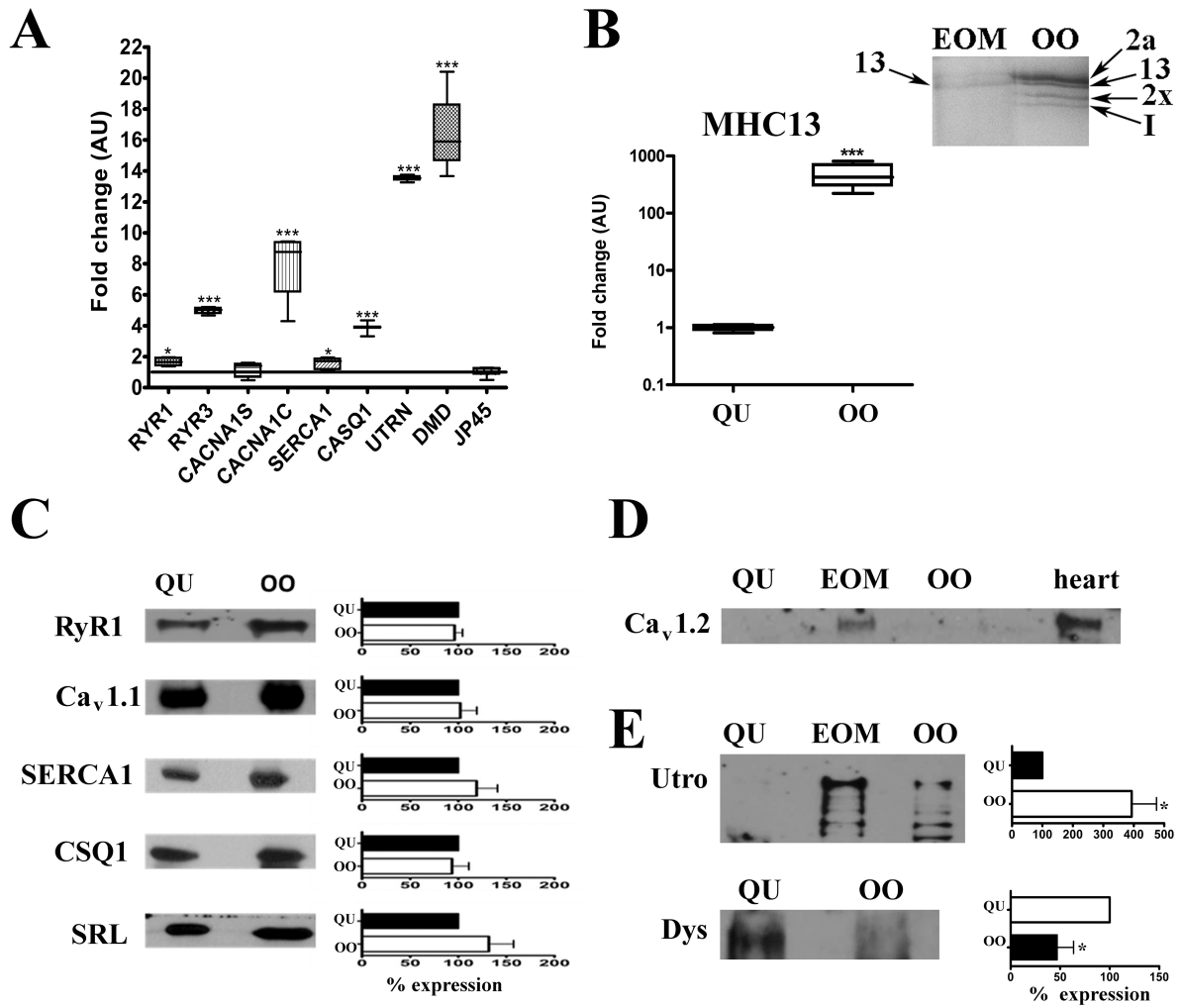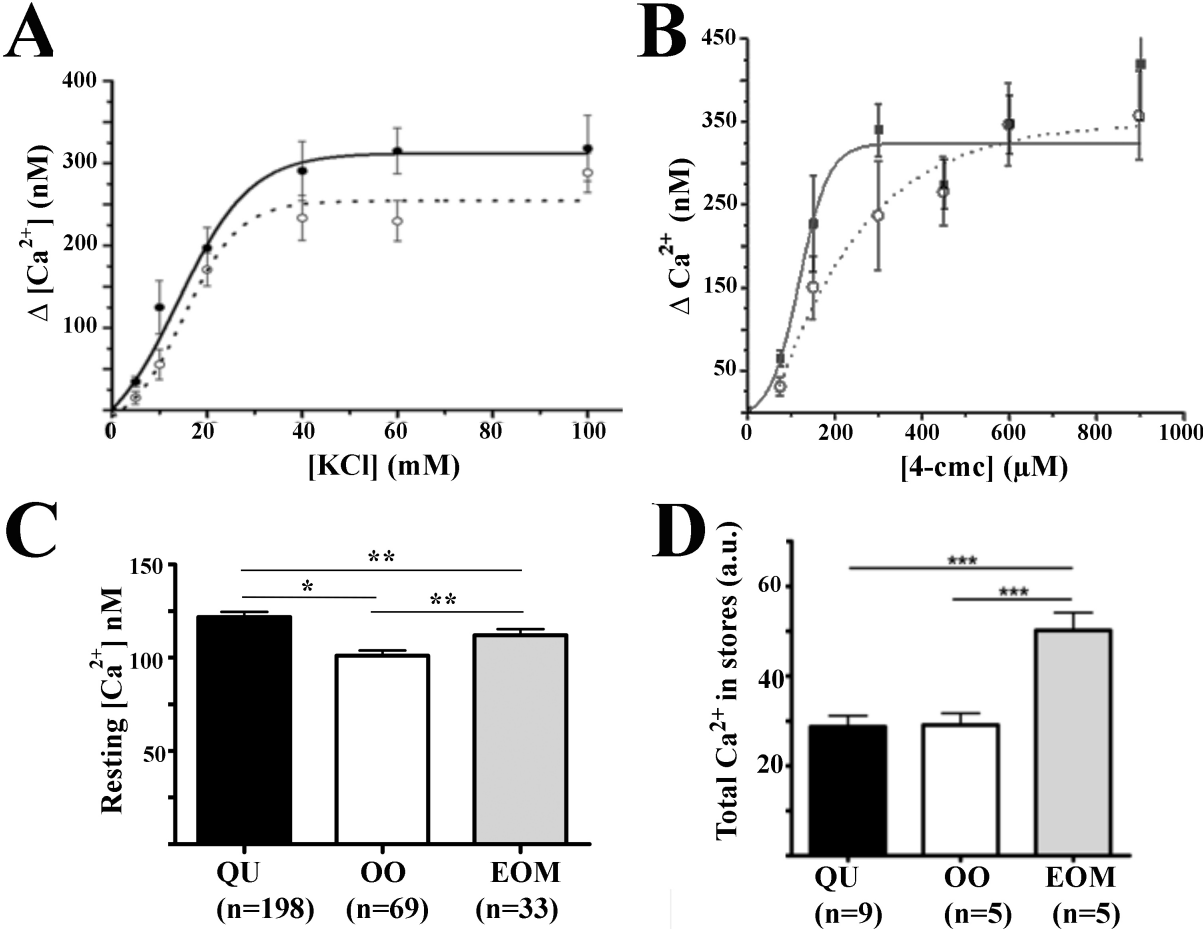**Figure 2**

Figure 3

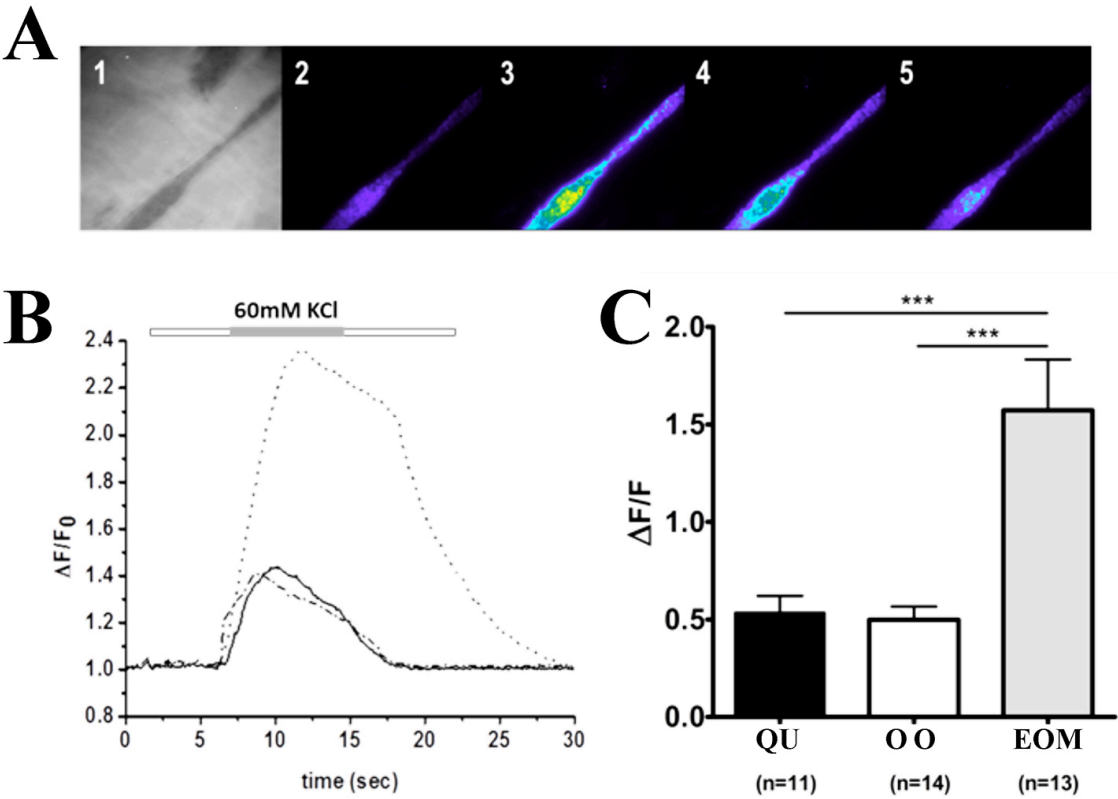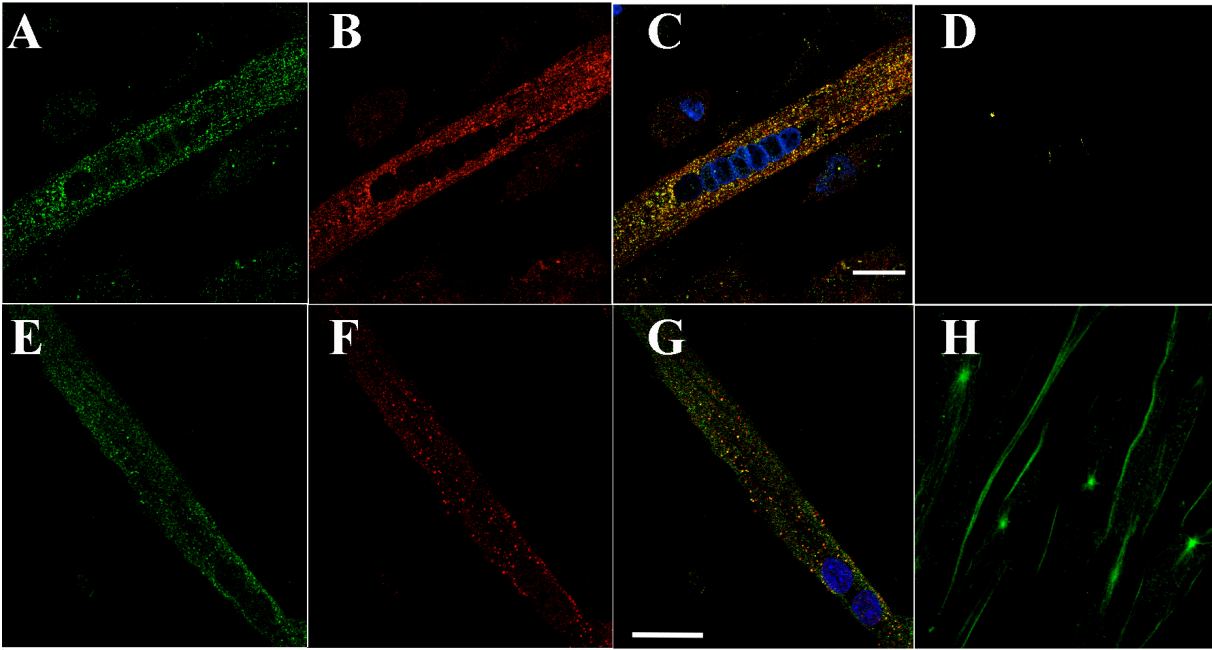**Figure 4**

2.2 Ryanodine receptors 1 and 3 – functional consequences of the mutations in human *RYR1* or the absence of *RYR3* in mice

2.2.1 Introduction

Ryanodine receptor 1 plays a crucial role in the process of the excitation contraction coupling in skeletal muscle. According to our study on human EOM, the expression of this receptor is decreased in EOM compared to that of human leg muscles. We were intrigued by this finding, as EOMs belong to the group of specialized skeletal muscles. Previous investigations in patients with recessive mutations in *RYR1* where one allele carries missense mutation and other stop mutation, indicated the presence of the weakness of the EOM muscles, known as ophthalmoplegia. In those patients muscle biopsies show a decrease in the content of the RyR1 protein [171]. For the purpose of investigating the effects of mutations found in these patients, we subcloned human *RYR1* cDNA into a mammalian bicistronic vector and used it for the insertion of specific mutations.

As mentioned in the previous sections RyR3 does not directly participate in ECC, as mature muscles express either very little or no RyR3 and still show normal excitation-contraction coupling and *RYR3* KO mice show no muscle impairment, no changes in muscle development and no alteration of other studied physiological parameters, except for a reported cognitive impairment [172].

In light of our findings on the low levels of RyR1 expression in EOM together with the low levels of skeletal alfa 1s of the DHPR and the presence of the cardiac alfa 1c isoform, we were prompted to investigate the EOM function in the *RYR3* KO mice in fact we hypothesize that this animal model has an impairment of EOM function and this was not investigated in previous studies.

2.2.2 Subcloning and introducing the mutations in human *RYR1*

In order to better understand the consequences of *RYR1* mutations, the human *RYR1* mRNA from healthy donor was used as template for cDNA synthesis which was further subcloned and finally used to establish a stably transfected cell culture of HEK 293 expressing RyR1. Furthermore RyR1-vector construct was used for introducing specific mutations found in patients.
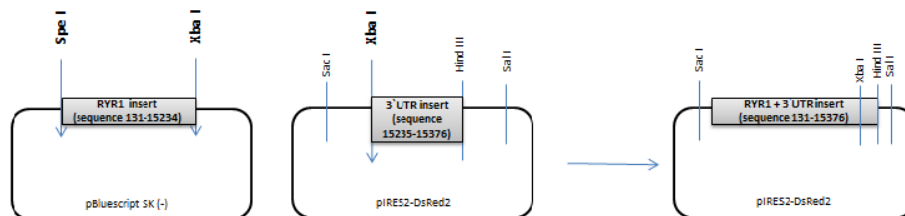
Assembling the RyR1-vector construct

RYR1 cDNA was synthesized using mRNA isolated from human skeletal muscle as a template (transcript variant 2, NCBI Reference Sequence: NM_001042723.1). When compared with the NCBI nucleotide database entry, six nucleotide changes that do not affect the amino acid sequence of the RyR1 protein were detected by sequencing. These were: c.724A>G, c.1207T>C, c.1798G>A, c.2416 C>T, c.3073G>A and c.9187C>T.

The full length *RYR1* cDNA was assembled through a series of subcloning steps in which fragments of different sizes (from 600bp-2629bp) were amplified by insertion in the pBSK (-) vector, followed by ligation and joining one insert at a time to obtain the full length construct (Fig. 17). Each fragment was checked by direct sequencing before being ligated to the next clone. The final complete *RYR1* cDNA sequence inserted in pBSK(-) was confirmed to be from the first ATG start codon to the stop codon (positions 131-15234 of the *RYR1* sequence). The full length *RYR1* cDNA was inserted in pIRES-DsRed vector in order to achieve transfection and expression in mammalian cells.
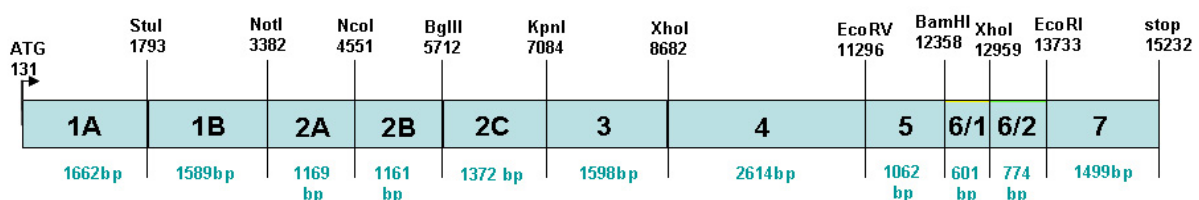
Figure 17: *RYR1* cDNA subcloning scheme. In the scheme are represented the restriction sites chosen to break the total cDNA into smaller clones to be used in a second phase of getting the full length cDNA.

3`untranslated region of *RYR1* was first inserted in pBSK(-) vector through digestion with HindIII/XbaI and this new construct was digested with SacI/SalI in order to transfer 3`UTR in pIRES-DsRed vector. In the final step, *RYR1* insert was cut out from the pBSK(-) with SpeI/XbaI and inserted in XbaI digested 3`UTR in pIRES-DsRed construct (Fig. 18).

Figure 18: Final assembling of *RYR1* insert with its 3`UTR fragment in pIRES-DsRed vector.

Stable transfection

HEK293 were stably transfected with the *RYR1* cDNA construct outlined above in order to ascertain that the appropriate recombinant protein was obtained. HEK293 cells were chosen for transfection because they do not express endogenous RyR1. The stably transfected clones D2 and A5 were observed for the DsRed fluorescence and as shown in figure 19, all the cells were positive for the DsRed signal. Transfected cells were collected and the microsomal fraction was prepared. As can be seen in figure 20, a high molecular weight immunoreactive band was present in the microsomes of transfected cells. The size of the immunoreactive band matched that of RyR1 present in rabbit terminal cisternae.
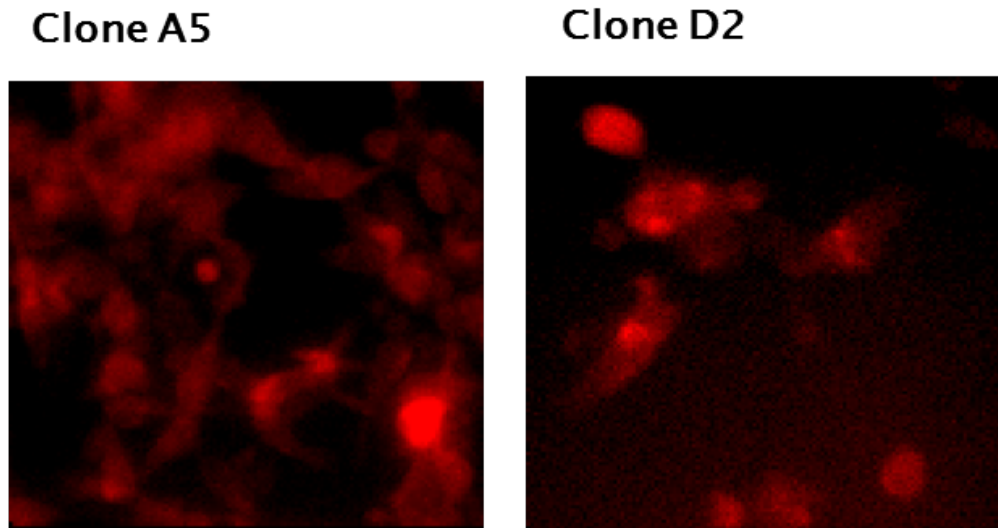
Figure 19. DsRed fluorescence present in the stably transfected HEK293 clones. Cells from clones A5 and D2 grown on laminin coated glass coverslips and observed for the DsRed fluorescence.
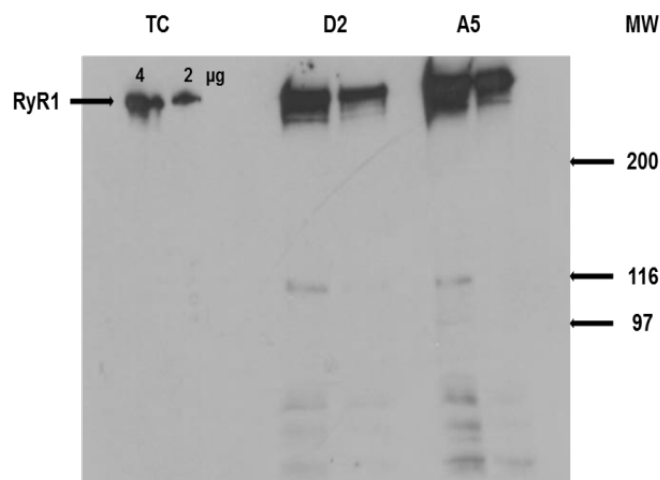
Figure 20: Western blot of microsomes from transfected Hek293 cells. (clones A5 and D2) 40μg and 80 μg protein were loaded per lane for each clone and separated on a 5% SDS-PAG. The blot was incubated with 0.5 μg/ml mAb 34C anti-RyR1 followed by anti–mouse peroxidase and the reaction was visualized by chemiluminescence.

The lanes on the left (positive control) were loaded with 4 and 2 μg rabbit skeletal muscle terminal cisternae and the arrow indicates the immunoreactive band corresponding to the RyR1 protomer.

Stably transfected cells from clone A5 were grown on a glass coverslip and fixed with 4% paraformaldehyde, permeabilized with 1% Triton in PBS for 20 min and stained with the mouse anti-RyR1 antibody. The staining was positive for the presence of the RyR1 protein in the cells as well as previously shown DsRed fluorescence (Fig. 21).
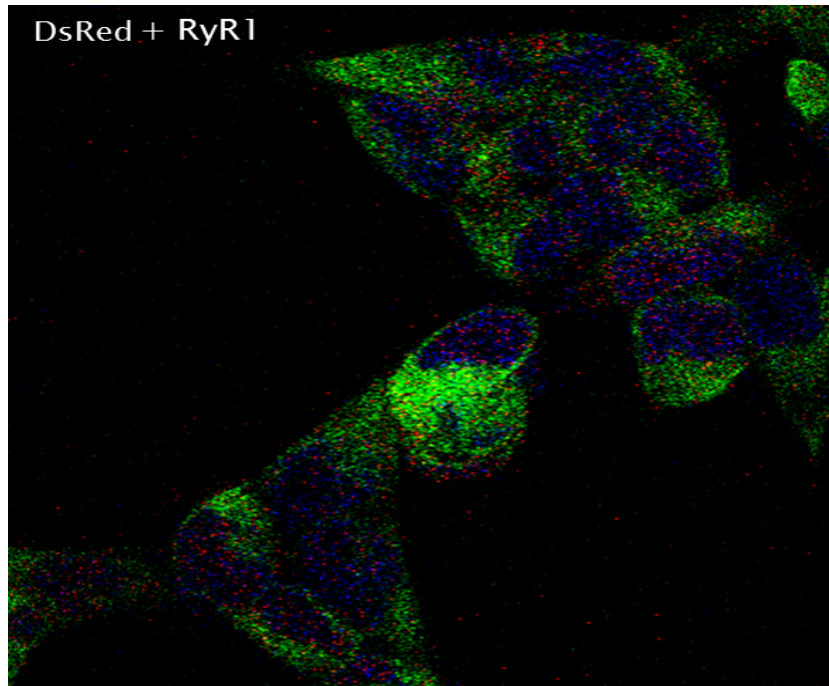
Figure 21: Cellular localization of RyR1 and DsRed. Merged image of cells stained with anti-RyR1 (green), nuclear counterstain DAPI (blue) and expressed DsRed protein fluorescence (red). Visualized with a Nikon A1R confocal microscope equipped with a CFI Apo TIRF 100X objective (1.49N.A.)

Ca^{2+} measurments

Clones were further tested for RyR1 function by monitoring calcium changes after stimulation with the RyR1 agonist 4-chloro-m-cresol (600μM) and caffeine (10mM). Positive clones were expanded and allowed to grow on glass coverslips; when enough cells were present, they were loaded with the ratiometric Ca^{2+} indicator fura-2 and changes in fluorescence were monitored. Figure 22 shows the results of a representative experiment. Traces A and B are showing that tranfected HEK293 respond to the addition of 10 mM caffeine and 600μM 4-cmc respectively. Panel C shows the pseudo colored ratiometric changes in fura-2 fluorescence elicited by the addition of 600μM 4-cmc in the latter cells.
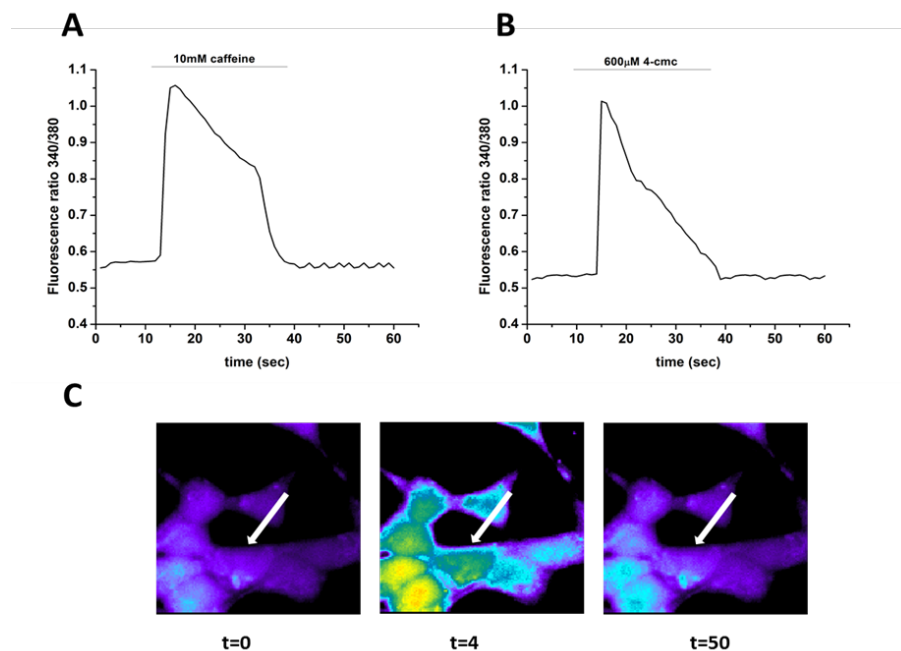
Figure 22: HEK293 cells transfected with human RYR1 respond to caffeine and 4-cmc addition. Cells from selected clones were grown on glass coverslips, loaded with 10μM fura-2 Ca^{2+} indicator and stimulated with **(A)** 10 mM caffeine and **(B)** 600μM 4-cmc in Krebs Ringer. **(C)** photographs of cells B showing 3 time points during caffeine stimulation. The trace shown in panel B was obtained from the cell indicated by the arrow in trace C.

After the stability of the expression of RyR1 in previously described clones was confirmed, the next step was to introduce mutations into RyR1 receptor sequence and test for the functional and protein expression changes. A premature stop mutation similar to one found in patients c.2367C>A was introduced into *RYR1* vector and using the electroporation protocol mutated cDNA was introduced into FDB. Briefly, cDNA from nucleotide 131 to 2367 was amplified by PCR and subcloned into the pIRES-DsRed vector (Clontech) into which the 3`UTR sequence of RyR1 (from nucleotide 15235-15376) had previously been inserted. The following primers were used for *RYR1*$_{TRUNC}$ subcloning: F 5`- GACCT CGA GGT CGA CGG TAT CGA TAA-3` and R 5`-GGATC TAG AAC GCT GAG GTC CAG TCA G -3`. All sequences were verified by Sanger sequencing.

Mouse FDB were then electroporated with the wild type or truncated *RYR1*; after one week FDB fibers were isolated and proteins were probed for the presence of the ubiquitin as a signal for degradation. As can be seen in figure 23A the band with truncated RyR1 protein is heavily marked with anti-ubiquitin antibody (Millipore 04-363), while at the same time the mRNA levels of truncated *RYR1* are highly increased compared to the control levels detected from the isolated FDB fibers of the other leg, indicating that electroporation was efficient (Fig. 23B), but the translated protein is being degraded.
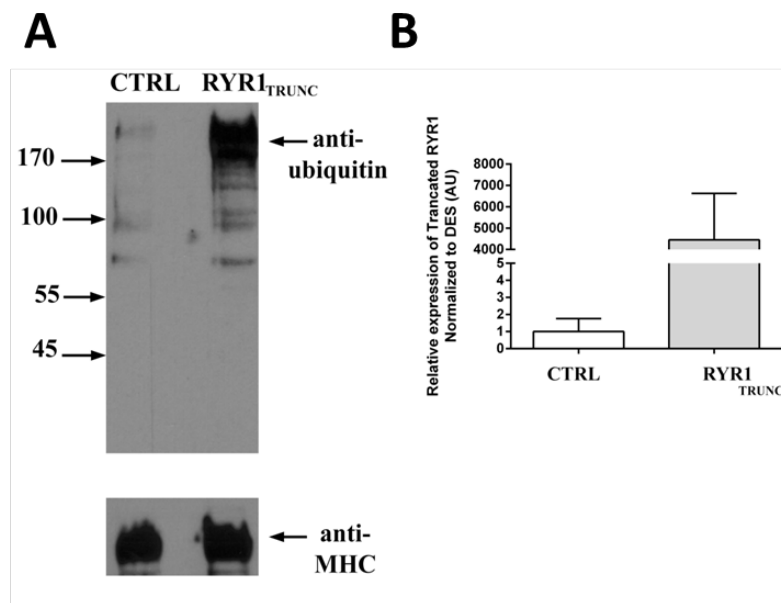
Figure 23: **Increase in ubiquitination of the truncated RyR1 protein**. **(A)** Western blot of the total homogenate from the isolated FDB fibers, from control leg and electroporated one, probed for anti-ubiquitin antibody and normalized to MyHC content. **(B)** Relative expression of truncated RYR1 in isolated transfected fibers compared to control fibers.

2.2.3 Extraocular muscle properties in RyR3 knockout mice

Considering that we found *RYR3* to be highly expressed in human EOM it was equally interesting to test *RYR3* levels in mouse EOM. As can be seen in figure 23, the pattern of *RYR1*, *CACNA1S*, and *CASQ2* expression was different in mouse EOM compared to human EOM, but the *RYR3* transcript levels were similarly increased, up to 100 fold compared to FDB fibers. This led us to investigate the function of the extraocular muscles in the *RYR3* knockout mice.
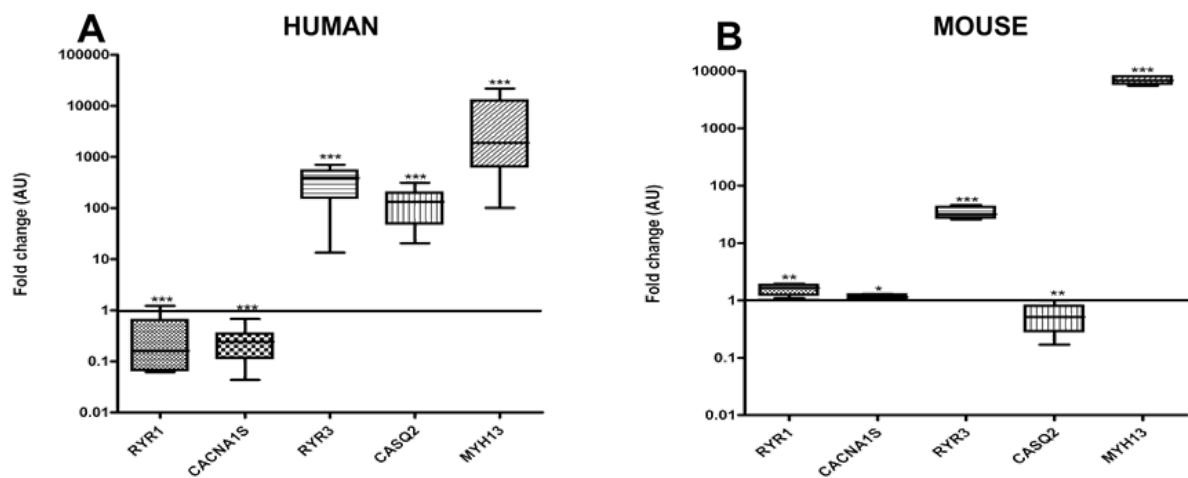
Figure 23: Expression of excitation-contraction coupling transcripts in human (A) and mouse (B) extraocular muscle biopsies. Gene expression was quantified by qPCR. Each reaction was carried out in triplicate, in pooled muscle samples from 4-5 biopsies from different individuals. Expression levels were normalized to *ACTN2* expression. Results are expressed as mean fold change of transcripts in EOM compared to human quadriceps muscles and to mouse FDB fibers, the latter were set as 1. Results were analyzed using the Student's t-test (***p<0.0001, **p<0.001, *p<0.01).

For the preliminary functional test, we chose to investigate the optokinetic reflex and measure visual acuity (clarity of vision), using the OptoMotry© system. Image stabilization is predominantly mediated by two types of oculomotor responses: the optokinetic reflex (OKR; also called optokinetic nystagmus or OKN) and the vestibulo-ocular reflex (VOR) The OKR is induced when the entire visual scene drifts across the retina, eliciting eye rotation in the same direction and at a velocity that minimizes the motion of the image on the retina. The VOR is an analogous response to head movement, with input coming from the vestibular system rather than the retina. Normally, the OKR and VOR work together to ensure image stabilization on the retina. Both the OKR and the VOR are controlled by subcortical circuits: the OKR is controlled by neurons in the retina, diencephalon and midbrain (the accessory optic system), pons, and dorsal medulla, and the VOR is controlled by neurons in the labyrinth of the inner ear, midbrain, pons, dorsal medulla, and cerebellum [173].

OptoMotry© is used for the rapid screening of functional vision using the opto-kinetic tracking/reflex (OKT/R) response. Spatial frequency thresholds can be measured by systematically increasing the spatial frequency of the grating at 100% contrast until animals no longer track. A contrast sensitivity function can be generated by identifying the minimum contrast that generates tracking, over a range of spatial frequencies. Single thresholds can be obtained in a few minutes in animals with no previous exposure to the task, and measurements can be repeated regularly. Rodents stand on an elevated platform in the epicenter of an arena surrounded by computer monitors, and a camera images the behavior of the animal from above (Fig. 24). A cylinder comprised of a sine wave grating is drawn in 3D coordinate space and rotates around the animal. Animals track the grating with reflexive head and neck movements (Fig. 25). A cursor placed on the forehead centers in real time the rotation of the cylinder at the animal's viewing position, thereby "clamping" the effective spatial frequency of the grating [174].
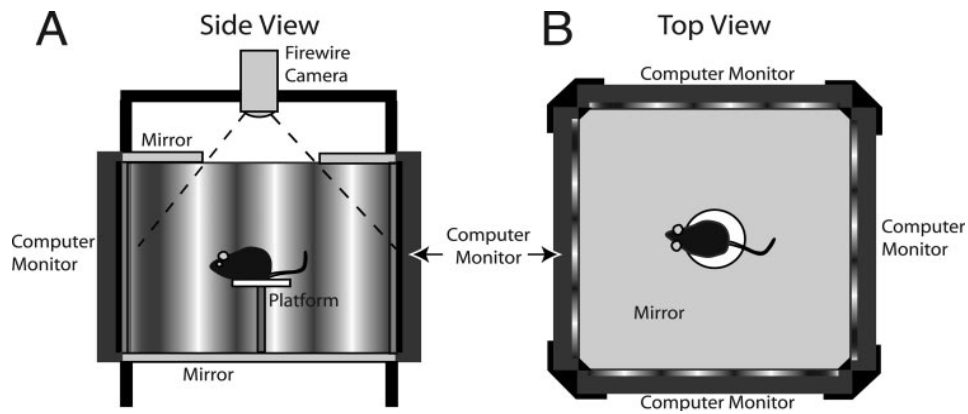
Figure 24: Schematic representation of the optomotor testing apparatus. **(A)** Side view. A mouse is placed on a platform positioned in the middle of an arena created by a quad-square of computer monitors. Sine wave gratings drawn on the screens are extended vertically with floor and ceiling mirrors. A video camera is used to monitor the animal's behavior from above. **(B)** Top view. The mouse is surrounded by 360° of gratings and is allowed to move freely on the platform [174].
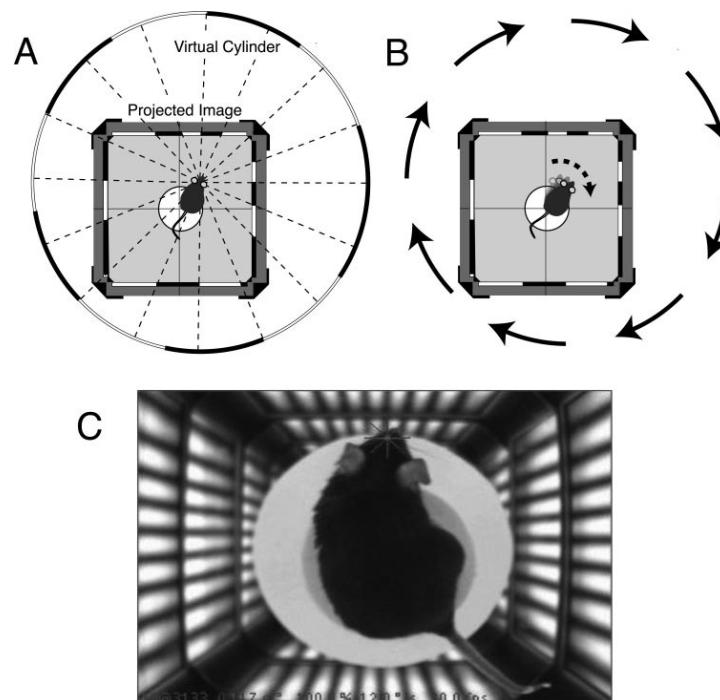
Figure 25: Virtual geometry and optomotor response. (**A**) A virtual cylinder is projected in 3-D coordinate space on the monitors. The head of the mouse centers the rotation of the cylinder. (**B**) When the cylinder is rotated, the mouse tracks the drifting grating with head and neck movements. (**C**) A single-frame video camera image of a mouse tracking the cylinder grating. The four-line crosshair is positioned between the eyes of the mouse, and the coordinates are used to center the rotation of the cylinder [174].

According to the results obtained after the first tests, there is a significant difference (***p<0.0001) in the visual acuity between *RYR3* KO mice and WT, in terms of poorer vision of the knockout mice (Fig. 26).
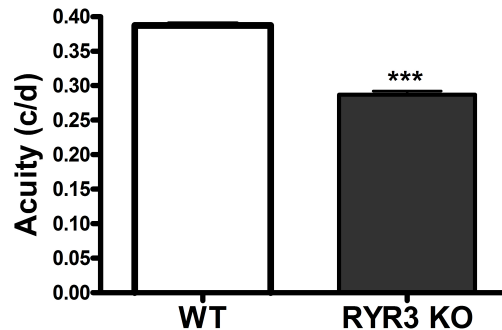
Figure 26: Visual acuity test of *RYR3* KO mice. OptoMotry© detection system. Unit for visual acuity used is c/d (cycle/degree). 10 WT and 10 *RYR3* KO mice tested in two independent measurements. Results were analyzed using the Student's t-test ***p<0.0001.

This was a good starting point for the measurements of EOM muscle function. The next planned experiment was a water maze test, where the visual impairment of *RYR3* KO mice was further investigated. Visual acuity was tested using the visual platform version of the Morris Water maze. A round gray tank of 1,7m diameter filled to a height of 30cm with water at room temperature of $23 \pm 1°C$ was used. The water was made opaque by the addition of non-toxic white paint. A video-camera fastened above the center of the pool recorded the swimming patterns of the mice, using a video tracking system (Ethovision™ XT11, Noldus Information Technology, Wageningen, Netherlands). The water surface was virtually divided into four quadrants. A white, round platform with a diameter of 10 cm, was placed in one quadrant, at a distance of 50 cm from the border and 2 cm above the water surface. 4 entry zones are marked outside the pool. The room was illuminated at an intensity of <150 Lux. Animals are transferred to the experimental room where they were given at least 72 h to acclimatize in 12 hourly light/dark cycles, the light being switched on at 6 am. Animals were provided with water and food ad libitum. On day 0, animals performed a habituation run, swimming for 60 sec in the water maze, after this period they were placed on the platform for 15 seconds. On day 1, animals were tested in a total of 4 trials with the platform at a fixed position, and varying each of the four entry zones. Test duration was 60

sec per run. If the animal did not find the platform after 60 sec, it was guided to it by hand and allowed to stay for 15 seconds. On day 2, tests were repeated in a similar way as day 1, except that the platform was moved in the opposite quadrant. Parameters that were evaluated are: swimming velocity, total distance moved and time to reach the platform. There was no difference in swimming velocity between two strains, which was good indicator that the swimming capacity is unchanged in *RYR3* KO and does not contribute to detected significantly higher time and distance to reach the platform (*p<0.05 and **p<0.005 respectively) (Fig. 27) .
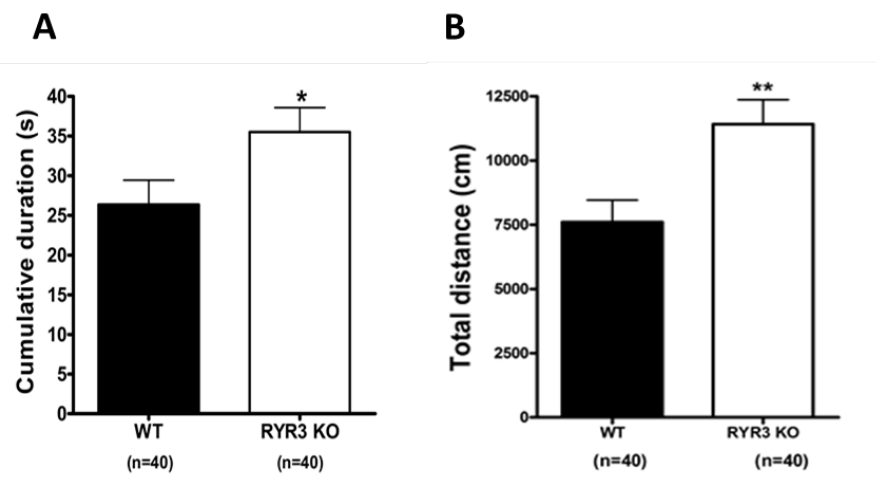
Figure 27: Water maze results show visual impairment in *RYR3* KO mice. The results are average per experimental group, per day. **(A)** Time spent to reach the platform; 10 mice were measured per strain and data from 4 different entry points are pooled. **(B)** Distance to reach the platform; 10mice were measured per strain and data from 4 different entry points were pooled; *p<0.05, p*<0.005.

Functional and biochemical testing of the isolated EOM fibers will be also part of the characterization of the *RYR3* KO EOM phenotype. So far, I have isolated mouse WT EOM fibers, and by confocal microscopy showed that the $Ca_v1.1$, RyR1 proteins are distributed as in skeletal muscle fibers, but the cardiac isoform of DHPR $Ca_v1.2$ was found to be expressed and localized only on the membrane of the fiber, as previously found in human EOM derived myotubes (Fig. 28).
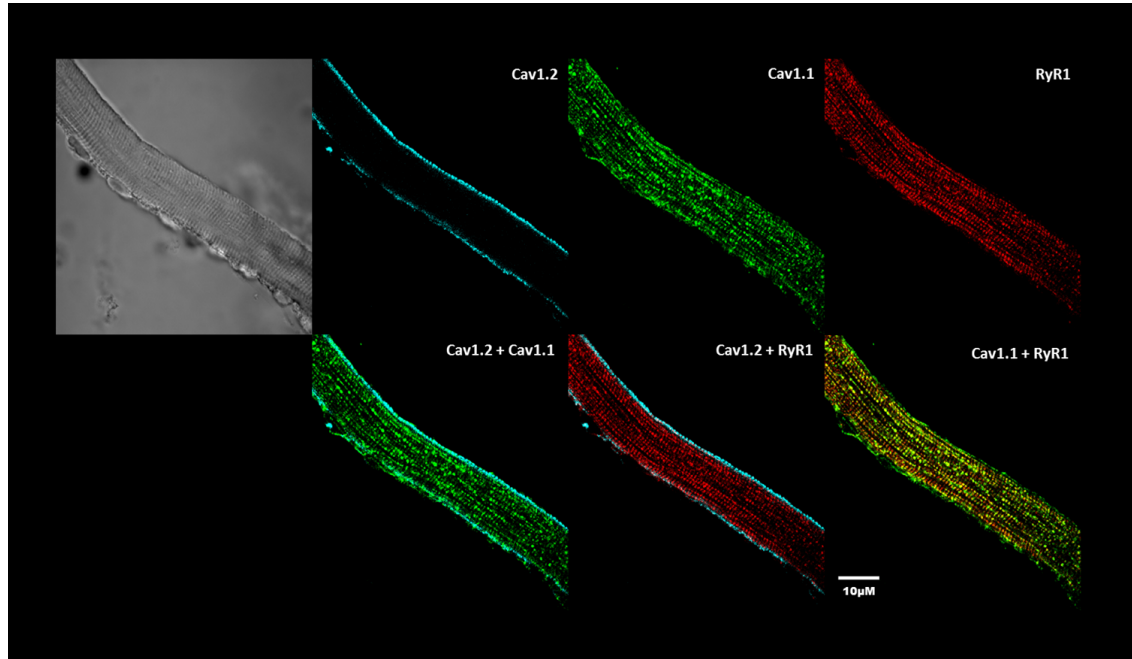
Figure 28: Cellular localization of RyR1, Cav1.1 and Cav1.2 in Mouse Extraocular muscle fiber. Samples were stained as previously described. Fiber was visualized with a Nikon A1R confocal microscope equipped with a CFI Apo TIRF 100X objective (1.49 N.A.).

CHAPTER 3: GENERAL CONCLUSION AND PERSPECTIVES

Extraocular muscles are affected in individuals carrying recessive *RYR1* mutations associated with multi-minicore disease, centronuclear myopathy and congenital fiber-type disproportion. Patients with severe congenital ophthalmoplegia and facial weakness in the setting of only mild skeletal myopathy harbor recessive mutations in *RYR1*, and are susceptible to malignant hyperthermia [175]. On the other hand, even within Malignant hyperthermia which is inherited in a dominant manner, there is a subgroup of patients which respond with masseter muscle rigidity - a severe, sustained contraction of the jaw muscle that may be observed after the administration of succinylcholine [176]. Our interest to investigate closer the properties of two muscle groups, the extraocular muscles and the facial orbicularis oculi muscles, led us to interesting discoveries. Finding that all major components of the skeletal excitation-contraction coupling in EOM were expressed at a lower levels was unexpected, as it is well known that EOM are one of the fastest muscles in the body. That was intriguing and made us question as to what additional signaling mechanism these muscles rely on. If it is not completely skeletal, might there be involvement of cardiac ECC components or some other factors? Indeed, the transcripts encoding RyR3, cardiac calsequestrin (CSQ2) and the α1 subunit of the cardiac dihydropyridine receptor were highly expressed in EOM compared to leg muscle. Cardiac DHPR was localized exclusively on the membrane of the EOM-derived myotubes and this was the first time that this isoform was detected in skeletal muscles. What is the exact role of this receptor in EOM muscles and how it contributes to the EOM phenotype is yet to be discovered. One explanation could be the increased depolarization induced Ca^{2+} influx in EOM that we reported, as it is practically abolished after adding of 50μM nifedipine to myotubes incubated in ryanodine. To what extent this effect can be attributed to the presence of cardiac DHPR cannot be resolved based on the experiments as nifedipine blocks the L-type calcium channels and is not specific for one isoform.

After discovering the high expression levels of *RYR3* transcript, we were interested to know its role in EOM, since this isoform is highly expressed only during muscle development and in low levels in adult muscle tissues, such as the diaphragm and soleus. It seems that RyR3 is not involved in ECC directly, as mice lacking this receptor show subtle changes in ECC and it seems that RyR1 successfully compensates for the absence of RyR3. This effect does not necessarily reflect the lack of RyR3 involvement in muscle, but might be the consequence of already low content of RyR3. In addition, when both receptors RyR1 and RyR3 are absent, functional and structural impairment is even more pronounced and this indicates that when RyR1 is absent, RyR3 does show some effect on myofibrilar organization. The reported reduction in the caffeine response of the RyR3 KO mice indicates that RyR3 could play a role in the CICR mechanism. Despite the fact that in RyR3 KO mice ECC is normal, a reduced CICR response was present at high Ca^{2+} concentrations [116, 177]. According to the results we have so far on extraocular muscles from RyR3 KO mice, their optokinetic reflex seems to be impaired and the water maze test confirmed a visual impairment, since RyR3 KO mice failed to see the platform and this was translated in a longer time and distance to reach the platform, compared to WT mice. At the same time the velocity of the RyR3 KO mice was not different compared to WT, which excludes the possibility that the lower values in time and distance for RyR3 KO mice were due to general weaker muscle performance. Further testing would give some additional insights in the EOM muscle and muscle fiber function of these mice, as EOM are constantly active and require an exquisite calcium management. Further experiments on the RyR3 KO mice will be conducted and will be combined with the biochemical characterization and Ca^{2+} measurements on isolated EOM fibers.

We have found that orbicularis oculi muscles exhibit more similarities with LM than with EOM in terms of protein and mRNA levels of skeletal ECC components. On a protein level, they seem not to express the cardiac isoform of the DHPR which was instead found to be present in EOM and this was supported by the unchanged ECCE compared to LM-derived myotubes. In Duchenne muscular dystrophy EOM are spared from pathology. The same is confirmed in mdx mice models where EOM are spared; while at the same time accessory EOM (retractor bulbi and LPS) are affected. We have found that human OO express higher levels of both dystrophin and utrophin. The next step would be to investigate the protein levels of utrophin and dystrophin in both OO and EOM and to see if there are any differences between them.

The second part of this thesis refers to RyR1 low protein levels found in patients with recessive *RYR1* mutations. The human *RYR1* cDNA was subcloned into a mammalian vector and used for the insertion of specific mutations found in patients. We thus discovered that introduction of a premature stop codon causes protein degradation. Further investigations will combine the insertion of several different mutations found in patients and following the functional effect on Ca^{2+} regulation, protein level expression and function in transfected cells. This investigation will hopefully clarify at least in part, what factors are involved in the pathophysiological mechanism of recessive *RYR1* mutations leading to disease and impaired muscle function.

References

1. Noden, D.M. and P. Francis-West, *The differentiation and morphogenesis of craniofacial muscles.* Dev Dyn, 2006. **235**(5): p. 1194-218.
2. Dudek, R.W. and J.D. Fix, *Embryology.* 2005: Lippincott Williams & Wilkins.
3. Sambasivan, R., S. Kuratani, and S. Tajbakhsh, *An eye on the head: the development and evolution of craniofacial muscles.* Development, 2011. **138**(12): p. 2401-15.
4. McLoon, L.K. and F. Andrade, *Craniofacial Muscles: A New Framework for Understanding the Effector Side of Craniofacial Muscle Control.* 2012: Springer New York.
5. Spencer, R.F. and J.D. Porter, *Biological organization of the extraocular muscles.* Prog Brain Res, 2006. **151**: p. 43-80.
6. Porter, J.D., et al., *Extraocular muscles: basic and clinical aspects of structure and function.* Surv Ophthalmol, 1995. **39**(6): p. 451-84.
7. Briggs, M.M. and F. Schachat, *The superfast extraocular myosin (MYH13) is localized to the innervation zone in both the global and orbital layers of rabbit extraocular muscle.* J Exp Biol, 2002. **205**(Pt 20): p. 3133-42.
8. Zacharias, A.L., et al., *Pitx2 is an upstream activator of extraocular myogenesis and survival.* Dev Biol, 2011. **349**(2): p. 395-405.
9. Diehl, A.G., et al., *Extraocular muscle morphogenesis and gene expression are regulated by Pitx2 gene dose.* Invest Ophthalmol Vis Sci, 2006. **47**(5): p. 1785-93.
10. Wasicky, R., et al., *Muscle Fiber Types of Human Extraocular Muscles: A Histochemical and Immunohistochemical Study.* Investigative Ophthalmology & Visual Science, 2000. **41**(5): p. 980-990.
11. McLoon, L.K., L. Rios, and J.D. Wirtschafter, *Complex three-dimensional patterns of myosin isoform expression: differences between and within specific extraocular muscles.* J Muscle Res Cell Motil, 1999. **20**(8): p. 771-83.
12. Spencer, R.F. and J.D. Porter, *Structural organization of the extraocular muscles.* Rev Oculomot Res, 1988. **2**: p. 33-79.
13. Stirn Kranjc, B., V. Smerdu, and I. Erzen, *Histochemical and immunohistochemical profile of human and rat ocular medial rectus muscles.* Graefes Arch Clin Exp Ophthalmol, 2009. **247**(11): p. 1505-15.
14. Demer, J.L., et al., *Evidence for fibromuscular pulleys of the recti extraocular muscles.* Invest Ophthalmol Vis Sci, 1995. **36**(6): p. 1125-36.
15. Demer, J.L., et al., *Innervation of extraocular pulley smooth muscle in monkeys and humans.* Invest Ophthalmol Vis Sci, 1997. **38**(9): p. 1774-85.
16. Wieczorek, D.F., et al., *Co-expression of multiple myosin heavy chain genes, in addition to a tissue-specific one, in extraocular musculature.* J Cell Biol, 1985. **101**(2): p. 618-29.
17. Lucas, C.A. and J.F. Hoh, *Extraocular fast myosin heavy chain expression in the levator palpebrae and retractor bulbi muscles.* Invest Ophthalmol Vis Sci, 1997. **38**(13): p. 2817-25.
18. Whalen, R.G., et al., *Three myosin heavy-chain isozymes appear sequentially in rat muscle development.* Nature, 1981. **292**(5826): p. 805-9.
19. Brueckner, J.K., O. Itkis, and J.D. Porter, *Spatial and temporal patterns of myosin heavy chain expression in developing rat extraocular muscle.* J Muscle Res Cell Motil, 1996. **17**(3): p. 297-312.

20.	Rushbrook, J.I., et al., *Identification of alpha-cardiac myosin heavy chain mRNA and protein in extraocular muscle of the adult rabbit.* Journal of Muscle Research & Cell Motility, 1994. **15**(5): p. 505-515.

21.	Park, K.A., et al., *Myosin heavy chain isoform expression in human extraocular muscles: longitudinal variation and patterns of expression in global and orbital layers.* Muscle Nerve, 2012. **45**(5): p. 713-20.

22.	Schiaffino, S. and C. Reggiani, *Fiber types in mammalian skeletal muscles.* Physiol Rev, 2011. **91**(4): p. 1447-531.

23.	Siebeck, R. and P. Krüger, *Die histologische Struktur der äußeren Augenmuskeln als Ausdruck ihrer Funktion.* Albrecht von Graefes Archiv für Ophthalmologie, 1955. **156**(6): p. 637-652.

24.	Durston, J.H., *Histochemistry of primate extraocular muscles and the changes of denervation.* Br J Ophthalmol, 1974. **58**(3): p. 193-216.

25.	Mayr, R., *Structure and distribution of fibre types in the external eye muscles of the rat.* Tissue Cell, 1971. **3**(3): p. 433-62.

26.	Ringel, S.P., et al., *HIstochemistry of human extraocular muscle.* Archives of Ophthalmology, 1978. **96**(6): p. 1067-1072.

27.	Hoogenraad, T.U., F.G. Jennekens, and K.E. Tan, *Histochemical fibre types in human extraocular muscles, an investigation of inferior oblique muscle.* Acta Neuropathol, 1979. **45**(1): p. 73-8.

28.	da Silva Costa, R.M., et al., *Nonclassical innervation patterns in mammalian extraocular muscles.* Curr Eye Res, 2012. **37**(9): p. 761-9.

29.	Hess, A., *The structure of slow and fast extrafusal muscle fibers in the extraocular muscles and their nerve endings in guinea pigs.* J Cell Comp Physiol, 1961. **58**: p. 63-79.

30.	Shimko, J.F., *Binocular Vision and Ocular Motility Theory and Management of Strabismus Gunter K. vonNoorden, M.D.; Emilio C. Campos, M.D. Mosby Inc., Sixth Edition 2002, $149.00; 631 pages, 315 illustrations.* Am Orthopt J, 2001. **51**: p. 161-2.

31.	Cooper, S. and J.C. Eccles, *The isometric responses of mammalian muscles.* The Journal of Physiology, 1930. **69**(4): p. 377-385.

32.	Denny-Brown, D.E., *The Histological Features of Striped Muscle in Relation to Its Functional Activity.* Proceedings of the Royal Society of London. Series B, Containing Papers of a Biological Character, 1929. **104**(731): p. 371-411.

33.	Lander, T., J.D. Wirtschafter, and L.K. McLoon, *Orbicularis oculi muscle fibers are relatively short and heterogeneous in length.* Invest Ophthalmol Vis Sci, 1996. **37**(9): p. 1732-9.

34.	*CUNNINGHAM'S TEXTBOOK OF ANATOMY.* The Ulster Medical Journal, 1972. **41**(2): p. 181-182.

35.	Cheng, N.C., et al., *Fiber type and myosin heavy chain compositions of adult pretarsal orbicularis oculi muscle.* J Mol Histol, 2007. **38**(3): p. 177-82.

36.	Nelson, C.C. and M. Blaivas, *Orbicularis oculi muscle in children. Histologic and histochemical characteristics.* Invest Ophthalmol Vis Sci, 1991. **32**(3): p. 646-54.

37.	Sandow, A., *Excitation-contraction coupling in muscular response.* Yale J Biol Med, 1952. **25**(3): p. 176-201.

38.	Caputo, C., *Pharmacological Investigations of Excitation-Contraction Coupling*, in *Comprehensive Physiology*. 2010, John Wiley & Sons, Inc.

39.	Fill, M. and J.A. Copello, *Ryanodine receptor calcium release channels.* Physiol Rev, 2002. **82**(4): p. 893-922.

40.   Bannister, R.A., I.N. Pessah, and K.G. Beam, *The skeletal L-type Ca(2+) current is a major contributor to excitation-coupled Ca(2+) entry.* J Gen Physiol, 2009. **133**(1): p. 79-91.

41.   Conklin, M.W., et al., *Comparison of Ca(2+) sparks produced independently by two ryanodine receptor isoforms (type 1 or type 3).* Biophys J, 2000. **78**(4): p. 1777-85.

42.   Franzini-Armstrong, C. and K.R. Porter, *SARCOLEMMAL INVAGINATIONS CONSTITUTING THE T SYSTEM IN FISH MUSCLE FIBERS.* J Cell Biol, 1964. **22**: p. 675-96.

43.   Edwards, J.N., et al., *Longitudinal and transversal propagation of excitation along the tubular system of rat fast-twitch muscle fibres studied by high speed confocal microscopy.* J Physiol, 2012. **590**(Pt 3): p. 475-92.

44.   Block, B.A., et al., *Structural evidence for direct interaction between the molecular components of the transverse tubule/sarcoplasmic reticulum junction in skeletal muscle.* J Cell Biol, 1988. **107**(6 Pt 2): p. 2587-600.

45.   Franzini-Armstrong, C. and A.O. Jorgensen, *Structure and development of E-C coupling units in skeletal muscle.* Annu Rev Physiol, 1994. **56**: p. 509-34.

46.   Anderson, K., A.H. Cohn, and G. Meissner, *High-affinity [3H]PN200-110 and [3H]ryanodine binding to rabbit and frog skeletal muscle.* Am J Physiol, 1994. **266**(2 Pt 1): p. C462-6.

47.   Meissner, G. and X. Lu, *Dihydropyridine receptor-ryanodine receptor interactions in skeletal muscle excitation-contraction coupling.* Biosci Rep, 1995. **15**(5): p. 399-408.

48.   Zorzato, F., R. Sacchetto, and A. Margreth, *Identification of two ryanodine receptor transcripts in neonatal, slow-, and fast-twitch rabbit skeletal muscles.* Biochem Biophys Res Commun, 1994. **203**(3): p. 1725-30.

49.   Garcia, J. and M.F. Schneider, *Calcium transients and calcium release in rat fast-twitch skeletal muscle fibres.* J Physiol, 1993. **463**: p. 709-28.

50.   Protasi, F., *Structural interaction between RYRs and DHPRs in calcium release units of cardiac and skeletal muscle cells.* Front Biosci, 2002. **7**: p. d650-8.

51.   Fabiato, A., *Calcium-induced release of calcium from the cardiac sarcoplasmic reticulum.* Am J Physiol, 1983. **245**(1): p. C1-14.

52.   Sun, X.H., et al., *Molecular architecture of membranes involved in excitation-contraction coupling of cardiac muscle.* J Cell Biol, 1995. **129**(3): p. 659-71.

53.   Bers, D., *Excitation-Contraction Coupling and Cardiac Contractile Force.* 2013: Springer Netherlands.

54.   Sham, J.S., L. Cleemann, and M. Morad, *Functional coupling of Ca2+ channels and ryanodine receptors in cardiac myocytes.* Proc Natl Acad Sci U S A, 1995. **92**(1): p. 121-5.

55.   Otsu, K., et al., *Molecular cloning of cDNA encoding the Ca2+ release channel (ryanodine receptor) of rabbit cardiac muscle sarcoplasmic reticulum.* J Biol Chem, 1990. **265**(23): p. 13472-83.

56.   Nixon, G.F., G.A. Mignery, and A.V. Somlyo, *Immunogold localization of inositol 1,4,5-trisphosphate receptors and characterization of ultrastructural features of the sarcoplasmic reticulum in phasic and tonic smooth muscle.* J Muscle Res Cell Motil, 1994. **15**(6): p. 682-700.

57.   Hakamata, Y., et al., *Primary structure and distribution of a novel ryanodine receptor/calcium release channel from rabbit brain.* FEBS Lett, 1992. **312**(2-3): p. 229-35.

58.   Lanner, J.T., et al., *Ryanodine receptors: structure, expression, molecular details, and function in calcium release.* Cold Spring Harb Perspect Biol, 2010. **2**(11): p. a003996.

59.   Lai, F.A., et al., *The ryanodine receptor-Ca2+ release channel complex of skeletal muscle sarcoplasmic reticulum. Evidence for a cooperatively coupled, negatively charged homotetramer.* J Biol Chem, 1989. **264**(28): p. 16776-85.

60.   McGrew, S.G., et al., *Positive cooperativity of ryanodine binding to the calcium release channel of sarcoplasmic reticulum from heart and skeletal muscle.* Biochemistry, 1989. **28**(4): p. 1686-91.

61.   Rogers, E.F., F.R. Koniuszy, and et al., *Plant insecticides; ryanodine, a new alkaloid from Ryania speciosa Vahl.* J Am Chem Soc, 1948. **70**(9): p. 3086-8.

62.   Meissner, G., *Ryanodine activation and inhibition of the Ca2+ release channel of sarcoplasmic reticulum.* J Biol Chem, 1986. **261**(14): p. 6300-6.

63.   Sabbadini, R.A., et al., *The effects of sphingosine on sarcoplasmic reticulum membrane calcium release.* J Biol Chem, 1992. **267**(22): p. 15475-84.

64.   *Single channel measurements of the calcium release channel from skeletal muscle sarcoplasmic reticulum. Activation by Ca2+ and ATP and modulation by Mg2+.* The Journal of General Physiology, 1986. **88**(5): p. 573-588.

65.   Tanabe, T., et al., *Regions of the skeletal muscle dihydropyridine receptor critical for excitation-contraction coupling.* Nature, 1990. **346**(6284): p. 567-9.

66.   Ikemoto, N., et al., *Intravesicular calcium transient during calcium release from sarcoplasmic reticulum.* Biochemistry, 1991. **30**(21): p. 5230-7.

67.   Wang, J. and P.M. Best, *Inactivation of the sarcoplasmic reticulum calcium channel by protein kinase.* Nature, 1992. **359**(6397): p. 739-41.

68.   Brillantes, A.B., et al., *Stabilization of calcium release channel (ryanodine receptor) function by FK506-binding protein.* Cell, 1994. **77**(4): p. 513-23.

69.   Chen, S.R. and D.H. MacLennan, *Identification of calmodulin-, Ca(2+)-, and ruthenium red-binding domains in the Ca2+ release channel (ryanodine receptor) of rabbit skeletal muscle sarcoplasmic reticulum.* J Biol Chem, 1994. **269**(36): p. 22698-704.

70.   Yang, H.C., et al., *Calmodulin interaction with the skeletal muscle sarcoplasmic reticulum calcium channel protein.* Biochemistry, 1994. **33**(2): p. 518-25.

71.   Ma, J., M.B. Bhat, and J. Zhao, *Rectification of skeletal muscle ryanodine receptor mediated by FK506 binding protein.* Biophys J, 1995. **69**(6): p. 2398-404.

72.   Mayrleitner, M., et al., *Phosphorylation with protein kinases modulates calcium loading of terminal cisternae of sarcoplasmic reticulum from skeletal muscle.* Cell Calcium, 1995. **18**(3): p. 197-206.

73.   Tripathy, A., et al., *Calmodulin activation and inhibition of skeletal muscle Ca2+ release channel (ryanodine receptor).* Biophys J, 1995. **69**(1): p. 106-19.

74.   Timerman, A.P., et al., *Selective binding of FKBP12.6 by the cardiac ryanodine receptor.* J Biol Chem, 1996. **271**(34): p. 20385-91.

75.   Nakai, J., et al., *Two regions of the ryanodine receptor involved in coupling with L-type Ca2+ channels.* J Biol Chem, 1998. **273**(22): p. 13403-6.

76.   Rodney, G.G., et al., *Regulation of RYR1 activity by Ca(2+) and calmodulin.* Biochemistry, 2000. **39**(26): p. 7807-12.

77.   Porter Moore, C., J.Z. Zhang, and S.L. Hamilton, *A role for cysteine 3635 of RYR1 in redox modulation and calmodulin binding.* J Biol Chem, 1999. **274**(52): p. 36831-4.

78. Takeshima, H., et al., *Primary structure and expression from complementary DNA of skeletal muscle ryanodine receptor.* Nature, 1989. **339**(6224): p. 439-45.

79. Zorzato, F., et al., *Molecular cloning of cDNA encoding human and rabbit forms of the Ca2+ release channel (ryanodine receptor) of skeletal muscle sarcoplasmic reticulum.* J Biol Chem, 1990. **265**(4): p. 2244-56.

80. Hwang, J.H., et al., *Mapping domains and mutations on the skeletal muscle ryanodine receptor channel.* Trends Mol Med, 2012. **18**(11): p. 644-57.

81. Franzini-Armstrong, C. and G. Nunzi, *Junctional feet and particles in the triads of a fast-twitch muscle fibre.* J Muscle Res Cell Motil, 1983. **4**(2): p. 233-52.

82. Neylon, C.B., et al., *Multiple types of ryanodine receptor/Ca2+ release channels are expressed in vascular smooth muscle.* Biochem Biophys Res Commun, 1995. **215**(3): p. 814-21.

83. Giannini, G., et al., *The ryanodine receptor/calcium channel genes are widely and differentially expressed in murine brain and peripheral tissues.* J Cell Biol, 1995. **128**(5): p. 893-904.

84. Nakai, J., et al., *Primary structure and functional expression from cDNA of the cardiac ryanodine receptor/calcium release channel.* FEBS Lett, 1990. **271**(1-2): p. 169-77.

85. Marks, A.R., et al., *Molecular cloning and characterization of the ryanodine receptor/junctional channel complex cDNA from skeletal muscle sarcoplasmic reticulum.* Proc Natl Acad Sci U S A, 1989. **86**(22): p. 8683-7.

86. Furuichi, T., et al., *Multiple types of ryanodine receptor/Ca2+ release channels are differentially expressed in rabbit brain.* J Neurosci, 1994. **14**(8): p. 4794-805.

87. Ottini, L., et al., *Alpha and beta isoforms of ryanodine receptor from chicken skeletal muscle are the homologues of mammalian RyR1 and RyR3.* Biochem J, 1996. **315 (Pt 1)**: p. 207-16.

88. Vukcevic, M., et al., *Functional properties of RYR1 mutations identified in Swedish patients with malignant hyperthermia and central core disease.* Anesth Analg, 2010. **111**(1): p. 185-90.

89. Samso, M., et al., *Coordinated movement of cytoplasmic and transmembrane domains of RyR1 upon gating.* PLoS Biol, 2009. **7**(4): p. e85.

90. Samso, M., T. Wagenknecht, and P.D. Allen, *Internal structure and visualization of transmembrane[Samso, 2005 #68] domains of the RyR1 calcium release channel by cryo-EM.* Nat Struct Mol Biol, 2005. **12**(6): p. 539-44.

91. Ludtke, S.J., et al., *The pore structure of the closed RyR1 channel.* Structure, 2005. **13[Ludtke, 2005 #69]**(8): p. 1203-11.

92. Ludtke, S.J., et al., *The pore structure of the closed RyR1 channel.* Structure, 2005. **13**(8): p. 1203-11.

93. Samso, M., T. Wagenknecht, and P.D. Allen, *Internal structure and visualization of transmembrane domains of the RyR1 calcium release channel by cryo-EM.* Nat Struct Mol Biol, 2005. **12**(6): p. 539-44.

94. Serysheva, II, et al., *Subnanometer-resolution electron cryomicroscopy-based domain models for the cytoplasmic region of skeletal muscle RyR channel.* Proc Natl Acad Sci U S A, 2008. **105**(28): p. 9610-5.

95. Sharma, M.R., et al., *Cryoelectron microscopy and image analysis of the cardiac ryanodine receptor.* J Biol Chem, 1998. **273**(29): p. 18429-34.

96. Sharma, M.R., et al., *Three-dimensional structure of ryanodine receptor isoform three in two conformational states as visualized by cryo-electron microscopy.* J Biol Chem, 2000. **275**(13): p. 9485-91.

97. Ludtke, S.J., et al., *The Pore Structure of the Closed RyR1 Channel.* Structure, 2005. **13**(8): p. 1203-1211.

98. Du, G.G., et al., *Topology of the Ca2+ release channel of skeletal muscle sarcoplasmic reticulum (RyR1).* Proc Natl Acad Sci U S A, 2002. **99**(26): p. 16725-30.

99. Yin, C.C. and F.A. Lai, *Intrinsic lattice formation by the ryanodine receptor calcium-release channel.* Nat Cell Biol, 2000. **2**(9): p. 669-71.

100. Yin, C.C., L.M. Blayney, and F.A. Lai, *Physical coupling between ryanodine receptor-calcium release channels.* J Mol Biol, 2005. **349**(3): p. 538-46.

101. Marx, S.O., K. Ondrias, and A.R. Marks, *Coupled gating between individual skeletal muscle Ca2+ release channels (ryanodine receptors).* Science, 1998. **281**(5378): p. 818-21.

102. Takeshima, H., et al., *Excitation-contraction uncoupling and muscular degeneration in mice lacking functional skeletal muscle ryanodine-receptor gene.* Nature, 1994. **369**(6481): p. 556-9.

103. Lai, F.A., et al., *Expression of a cardiac Ca(2+)-release channel isoform in mammalian brain.* Biochem J, 1992. **288 (Pt 2)**: p. 553-64.

104. Kuwajima, G., et al., *Two types of ryanodine receptors in mouse brain: skeletal muscle type exclusively in Purkinje cells and cardiac muscle type in various neurons.* Neuron, 1992. **9**(6): p. 1133-42.

105. Wehrens, X.H., S.E. Lehnart, and A.R. Marks, *Intracellular calcium release and cardiac disease.* Annu Rev Physiol, 2005. **67**: p. 69-98.

106. McCauley, M.D. and X.H.T. Wehrens, *Ryanodine Receptor Phosphorylation, Calcium/Calmodulin-dependent Protein Kinase II, and Life-threatening Ventricular Arrhythmias.* Trends in Cardiovascular Medicine, 2011. **21**(2): p. 48-51.

107. Meissner, G., *Molecular regulation of cardiac ryanodine receptor ion channel.* Cell Calcium, 2004. **35**(6): p. 621-8.

108. Magee, K.R. and G.M. Shy, *A new congenital non-progressive myopathy.* Brain, 1956. **79**(4): p. 610-21.

109. Napolitano, C., et al., *Clinical utility gene card for: Catecholaminergic polymorphic ventricular tachycardia (CPVT).* Eur J Hum Genet, 2014. **22**(1).

110. Jeyakumar, L.H., et al., *Purification and characterization of ryanodine receptor 3 from mammalian tissue.* J Biol Chem, 1998. **273**(26): p. 16011-20.

111. Tarroni, P., et al., *Expression of the ryanodine receptor type 3 calcium release channel during development and differentiation of mammalian skeletal muscle cells.* J Biol Chem, 1997. **272**(32): p. 19808-13.

112. Takeshima, H., et al., *Generation and characterization of mutant mice lacking ryanodine receptor type 3.* J Biol Chem, 1996. **271**(33): p. 19649-52.

113. Takeshima, H., et al., *Embryonic lethality and abnormal cardiac myocytes in mice lacking ryanodine receptor type 2.* The EMBO Journal, 1998. **17**(12): p. 3309-3316.

114. Takeshima, H., et al., *Ca(2+)-induced Ca2+ release in myocytes from dyspedic mice lacking the type-1 ryanodine receptor.* The EMBO Journal, 1995. **14**(13): p. 2999-3006.

115. Clancy, J.S., et al., *Contractile function is unaltered in diaphragm from mice lacking calcium release channel isoform 3.* Am J Physiol, 1999. **277**(4 Pt 2): p. R1205-9.

116. Felder, E. and C. Franzini-Armstrong, *Type 3 ryanodine receptors of skeletal muscle are segregated in a parajunctional position.* Proceedings of the National Academy of Sciences of the United States of America, 2002. **99**(3): p. 1695-1700.
117. Ahern, G.P., P.R. Junankar, and A.F. Dulhunty, *Subconductance states in single-channel activity of skeletal muscle ryanodine receptors after removal of FKBP12.* Biophys J, 1997. **72**(1): p. 146-62.
118. Samso, M., X. Shen, and P.D. Allen, *Structural characterization of the RyR1-FKBP12 interaction.* J Mol Biol, 2006. **356**(4): p. 917-27.
119. Benacquista, B.L., et al., *Amino acid residues 4425-4621 localized on the three-dimensional structure of the skeletal muscle ryanodine receptor.* Biophys J, 2000. **78**(3): p. 1349-58.
120. Buratti, R., et al., *Calcium dependent activation of skeletal muscle Ca2+ release channel (ryanodine receptor) by calmodulin.* Biochem Biophys Res Commun, 1995. **213**(3): p. 1082-90.
121. Maximciuc, A.A., et al., *Complex of calmodulin with a ryanodine receptor target reveals a novel, flexible binding mode.* Structure, 2006. **14**(10): p. 1547-56.
122. Yamaguchi, N., C. Xin, and G. Meissner, *Identification of apocalmodulin and Ca2+-calmodulin regulatory domain in skeletal muscle Ca2+ release channel, ryanodine receptor.* J Biol Chem, 2001. **276**(25): p. 22579-85.
123. Samso, M. and T. Wagenknecht, *Apocalmodulin and Ca2+-calmodulin bind to neighboring locations on the ryanodine receptor.* J Biol Chem, 2002. **277**(2): p. 1349-53.
124. Beard, N.A., L. Wei, and A.F. Dulhunty, *Ca(2+) signaling in striated muscle: the elusive roles of triadin, junctin, and calsequestrin.* Eur Biophys J, 2009. **39**(1): p. 27-36.
125. Zalk, R., S.E. Lehnart, and A.R. Marks, *Modulation of the ryanodine receptor and intracellular calcium.* Annu Rev Biochem, 2007. **76**: p. 367-85.
126. Wehrens, X.H., et al., *Ca2+/calmodulin-dependent protein kinase II phosphorylation regulates the cardiac ryanodine receptor.* Circ Res, 2004. **94**(6): p. e61-70.
127. Van Petegem, F., *Ryanodine receptors: structure and function.* J Biol Chem, 2012. **287**(38): p. 31624-32.
128. Catterall, W.A., et al., *International Union of Pharmacology. XL. Compendium of voltage-gated ion channels: calcium channels.* Pharmacol Rev, 2003. **55**(4): p. 579-81.
129. Lipscombe, D., T.D. Helton, and W. Xu, *L-type calcium channels: the low down.* J Neurophysiol, 2004. **92**(5): p. 2633-41.
130. Periasamy, M. and A. Kalyanasundaram, *SERCA pump isoforms: their role in calcium transport and disease.* Muscle Nerve, 2007. **35**(4): p. 430-42.
131. Treves, S., et al., *Minor sarcoplasmic reticulum membrane components that modulate excitation-contraction coupling in striated muscles.* J Physiol, 2009. **587**(Pt 13): p. 3071-9.
132. Yoshida, M., et al., *Impaired Ca2+ store functions in skeletal and cardiac muscle cells from sarcalumenin-deficient mice.* J Biol Chem, 2005. **280**(5): p. 3500-6.
133. Shimura, M., et al., *Sarcalumenin alleviates stress-induced cardiac dysfunction by improving Ca2+ handling of the sarcoplasmic reticulum.* Cardiovasc Res, 2008. **77**(2): p. 362-70.
134. Marty, I., *Triadin regulation of the ryanodine receptor complex.* J Physiol, 2014.

135. Zhang, L., et al., *Complex formation between junctin, triadin, calsequestrin, and the ryanodine receptor. Proteins of the cardiac junctional sarcoplasmic reticulum membrane.* J Biol Chem, 1997. **272**(37): p. 23389-97.

136. Pan, Z., et al., *Co-expression of MG29 and ryanodine receptor leads to apoptotic cell death: effect mediated by intracellular Ca2+ release.* J Biol Chem, 2004. **279**(19): p. 19387-90.

137. Yasuda, T., et al., *JP-45/JSRP1 variants affect skeletal muscle excitation-contraction coupling by decreasing the sensitivity of the dihydropyridine receptor.* Hum Mutat, 2013. **34**(1): p. 184-90.

138. Mosca, B., et al., *Enhanced dihydropyridine receptor calcium channel activity restores muscle strength in JP45/CASQ1 double knockout mice.* Nat Commun, 2013. **4**: p. 1541.

139. Schwaller, B., et al., *Prolonged contraction-relaxation cycle of fast-twitch muscles in parvalbumin knockout mice.* Am J Physiol, 1999. **276**(2 Pt 1): p. C395-403.

140. Betzenhauser, M.J. and A.R. Marks, *Ryanodine receptor channelopathies.* Pflugers Arch, 2010. **460**(2): p. 467-80.

141. MacLennan, D.H. and E. Zvaritch, *Mechanistic models for muscle diseases and disorders originating in the sarcoplasmic reticulum.* Biochimica et Biophysica Acta (BBA) - Molecular Cell Research, 2011. **1813**(5): p. 948-964.

142. Treves, S., et al., *Congenital muscle disorders with cores: the ryanodine receptor calcium channel paradigm.* Curr Opin Pharmacol, 2008. **8**(3): p. 319-26.

143. Clarke, N.F., et al., *Recessive mutations in RYR1 are a common cause of congenital fiber type disproportion.* Hum Mutat, 2010. **31**(7): p. E1544-50.

144. Wilmshurst, J.M., et al., *RYR1 mutations are a common cause of congenital myopathies with central nuclei.* Ann Neurol, 2010. **68**(5): p. 717-26.

145. Denborough, M.A., et al., *Anaesthetic deaths in a family.* Br J Anaesth, 1962. **34**: p. 395-6.

146. Rosenberg, H., et al., *Malignant hyperthermia.* Orphanet J Rare Dis, 2007. **2**: p. 21.

147. Capacchione, J.F. and S.M. Muldoon, *The relationship between exertional heat illness, exertional rhabdomyolysis, and malignant hyperthermia.* Anesth Analg, 2009. **109**(4): p. 1065-9.

148. Krause, T., et al., *Dantrolene--a review of its pharmacology, therapeutic use and new developments.* Anaesthesia, 2004. **59**(4): p. 364-73.

149. Paul-Pletzer, K., et al., *Identification of a dantrolene-binding sequence on the skeletal muscle ryanodine receptor.* J Biol Chem, 2002. **277**(38): p. 34918-23.

150. Jiang, D., et al., *Reduced threshold for luminal Ca2+ activation of RyR1 underlies a causal mechanism of porcine malignant hyperthermia.* J Biol Chem, 2008. **283**(30): p. 20813-20.

151. Jungbluth, H., C.A. Sewry, and F. Muntoni, *Core myopathies.* Semin Pediatr Neurol, 2011. **18**(4): p. 239-49.

152. Lyfenko, A.D., et al., *Two central core disease (CCD) deletions in the C-terminal region of RYR1 alter muscle excitation-contraction (EC) coupling by distinct mechanisms.* Hum Mutat, 2007. **28**(1): p. 61-8.

153. McCarthy, T.V., K.A. Quane, and P.J. Lynch, *Ryanodine receptor mutations in malignant hyperthermia and central core disease.* Hum Mutat, 2000. **15**(5): p. 410-7.

154. Monnier, N., et al., *Familial and sporadic forms of central core disease are associated with mutations in the C-terminal domain of the skeletal muscle ryanodine receptor.* Hum Mol Genet, 2001. **10**(22): p. 2581-92.

155. Tilgen, N., et al., *Identification of four novel mutations in the C-terminal membrane spanning domain of the ryanodine receptor 1: association with central core disease and alteration of calcium homeostasis.* Hum Mol Genet, 2001. **10**(25): p. 2879-87.

156. Avila, G. and R.T. Dirksen, *Functional effects of central core disease mutations in the cytoplasmic region of the skeletal muscle ryanodine receptor.* J Gen Physiol, 2001. **118**(3): p. 277-90.

157. Zorzato, F., et al., *Clinical and functional effects of a deletion in a COOH-terminal lumenal loop of the skeletal muscle ryanodine receptor.* Hum Mol Genet, 2003. **12**(4): p. 379-88.

158. Jungbluth, H., *Multi-minicore Disease.* Orphanet Journal of Rare Diseases, 2007. **2**: p. 31-31.

159. Jungbluth, H., et al., *Minicore myopathy in children: a clinical and histopathological study of 19 cases.* Neuromuscul Disord, 2000. **10**(4-5): p. 264-73.

160. Ferreiro, A., et al., *A recessive form of central core disease, transiently presenting as multi-minicore disease, is associated with a homozygous mutation in the ryanodine receptor type 1 gene.* Ann Neurol, 2002. **51**(6): p. 750-9.

161. Jungbluth, H., et al., *Centronuclear myopathy due to a de novo dominant mutation in the skeletal muscle ryanodine receptor (RYR1) gene.* Neuromuscul Disord, 2007. **17**(4): p. 338-45.

162. Cavanagh, N.P., B.D. Lake, and P. McMeniman, *Congenital fibre type disproportion myopathy. A histological diagnosis with an uncertain clinical outlook.* Arch Dis Child, 1979. **54**(10): p. 735-43.

163. Laing, N.G., et al., *Actin mutations are one cause of congenital fibre type disproportion.* Ann Neurol, 2004. **56**(5): p. 689-94.

164. Monnier, N., et al., *Null mutations causing depletion of the type 1 ryanodine receptor (RYR1) are commonly associated with recessive structural congenital myopathies with cores.* Hum Mutat, 2008. **29**(5): p. 670-8.

165. Jungbluth, H., et al., *Minicore myopathy with ophthalmoplegia caused by mutations in the ryanodine receptor type 1 gene.* Neurology, 2005. **65**(12): p. 1930-5.

166. Rosenberg, P.B., *Calcium entry in skeletal muscle.* The Journal of Physiology, 2009. **587**(13): p. 3149-3151.

167. Cheng, H., W.J. Lederer, and M.B. Cannell, *Calcium sparks: elementary events underlying excitation-contraction coupling in heart muscle.* Science, 1993. **262**(5134): p. 740-4.

168. Endo, M., *Calcium-induced calcium release in skeletal muscle.* Physiol Rev, 2009. **89**(4): p. 1153-76.

169. Gomez, A.M., et al., *Ca2+ diffusion and sarcoplasmic reticulum transport both contribute to [Ca2+]i decline during Ca2+ sparks in rat ventricular myocytes.* J Physiol, 1996. **496 (Pt 2)**: p. 575-81.

170. Nelson, M.T., et al., *Relaxation of arterial smooth muscle by calcium sparks.* Science, 1995. **270**(5236): p. 633-7.

171. Zhou, H., et al., *Characterization of recessive RYR1 mutations in core myopathies.* Hum Mol Genet, 2006. **15**(18): p. 2791-803.

172. Protasi, F., et al., *RYR1 and RYR3 have different roles in the assembly of calcium release units of skeletal muscle.* Biophys J, 2000. **79**(5): p. 2494-508.

173. Cahill, H. and J. Nathans, *The optokinetic reflex as a tool for quantitative analyses of nervous system function in mice: application to genetic and drug-induced variation.* PLoS One, 2008. **3**(4): p. e2055.

174. Prusky, G.T., et al., *Rapid quantification of adult and developing mouse spatial vision using a virtual optomotor system.* Invest Ophthalmol Vis Sci, 2004. **45**(12): p. 4611-6.

175. Shaaban, S., et al., *RYR1 mutations as a cause of ophthalmoplegia, facial weakness, and malignant hyperthermia.* JAMA Ophthalmol, 2013. **131**(12): p. 1532-40.

176. O'Flynn, R.P., et al., *Masseter muscle rigidity and malignant hyperthermia susceptibility in pediatric patients. An update on management and diagnosis.* Anesthesiology, 1994. **80**(6): p. 1228-33.

177. Barone, V., et al., *Contractile impairment and structural alterations of skeletal muscles from knockout mice lacking type 1 and type 3 ryanodine receptors.* FEBS Lett, 1998. **422**(2): p. 160-4.

CURRICULUM VITAE

Name: Marijana

First name: Sekulic

Birth Date/Place: 19/08/1985, Novi Sad, (Serbia)

Education:

Feb, 2012 – Feb, 2016   PhD studies /Cell Biology/: Perioperative Patient Safety group, Department of Biomedicine, University Hospital Basel, University of Basel

2009   Master Studies /Molecular Biology/ Faculty of Science, University of Novi Sad, Serbia

2004 - 2008   Undergraduate studies, four-year program /Molecular Biology/, Faculty of Science, University of Novi Sad, Serbia

2000 - 2004   High School: /Medical High School/, four-year program, Novi Sad, Serbia

Publications:

1. **Characterization of excitation-contraction coupling components in human extraocular muscles**. Sekulic-Jablanovic M., Palowski-Wolfe A., Zorzato F. and Treves S. *Biochemical Journal*, 2015 Feb 15; **466**(1):29-36. doi: 10.1042/BJ20140970.

2. **Epigenetic changes as a common trigger of muscle weakness in congenital myopathies.** Rokach O, Sekulic-Jablanovic M, Voermans N, Wilmshurst J, Pillay K, Heytens L, Zhou H, Muntoni F, Gautel M, Nevo Y, Mitrani-Rosenbaum S, Attali R, Finotti A, Gambari R, Mosca B, Jungbluth H, Zorzato F, Treves S. *Hum Mol Genet*. 2015 Aug 15; **24**(16):4636-47. doi: 10.1093/hmg/ddv195. Epub 2015 May 27